Proliferation and lineage potential in fetal thymic epithelial progenitor cells

Alistair Martin Cook

Thesis presented for the degree of Doctor of Philosophy

The University of Edinburgh

2010

Declaration

The work in this thesis is my own, except where otherwise stated.

Alistair Martin Cook

Acknowledgements

Firstly I would like to thank my supervisor, Dr Clare Blackburn, for giving me the opportunity to carry out this project in her lab, for her helpful comments on my thesis, and for her patience. I would also like to thank the rest of the Blackburn lab members, past and present. Their assistance with endless embryo microdissections, and for technical advice has been second to none. Special thanks go out to Craig, Al, Nick, Adam and Christele for banter, cups of coffee, and 'interesting' conversations in the write-up room. I must also thank other members of the wider ISCR, in particular Ron Wilkie for histology advice, and Jan Vrana for excellent flow cytometric cell sorting. I owe a massive thankyou to Carol, John, and all other members of the animal house for breeding, looking after and keeping track of all those mice, and supplying them with vast quantities of cheese.

Thanks to Mum, Dad, Graham and Grandpa for all the support and advice you have given me over the last few years - I couldn't have done it without you, and I will endeavour to see more of you now! Thanks to Pip for her love, support, patience and understanding, for helping me put things into perspective on occasion, and for being my light at the end of the tunnel. Finally, apologies to the many friends whom I have been ignoring, but who have nevertheless been there whenever I needed some moral support in the form of a few beers (Dougie), or a good whinge.

Abstract

The thymic stroma primarily comprises epithelial, mesenchymal and endothelial cells, interspersed with those of haematopoietic origin. Thymic epithelial cells (TECs) are highly heterogeneous, but can be divided into two broad lineages, cortical and medullary, based on phenotype, functionality and location. A population of Plet1^{+} TEC progenitors have been identified which, when isolated from mouse E12.5 or E15.5 fetal thymus, reaggregated, and grafted, can produce a functional thymus. However, the potential of individual progenitors to form cortex and/or medulla is undefined. The main aim of this thesis was to use retrospective clonal analysis to ascertain the point during thymus ontogeny at which the cortical and medullary lineages diverge. To this end, I used transgenic mice carrying a ubiquitous *ROSA26laacZ* reporter gene (where a duplication within *lacZ* encodes non-functional β-galactosidase). Here, rare, random *laacZ-lacZ* genetic recombinations result in heritable expression of functional β-gal, producing labelled clones. As this occurs at a known frequency, determination of TEC numbers would enable calculation of the expected number of TEC clones present throughout ontogeny. Due to the lack of quantitative data on all thymic cell populations, I determined the size not only of TEC (lin^{-}EpCAM^{+}), but also haematopoietic (CD45^{+}), mesenchymal (lin^{-}PDGFRα^{+} and/or lin^{-}PDGFRβ^{+}) and endothelial (lin^{-}CD31^{+}) populations from E12.5 until E17.5. I then showed that the absolute number of Plet1^{+} TECs remains constant during this time, although the proportion of Plet1^{+} cells in cycle decreases. From these collective data, I propose a model for the role of the Plet1^{+} population in thymus development, in which Plet1^{+} cells continually give rise to Plet1^{-} TECs in a self-renewing manner. Finally, I present a 'dual origin coefficient' strategy for analysis of a library of prospective TEC clones. I calculated the number of TEC lacZ^{+} clones expected to be present throughout thymus ontogeny, selecting an appropriate developmental stage for analysis. Although I observed several clones of apparent mesenchymal origin, supporting a single origin for intrathymic and capsular mesenchyme at E15.5, I observed no TEC clones in this extensive analysis. The CpG content of the ROSA26 promoter suggests a possibility of methylation-induced silencing brought about by *de novo* methylation of the *lacZ* reporter gene.

Table of contents

Abbreviations

AIRE	autoimmune regulator
APC	antigen-presenting cell
BM	bone marrow
Cld	claudin
CMJ	corticomedullary junction
cTEC	cortical thymic epithelial cell
CTES	clusters of thymic epithelial staining
DC	dendritic cell
DN	double negative
DP	double positive
ECM	extracellular matrix
EGF	epidermal growth factor
EpCAM	epithelial cell adhesion molecule
ES	embryonic stem cell
FGF	fibroblast growth factor
H & E	hematoxylin & eosin
HC	Hassal's corpuscle
HP	haematopoietic progenitor
IGF	insulin-like growth factor
IL	interleukin
K	cytokeratin
LTBR	lymphotoxin beta receptor
Mab	monoclonal antibody
MDC	macrophage-derived chemokine
MHC	major histocompatibility complex
mTEC	medullary thymic epithelial cell
MTS	mouse thymic stroma
NC	neural crest
NH	nonhaematopoietic
NK	natural killer
NLS	nuclear localisation sequence

OEF	old embryo fix
PBS	phosphate buffered saline
PDGF	platelet-derived growth factor
PFA	paraformaldehyde
PVS	perivascular space
RAG	recombinase activating gene
RFTOC	reaggregated fetal thymic organ culture
RRV	recombinant retrovirus
RT	room temperature
SCID	severe combined immunodeficiency
SDF	stromal cell derived factor
SP	single positive
TCR	T cell receptor
TEC	thymic epithelial cell
TEPC	thymic epithelial progenitor cell
TGF	transforming growth factor
TN	triple negative
TNC	thymic nurse cell
TRA	tissue-restricted antigen
TSLP	thymic stromal lymphopoietin
WT	wild type

Chapter 1. Introduction

1.1. The mature thymus

1.1.1. Summary of thymus function

The thymus is the principal site of T-cell development. Bone-marrow (BM) derived T-cell precursor cells enter the organ from the circulation, in an immature state. These are guided through a series of complex maturation and selection steps to ensure the output of an immunologically self-tolerant repertoire of functional T-cells, that can recognise and bind to self-major histocompatibility complexes (MHC) with the correct degree of avidity.

1.1.2. Organ structure and composition

1.1.2.1. Overview

The mature mouse thymus consists of two conjoined lobes, situated on the midline, just above the heart. These lobes are covered in a thick capsule of connective tissue, from which trabeculae penetrate inward on a regular basis and further divide the thymus into a series of lobulations (Figure 1.1A). Within these lobules, the organ can be said to consist of two zones – an inner medulla, surrounded by an outer cortex. These areas can be designated on a histological basis; staining with hematoxylin and eosin (H&E) results in a darker cortex, due to a higher cell density (Figure 1.1A).

Thymic epithelial cells (TECs) comprise the major functional component of the thymic stroma, and form a complex, strictly regulated 3-dimensional network. Amongst this epithelial network reside many tightly packed thymocytes, at various stages of development (Figure 1.1B). Other stromal components include cells of mesenchymal origin such as fibroblasts and pericytes, and BM derived cells such as macrophages and dendritic cells (DCs). The interior of the thymus is heavily vascularised and innervated.

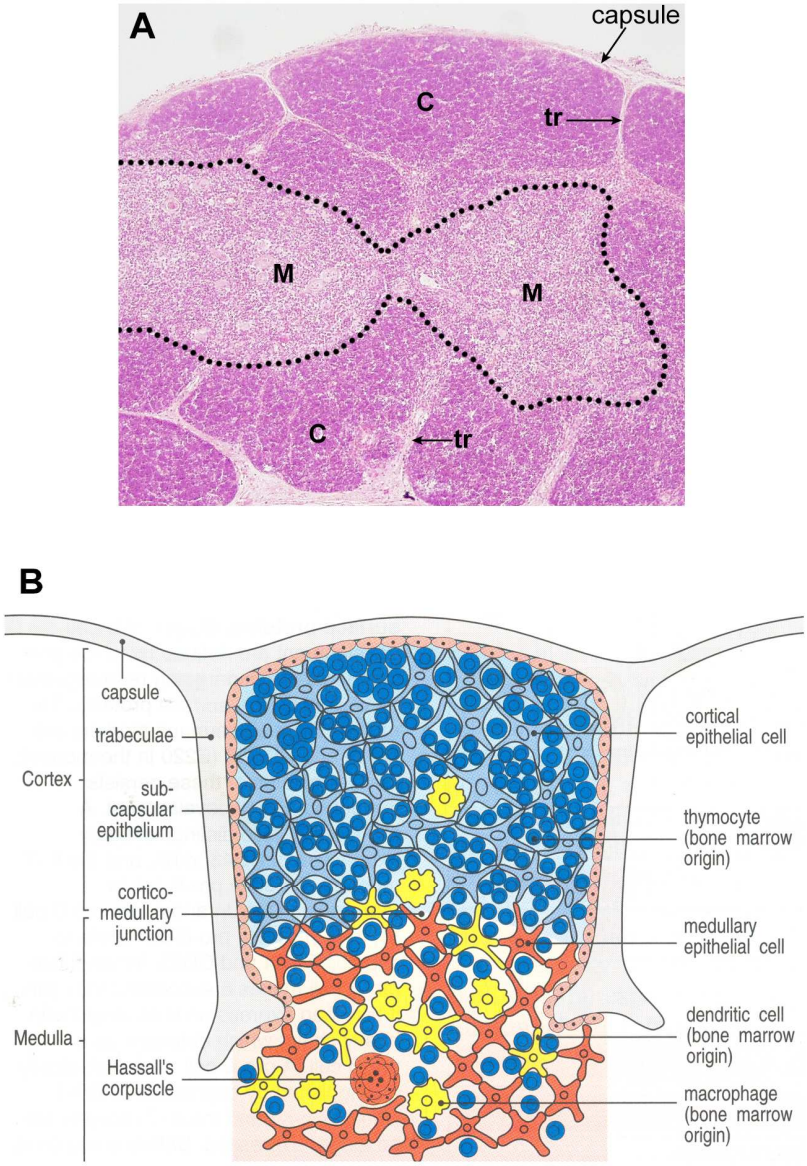

Figure 1.1 Thymus structure and cellular organisation

A) H&E stain of thymus, showing histologically distinct dark cortex (C) and lighter medulla (M). Cortex appears darker owing to a higher density of thymocytes than in the medulla. The connective tissue of the surrounding capsule and dividing trabeculae (tr) are also indicated.

Picture adapted from http://www.lab.anhb.uwa.edu.au/mb140/

B) Cartoon showing cellular organisation in the mature thymus. Bounded by subcapsular epithelium, the thymic parenchyma consists of an outer cortex and an inner medulla. Distinct cortical and medullary epithelial cells inhabit these regions, with the cortex being particularly tightly packed with thymocytes. Picture taken from Janeway et al., 2001.

1.1.2.2. Thymic epithelium

Although generally designated into three broad types (subcapsular, cortical and medullary), thymic epithelial cells are highly heterogeneous and have been subject to various methods of classification. Firstly an ultrastructural study of human thymus classified TECs into 6 different types – "subcapsular-perivascular" (type 1); "pale" (type 2); "intermediate" (type 3); "dark" (type 4); "undifferentiated" (type 5); and "large-medullary" (type 6) (van de Wijngaert et al., 1984). A second means of TEC classification has been according to profiles of staining with monoclonal antibodies (MAbs), in chicken, human, mouse and rat, assigning them to 'clusters of thymic epithelial staining' (CTES) groups, summarised in Table 1.1 (Kampinga et al., 1989, Brekelmans and van Ewijk, 1990, Van Vliet et al., 1984, Godfrey et al., 1990, Boyd et al., 1992).

If one were to move inward from the outer capsule toward the medulla, different TEC types would be sequentially encountered (Figure 1.1B). Firstly, a flattened epithelial cell type lines the thymic parenchyma, separating it from the thymic structural elements of the capsule and trabeculae (van de Wijngaert et al., 1984). This 'subcapsular' (or 'type 1') epithelium is supported on a basement membrane, creating a barrier between the internal and external thymic microenvironments. Type 1 epithelium is also continuous in surrounding large thymic blood vessels and cortical capillaries, creating perivascular spaces (PVS) and maintaining the 'blood-thymus barrier' in the cortex and at the cortico-medullary junction (CMJ) (Kendall, 1989). These cells are stained by CTES II MAbs, and are MHC class II negative (Boyd et al., 1992, Kampinga et al., 1989).

Type 1 epithelium apart, the most striking feature of epithelial cells in the thymus is their 3-dimensional arrangement. In contrast to the classical 2-dimensional sheets or stratified arrangements found in the majority of epithelial structures, TECs form an organised open network.

Immediately beneath the subcapsular epithelium lies the cortex. Cortical epithelial cells (cTECs) typically form an inter-connected meshwork, extending out long finger-like processes that join to their neighbouring cTECs by way of desmosomes.

TECs in the outermost cortex are 'type 2', appearing as "pale" on electron-micrographs (van de Wijngaert et al., 1984). Directly beneath these lie 'type 3' cTECs, characterised by an "intermediate" electron lucency, followed by 'type 4' cTECs that appear as "dark" on electron-micrographs (van de Wijngaert et al., 1984). Type 2, 3 and 4 cTECs are seen to stain with the CTES III group of antibodies and are also MHC class II positive, to a varying degree (Boyd et al., 1993, Kampinga et al., 1989, Gray et al., 2006). In the ultrastructural TEC analysis it was considered that TEC types 2 and 3 were very metabolically active, and presumed that cytokine production was occurring. Conversely, type 4 TECs have "features of dying cells" and may represent a terminal cTEC stage (Boyd et al., 1993, van de Wijngaert et al., 1984). On the basis of staining with MAbs to different species of keratin (K), two distinct cTEC subsets have been observed: a predominating $K8^{+}K18^{+}K5^{-}K14^{-}$ subset, and an infrequent $K8^{+}K18^{+}K5^{+}K14^{-}$ subset concentrated at the CMJ (Klug et al., 1998, Savino and Dardenne, 1988b, Savino and Dardenne, 1988a).

Some cTECs are known to form multicellular complexes, termed 'thymic nurse cells' (TNC). These are of enormous size, having appeared to engulf as many as 50-200 thymocytes (Wekerle and Ketelsen, 1980, Wekerle et al., 1980). Although little is known about the function of TNC, there is little evidence for phagocytic degradation of internalised thymocytes (Wekerle et al., 1980). Instead, these are completely sequestered within caveolae, and are often seen to be mitotically active (Wekerle et al., 1980). It has been postulated that these structures are involved in thymocyte maturation. In hanging drop culture experiments, an isolated cell line of rat 'TNC' was indicated to have the ability to internalise, and induce maturation of, immature $CD4^{-}CD8^{+}$ thymocytes to the $CD4^{+}CD8^{+}$ stage (Li et al., 2005). However, other studies have implied that it is in fact the $CD4^{+}CD8^{+}$ subset which are internalised and that TNC are involved in the process of MHC restriction (Martinez et al., 2007, Li et al., 1992).

In the innermost portion of the thymus lies the medulla. Medullary epithelial cells (mTEC) occur at a higher density than cTEC, are more compact in appearance, and are interspersed by fewer, less tightly packed thymocytes. Nearly all mTECs stain with CTES II or IV MAbs. By ultrastructural analysis, 'type 5' ("undifferentiated")

mTECs can be identified in small clusters at the CMJ (van de Wijngaert et al., 1984). Type 3 cells comprise the major proportion of mTECs within the main body of the medulla, interspersed with isolated type 6 "large medullary" cells – secretory cells with extensive endoplasmic reticulum (van de Wijngaert et al., 1984). All mTECs express MHC class I, and MHC class II expression is seen to vary between high and low expression (Farr and Nakane, 1983, Surh et al., 1992, Van Ewijk et al., 1980, Gray et al., 2006). As in the cortex, mTEC subpopulations have been identified on the basis of anti-keratin antibody staining. A major, centrally located $K8^{-}K18^{-}$ $K5^{+}K14^{+}$ population of cells exhibits a stellate morphology and reacts with the MAb MTS10, whereas a smaller, globular $K8^{+}K18^{+}K5^{-}K14^{-}$ population is localised in the outer medulla and is seen to bind the lectin UEA-1 with high affinity whilst being MHC class II^{hi} (Klug et al., 1998, Yang et al., 2006). Within the $UEA\text{-}1^{+}$ population, another scattered mTEC subpopulation expresses specific tight-junction components (the claudins Cld3 and Cld4 and occludin) (Hamazaki et al., 2007). This mTEC subset is predominantly MHC class $II^{hi}CD80^{+}MTS10^{-}$ and is known to also express the autoimmune regulator (Aire) transcription factor - involved in the expression of tissue-restricted antigens (TRAs) to facilitate negative selection (see section 1.1.3.3).

Multicellular complexes, Hassall's Corpuscles (HC), also occur in the medulla (Hassall, 1849). More commonly observed and well-developed in the human and guinea-pig thymus than in the mouse or rat, the role of these whorl-like groups of epithelial cells is still debated (Farr et al., 2002). HC have been proposed to be involved in the removal of apoptotic thymocytes, or in their maturation (Blau, 1973, Senelar et al., 1976). They have been shown to be active cytokine-producers; expressing interleukin (IL)-7, transforming growth factor (TGF)-α, CD30 ligand, stromal-cell-derived factor (SDF)-1 and macrophage-derived chemokine (MDC) (Annunziato et al., 2000, He et al., 1995, Le et al., 1991, Romagnani et al., 1998, Zaitseva et al., 2002). Expression of various elements of the mitogen-activated protein kinase (MAPK) signalling pathway suggest that the mTECs within HC may be in varying states of maturity (Nishio et al., 2001). Recently, it has been indicated that HC may play an indirect role, in inducing $CD4^{+}CD25^{+}$ regulatory T cells in human thymus. HC were shown to produce thymic stromal lymphopoietin (TSLP),

which activated $CD11c^+$ DCs to express CD80 and CD86. These ligands in turn activated $CD4^+CD8^-CD25^-$ thymocytes to proliferate and differentiate along the regulatory T cell pathway (Watanabe et al., 2005).

Table 1.1 CTES phenotypic classification in response to monoclonal antibody staining

CTES Group	Specificity
I	All TEC
II	Subcapsular/perivascular/medullary TEC
III.A	Cortical TEC
III.B	Cortical TEC, isolated medullary TEC
III.C.1	Cortical TEC, macrophages
III.C.2	Cortical TEC, thymocytes
IV	Medullary TEC, Hassal's corpuscles
V.A	Hassal's corpuscles
V.B	Hassal's corpuscles, myeloid cells
V.C	Hassal's corpuscles, associated medullary TECs
V.D	Hassal's corpuscles, associated medullary TECs, some leukocytes
V.E	Hassal's corpuscles, associated medullary TECs, subcapsular TEC
VI	Type 1 epithelium
XX.A	Most corticall and medullary TEC, isolated subcapsular TECs
XX.B	Minority of cortical and medullary TEC
XX.C	Minority of medullary TEC, cortical thymocytes

Summary of 'clusters of thymic epithelial staining' (CTES), where TEC subpopulations were assigned in response to monoclonal antibody staining patterns.

1.1.2.3. Thymic vasculature and innervation

Major blood vessels and lymphatics from the thymic exterior arrive at the cortico-CMJ from within trabecular connective tissue. These subsequently diverge into the thymic parenchyma, connecting to a fine network of capillaries that lead into the cortex and medulla (Kato, 1997, Kato and Schoefl, 1989). Cortical capillaries extend out toward the subcapsule, whereupon the vasculature loops back toward the CMJ and drains into postcapillary venules (Kato and Schoefl, 1989). Around large blood vessels of the thymic parenchyma, in the medulla and at the CMJ, an additional sheath of perivascular cells is present which form close contact to type 1 simple epithelium. The gap formed between the inner and outer perivascular cells is known as the perivascular space, and is involved in the selective transport of haematopoietic precursors and mature thymocytes between the circulation and the thymic stroma (Mori et al., 2007, Kato and Schoefl, 1989).

Dense nerve plexuses from the sympathetic nervous system enter the thymus associated with large blood vessels, with which they reach the inner cortex and medulla. Nerve fibres also enter the outer cortex from the capsule and interlobular septae. Innervation is particularly dense at the CMJ (Kendall, 1991, Kendall and al-Shawaf, 1991, Mignini et al., 2003).

1.1.2.4. Other stromal components

In the mature organ, mesenchyme-derived cells are present in a number of structural components such as the outer capsule, inner connective tissue and trabeculae, intrathymic fibroblasts, and the pericytes and smooth muscle cells that surround many blood vessels. Extra-cellular matrix (ESM) produced by fibroblasts is an important contributor to thymus structure, and is involved in signalling with epithelial, endothelial and haematopoietic cells. Thymic mesenchyme is heterogeneous - for example, sub-populations showing staining with the monoclonal antibody MTS15 have been identified, lining the subcapsule and large blood vessels (Gray et al., 2007b, Gray et al., 2002).

1.1.3. Intrathymic T-cell development in the mature thymus

1.1.3.1. Initial stages

Because of the need to establish a self-tolerant repertoire with a propensity to recognise self-MHC, via combinational gene rearrangement, a number of gating or "selection" steps are imposed during T cell development. As a result, only 3-5% of candidates pass all these stringent selection criteria (Scollay et al., 1984, Merkenschlager et al., 1997). In the steady-state adult thymus, T-cell precursors enter from the circulation at the CMJ (Figure 1.2). These then move outward through the cortex toward the subcapsular area, passing through defined zones (region 1-4, see Figure 1.2) that are inhabited by thymocytes of increasing maturity (Lind et al., 2001). Thymocyte migration between different zones of the thymus is largely induced by a range of chemokines (for a recent review see (Takahama, 2006)).

Upon entering the thymus, prospective thymocytes are $CD4^-CD8^-$ double negative (DN) (Petrie et al., 1990). These are heterogeneous in their potential to generate T cells or other BM-derived cells such as natural killer (NK) cells, DCs and macrophages (Porritt et al., 2004, Balciunaite et al., 2005). These DN cells can be further subdivided into subsets of progressive maturation, based on expression of CD44 and CD25 (Godfrey et al., 1993). Initially $CD44^+CD25^-$ (DN1) thymic immigrants move from region 1 to region 2 (Figure 1.2) – undergoing proliferative expansion, and adopting a $CD44^+CD25^+$ (DN2) phenotype (Godfrey et al., 1993, Penit et al., 1995).

Transition to the $CD44^-CD25^+$ (DN3) stage in region 3 is followed by rearrangement of the T-cell receptor (TCR) gene segments. Supported by IL7 signalling from stromal cells, and under the control of recombination activating gene (RAG) 1 and RAG 2, the β-, γ- and δ-TCR genes begin rearrangement virtually simultaneously (Wilson et al., 1994a, Hofmeister et al., 1999, Muegge et al., 1993). The choice between α:β or γ:δ T-cell lineage is regulated by whichever TCR genes are productively rearranged first (known as the β-selection checkpoint). Signalling

occurs via expression of the corresponding TCR chains on the cell surface, leading to shutdown of further TCR gene rearrangement. This process, termed allelic exclusion, thus blocks productive recombination of gene segments for the alternate lineage in that cell. The γ:δ lineage requires expression of both functional γ- and δ-chains; the α:β lineage initially requires only a functional β-chain (which pairs with a surrogate α-chain to form the β:pTα pre T-cell receptor), hence 95% of thymocytes are of the α:β lineage (Godfrey and Zlotnik, 1993, Groettrup and von Boehmer, 1993). The γ:δ T-cells remain DN and show little proliferation. β:pTα cells are stimulated to proliferate and subsequently undergo α-TCR rearrangement to become α:β T-cells (Dudley et al., 1994). The α-TCR gene segments continuously rearrange until a functional α-TCR chain is produced, maximizing the production of useful thymocytes (Petrie et al., 1993).

Thymocytes subsequently migrate to the outermost subcapsular region (region 4, Figure 1.1) thymocytes become $CD44^{-}CD25^{-}$ (DN4/preDP) and undergo further proliferation followed by a switch to the $CD4^{+}CD8^{+}$ double-positive (DP) phenotype (Godfrey et al., 1993).

1.1.3.2. Positive selection

DP thymocytes migrate back toward the CMJ, on the way undergoing positive selection – a process mediated by cortical TECs (Anderson et al., 1994, Laufer et al., 1996). Positive selection ensures that the TCR gene rearrangement step has produced a TCR that is able to recognise self-MHC with the correct avidity. Any thymocyte that is not MHC-restricted will subsequently undergo apoptosis.

Upon completing positive selection, thymocytes become either $CD4^{+}CD8^{-}$ or $CD4^{-}CD8^{+}$ single-positive (SP) (also known as helper and cytotoxic T-cells respectively). This fate choice is based on the strength and duration of MHC-induced signalling through the TCR during positive selection. Initial MHC recognition by the TCR leads to uniform downregulation of CD8, the MHC class-I-specific co-receptor. It therefore follows that thymocytes interacting with MHC class-I molecules will experience disrupted, transient signalling. Conversely, MHC class-II interaction will produce strong, sustained TCR signalling since expression of the MHC class-II-

specific CD4 co-receptor is maintained (Singer, 2002). These MHC-TCR signals are mediated by the *src*-family kinase $p56^{lck}$ (Lck) (Liu and Bosselut, 2004, Salmond et al., 2009, Brugnera et al., 2000). Strong, sustained signalling from MHC-II-specific TCRs activates initial $CD4^+$ thymocyte differentiation via the transcription factor GATA-3 (Pai et al., 2003). ThPOK, another transcription factor, acts downstream to commit these cells to the $CD4^+$ fate (Egawa and Littman, 2008, Muroi et al., 2008, Wang et al., 2008). In contrast, transient signalling by MHC-I specific TCRs activates Runx3, which supports $CD8^+$ thymocyte differentiation (Kohu et al., 2005).

1.1.3.3. Negative selection

Upon crossing the CMJ, SP thymocytes undergo the process of negative selection to create a self-tolerant repertoire. This serves to identify and neutralise any T-cells that may have an affinity toward self-antigens through clonal deletion – thereby preventing autoimmune attack. Negative selection is mediated by contact with various antigen-presenting cells (APCs) in the medulla. Dendritic cells are able to ingest and present extracellular self-antigens from dead cells, in addition to presenting antigens of self-haematopoietic origin, via surface MHC complexes. MTECs also present self-antigens to T-cells. MTECs express one of the highest levels of different genes in any cell – organ-specific antigens from peripheral areas, e.g. liver, stomach, are found to be expressed (often as thymic splice variants) by mTECs, each usually by only a small number of cells per individual mouse (Derbinski et al., 2001, Kyewski et al., 2002). This elevated expression of peripheral tissue-restricted antigens (TRAs) aids in identification of self-reactive thymocytes during negative selection.

Mature T cells can remain in the thymus for up to 2 weeks before emigrating from the thymus via blood vessels to the circulation.

1.1.3.4. $Aire^+$ mTECs

The promiscuous expression of TRAs in the thymus is regulated, at least in part, by expression of the autoimmune regulator protein (Aire) (Anderson et al., 2002, Kuroda et al., 2005, Liston et al., 2003). *AIRE* was originally identified in humans, as the gene responsible for a multiorgan autoimmune disease, autoimmune

polyendocrinopathy candidiases ectodermal dystrophy (APECED) (Aaltonen et al., 1997). Mouse studies have shown that *Aire*, now known to be a transcriptional regulator, is expressed by a specific subset of mTECs (Derbinski et al., 2001, Hubert et al., 2008).

It has also recently been suggested that the Aire protein itself may play a role in inducing apoptosis of mTECs that express TRAs and that are becoming terminally differentiated, possibly to facilitate cross-presentation of ectopically expressed antigens within the thymus (Dooley et al., 2008). In support of this, $Aire^{-/-}$ mice display a large number of $K8^{+}K14^{-/lo}$ 'globular' mTECs. These are found as a minor subset in WT mice, perhaps indicating that in the $Aire^{-/-}$ thymus they are able to terminally differentiate and persist instead of being induced to die. Thus, it may be that $K14^{+}K8^{-}p63^{+}Aire^{-}$ cells give rise to $K14^{+}K8^{+}p63^{-}Aire^{+}$ cells, and that these – if not eliminated by apoptosis – may terminally differentiate into $K8^{+}K14^{-/lo}$ mTECs.

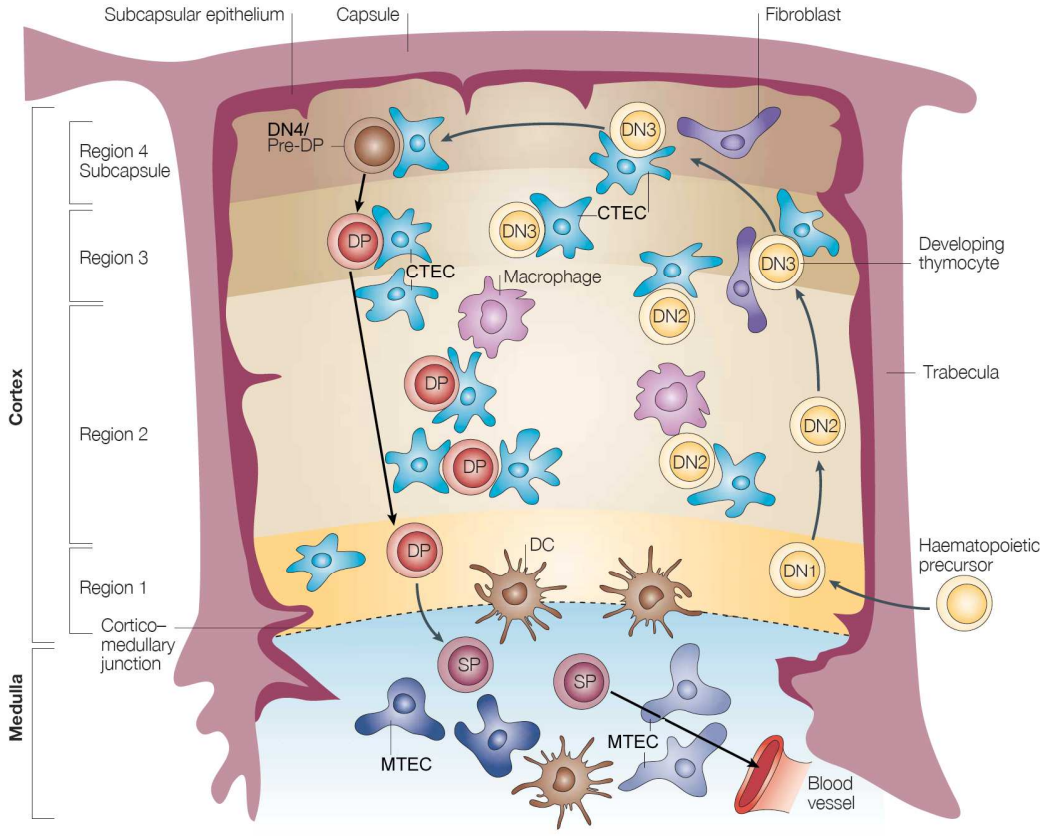

Figure 1.2 Intrathymic T-cell development

Developing thymocytes migrate through defined zones of the thymus in a stepwise manner, progressing through a highly ordered differentiation programme. Uncommitted DN1 precursors enter at the CMJ and migrate out toward the subcapsule. During this time they undergo proliferative expansion and lose NK- and B-cell potential (DN2), and begin TCR gene rearrangement (DN3). In the subcapsular region thymocytes become DP. They then migrate back through the cortex, becoming either $CD4^+$ or $CD8^+$ SP, and finally into the medulla prior to export to the periphery (subject to surviving positive and negative selection).

(Figure adapted from Blackburn and Manley, 2004)

1.2. The developing thymus

1.2.1. Overview of early organogenesis

Developing separately and bilaterally on opposite sides of the embryo, the murine thymus lobes originate in the pharyngeal region of the embryonic foregut (Figure 1.3A). This region consists of a series of mesodermal bulges, known as the pharyngeal arches. These arches (of which there are 5 in the mouse) form by day 9 of embryonic development (E9), in a rostral to caudal manner. The arches are separated by bilateral out-pocketings of endoderm, termed the pharyngeal pouches, and invaginations of ectoderm immediately opposite, termed the pharyngeal clefts (Figure 1.3B). The pharyngeal endoderm and ectoderm are at this stage composed of single layers of simple epithelium. Between E9.5 and E10 third pouch endoderm and third cleft ectoderm are in close contact, but separation subsequently occurs.

By E11, following proliferation of the endodermal epithelium, the thymus has begun to form an outgrowing bud and is morphologically visible (Manley, 2000). This anlage contains the primordia of both the thymus (distal region) and parathyroid, and is surrounded by a neural-crest-derived mesenchymal capsule (Figure 1.3C). Lymphocyte precursors arrive in the capsule from E11 (Itoi et al., 2001). At this early stage, thymic epithelium exists as a bilayered epithelial sheet with an inner lumen. At E11.5 this epithelium is $K5^{+}K8^{+}$, with the apical layer expressing claudin-3 and claudin-4 (Hamazaki et al., 2007, Bennett et al., 2002).

By E12, the thymus/parathyroid primordia have completely separated from the pharynx (Figure 1.3E), following apoptosis on opposing sides of surface ectoderm and connective endoderm (Gordon et al., 2004). Thymus structure has now changed from a two-dimensional sheet to a three-dimensional clustered formation, and lymphocytes begin to invade the thymic epithelium from the capsule (Itoi et al., 2001). By E12.5, patterning and differentiation within the thymus has begun. Epithelial cells are predominantly $K5^{+}K8^{+}$, with a minor subset of $K5^{-}K8^{+}$ appearing around the periphery (Klug et al., 2002). TEC are negative for MHC class II (a

marker of mature thymic epithelium) at this stage (Bennett et al., 2002, Jenkinson et al., 1981).

The thymus and parathyroid begin physical separation by E13, with the thymic rudiment beginning to migrate in a ventro-medial and caudal manner toward its final location (Figure 1.3E), in a central position just above the heart (Manley and Blackburn, 2003). The centre of the E13.5 thymus remains predominantly $K5^{+}K8^{+}$, with an increasing $K5^{-}K8^{+}$ population around the outside. The central region of the $K5^{+}K8^{+}$ clusters stains brightly with MTS10, a marker of the predominant mature medullary subset (Klug et al., 2002).

By E15.5 $K5^{+}K8^{+}$ TECs persist as small clusters (~13% of total TECs) within the predominant (~60% of TECs) $K5^{-}K8^{+}$ subset, emanating out from the central area of the thymus. Cells in the centre of these clusters generally express the highest levels of K5, and some of those on the outer boundaries of the clusters are $K5^{+}K8^{lo}$ (~27% of all TECs) (Klug et al., 2002, Jenkinson et al., 2005).

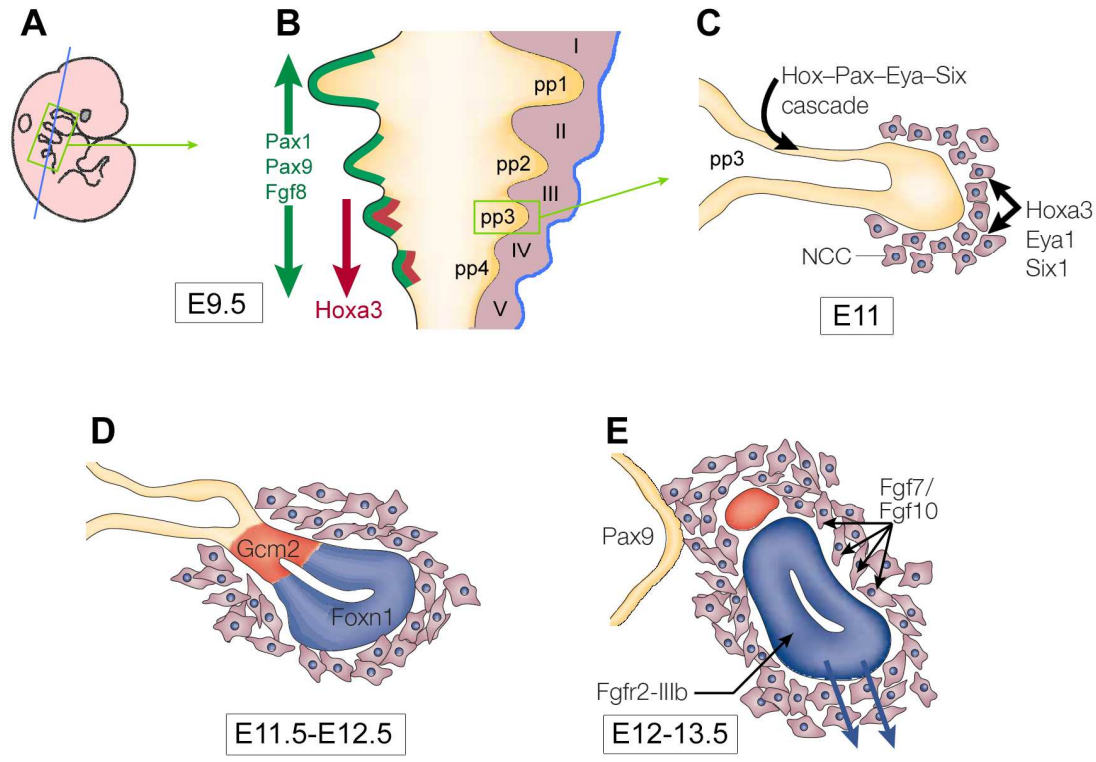

Figure 1.3 Early thymus organogenesis

A) Embryo showing location of pharyngeal region (green box). The blue line depicts a coronal section through the pharyngeal region. (Modified from Manley, 2000)

B) Cartoon representing the coronal section from **A**, at E9.5. Right side of figure indicates positioning of endodermal pharyngeal pouches (pp1-pp4); this side also depicts mesenchymal/mesodermal pharyngeal arches (purple, I-V) and pharyngeal ectoderm (shown in blue). Left side of figure shows pharyngeal pouches only, indicating expression patterns of Pax1, Pax9 and Fgf8 (required for pharyngeal pouch formation) and Hoxa3 (required for pp3 axial identity).

C) Rudiment outgrowth begins. Continued development is dependent on activity of the transcription factors Hoxa3, Pax1, Pax9, Eya1 and Six1. These are all expressed in the endoderm, with Hoxa3, Eya1 and Six1 also expressed in NCC and ectoderm.

D) Outgrowth and patterning of rudiment. This begins at E10 with the onset of Gcm2 expression, indicating the parathyroid domain of pp3 (red). Foxn1 is expressed in the thymus domain of pp3 at high levels from E11.25 (blue).

E) Separation from the pharynx and migration of the thymic rudiment. Separation requires Pax9. Production of Fgf7/Fgf10 by NCC stimulates epithelial proliferation via the Fgfr2-IIIb receptor.

(B, C, D & E modified from Blackburn and Manley, 2004)

1.2.2. Genetic factors influencing thymus development

1.2.2.1. Tbx1

One of the first genes to act in the process of thymus organogenesis is the T-box transcription factor *Tbx1*. Expressed during development from E7.5 until E12.5, *Tbx1* is active in a variety of structures including pharyngeal endoderm and pharyngeal mesoderm (Chapman et al., 1996). *Tbx1* plays a role in pharyngeal segmentation, with loss of its expression resulting in severe hypoplasia or aplasia of most pharyngeal arches and pouches, and also severe hypoplasia of the pharynx (Jerome and Papaioannou, 2001, Vitelli et al., 2002).

Findings from the lab of Baldini and colleagues have revealed a crucial time window for *Tbx1* function in thymus formation. Tamoxifen-inducible cre recombinase was used to produce timed *Tbx1*-null mutant mouse embryos. Cre-induction at E8.5 or earlier resulted in athymic embryos when examined at E18.5 (Xu et al., 2005). In further experiments, tamoxifen-inducible cre was knocked into the *Tbx1* allele and used to activate permanent β-galactosidase expression. Here, E12.5 lobes were heavily labelled when β-gal was activated at E8.5, but not at E9.5 – indicating *Tbx1* is not active in TECs at E9.5 (Xu et al., 2005). These results indicate the importance of *Tbx1* function during the E8.5-9.5 time interval – coinciding with the formation of the third pharyngeal pouch. *Tbx1* appears to also play a role in subsequent thymus organogenesis, with *Tbx1*-null mice induced at E10.5 exhibiting a slightly hypoplastic thymus at E18.5 (Xu et al., 2005).

1.2.2.2. Hoxa3

The homeobox transcription factor *Hoxa3* is also known to play a role in pharyngeal development. The *Hox* family are known to regulate the anterior/posterior axis in embryogenesis (Krumlauf, 1994). *Hoxa3* is expressed in the pharyngeal endoderm and surrounding mesenchyme from E9.5, with its anterior boundary of expression being the third pouch (Figure 1.3B) (Manley and Capecchi, 1995). *Hoxa3* homozygous mutations are lethal, showing deletions of both parathyroid and thymus, and thyroid hypoplasia (Manley and Capecchi, 1998).

1.2.2.3. Pax1 and Pax9

The paired box transcription factor genes *Pax1* and *Pax9*, both of which are expressed in the third pharyngeal pouch from E9.5 (Figure 1.3), are affected by *Hoxa3* expression (Manley and Capecchi, 1995, Neubuser et al., 1995). *Pax1* inactivation results in a hypoplastic parathyroid and thymus, with disturbed thymocyte maturation (Wallin et al., 1996). *Pax9* null mutants result in the ectopic location of the early thymus rudiment; this is followed by failure of thymopoiesis, and subsequently by atrophy (Hetzer-Egger et al., 2002).

1.2.2.4. Eya1 and Six1

A homologue of the drosophila transcription factor gene *eyes absent* (*Eya1*) is present in second, third and fourth pouch endoderm and adjacent NC-derived mesenchyme (Figure 1.3), expressed form E9.5 until E10.5 (Xu et al., 2002). In *Eya1* deficient mice, thymus and parathyroid organ primordia fail to form. Expression of the *sine oculis* (*Six1*) transcription factor gene, also expressed in the above tissues, is also markedly reduced in *Eya1* null mice, suggesting dependence on *Eya1* (Xu et al., 2002). *Six1*$^{-/+}$ mutants lack a thymus (Laclef et al., 2003). In drosophila, the homologues of *Pax*, *Eya* and *Six* form a pathway, which appears to be conserved to some degree in mammalian development. A more recent study, however, has placed *Pax1* downstream of *Eya1* and *Six1* (Zou et al., 2006).

1.2.2.5. Gcm2 and Rhox4

A further transcription factor, glial cells missing 2 (*Gcm2*), is thought to be regulated by the *Hox-Pax-Eya-Six* cascade – its expression is reduced in *Pax1*$^{-/-}$ single mutants, and further reduced in *Hoxa3*$^{+/-}$*Pax1*$^{-/-}$ mutants (Su et al., 2001). *Gcm2* expression has also been shown to be *Eya1* dependent (Xu et al., 2002). Expressed after E9.5 in the anterior part of the third pouch, *Gcm2* marks the parathyroid-specific area (Gordon et al., 2001). *Gcm2* null mice lack parathyroid glands (Gunther et al., 2000).

Recently, the reproductive homeobox 4 (*Rhox4*) gene was found to be expressed in the third pharyngeal pouch, in a pattern complementary to *Gcm2* from E9.5 until E11.0. In *Gcm2* null mice, *Rhox4* continues to be limited to the ventral third pouch.

Rhox4 expression remains unaltered in *Hoxa3* null mice indicating that, unlike *Gcm2*, its regulation is controlled by a means other than *Hoxa3* (Morris et al., 2006).

1.2.2.6. Foxn1

Formerly known as winged-helix nude (Whn), the forkhead box transcription factor *Foxn1* is present in a mutant form in Nude (*nu*) mice (Nehls et al., 1996). In the *nu* mouse only a rudimentary, non-functional thymus is present, with its epithelial compartment composed of cells seemingly in an undifferentiated state. These cells appear phenotypically similar to the thymic epithelial progenitor population discussed in section 1.2.4.1, expressing the marker MTS24. During normal thymus development, *Foxn1* complements *Gcm2* expression in the third pharyngeal pouch at E11.25 (Figure 1.3D) (Gordon et al., 2001). Heterozygous, $nu^{+/-}$ thymus lobes show reduced colonisation by lymphoid progenitors (Scheiff et al., 1978).

A study by Blackburn et al demonstrated that *Foxn1* acts in a cell autonomous manner. Here, *nu*/WT chimeras were created by blastocyst complementation and some *nu*-derived cells were seen to contribute to the thymus. However, these cells remained clustered in the medulla, in an apparently undifferentiated state, and were not incorporated into the WT-derived normal thymic epithelial architecture (Blackburn et al., 1996). Studies involving the targeting of *Foxn1* to express reporter genes reveal continued expression of *Foxn1* by TECs throughout thymus ontogeny (Gordon et al., 2007, Nehls et al., 1996). It has recently been shown, by the absence of the cortical cell-surface marker CD205 and the cTEC-specific proteasome subunit β5t in the nude thymus, that the appearance of cells expressing cTEC markers at E12 occurs via a *Foxn1*-dependent mechanism (Shakib et al., 2009). Within the postnatal thymus, it appears that *Foxn1* expression is necessary to maintain the thymic microenvironment, and its artificial down-regulation reveals a dosage-dependent effect on the loss of specific TEC subsets (Chen et al., 2009).

1.2.3. Cellular origin and interaction during thymus ontogeny

1.2.3.1. Thymic epithelial origin

Derivation of the thymic epithelium had, until relatively recently, been subject to a degree of controversy. It was generally agreed that the medullary epithelium originates from the endoderm of the third pharyngeal pouch. However, it was a matter of dispute whether the cortex also originated from this structure, or whether it in fact had an ectodermal origin in the third pharyngeal cleft, as was the traditionally held view.

The dual-origin model was based primarily on a study in *nude* mice, in which thymus development is halted at the primordial stage between E11.5 and E12.0. Here, in homozygous *nu/nu* embryos, proliferation of the pharyngeal ectoderm was reported as being greatly reduced. The authors concluded that the *nude* phenotype rendered the ectoderm unable to fulfil its role in thymus development (Cordier and Haumont, 1980, Cordier and Heremans, 1975).

More recent studies, however, have verified the single origin model, initially demonstrated by the sufficiency of pharyngeal endoderm alone to develop into a thymus in chick/quail chimera studies (Le Douarin and Jotereau, 1973). In a study on whole mouse embryos, E10.5 pharyngeal ectoderm was labelled with tracking dye (Gordon et al., 2004). Following 30 hours in whole-embryo culture, the labelled cells showed no sign of contribution to the resultant thymus lobes. In the same study, E8.5-E9.0 second and third pharyngeal pouch endoderm was isolated and grafted under the kidney capsule of athymic *nude* mice. This resulted in thymus-like structures that contained distinct cortical and medullary areas, thus verifying the single origin model (Gordon et al., 2004).

1.2.3.2. Thymic mesenchymal origin

Mesenchymal cells migrate into the pharyngeal arches from E9.0, encapsulating the thymus during early organogenesis. These are neural crest (NC) derived, as shown in chick/quail chimera experiments (Le Douarin and Jotereau, 1975, Le Lievre and Le Douarin, 1975). The requirement for NC mesenchyme in the proliferation of

thymic epithelium has been demonstrated, with extirpation of cephalic NC areas in chick embryos resulting in thymus hypoplasia or absence (Bockman and Kirby, 1984). Culture of the mouse thymic rudiment minus the surrounding mesenchyme also results in failure of normal thymus development (Anderson et al., 1993, Auerbach, 1960, Suniara et al., 2000, Jenkinson et al., 2007).

To assess NC contribution to mature thymus, lineage-tracing experiments using a silent *ROSA26R* lacZ reporter activated by myelin protein zero-Cre (Yamazaki et al., 2005) and Wnt1-Cre (Jiang et al., 2000) reporter mice have been performed, labelling NC-derived mesenchyme. Results from these studies appeared to suggest that, although present in large numbers in earlier organogenesis, NC contribution to mesenchymal structures in the mature thymus is trivial or absent.

However, more recent studies - using Cre under the control of Wnt1 and Sox10 promoters to reactivate silent *ROSA26R*-eYFP in the embryonic NC - have demonstrated the persistence of NC-derived cells in the adult thymus, as perivascular cells and in the thymic capsule (Foster et al., 2008, Muller et al., 2008). The difference between these and the earlier studies using lacZ may be a result of poor sensitivity in the *lacZ* system, or perhaps age-related silencing of the *lacZ* gene (Chevalier-Mariette et al., 2003). It remains to be confirmed as to whether or not a mesodermally derived mesenchyme population also contributes to thymus development.

1.2.3.3. Role of mesenchyme in thymus ontogeny

From around E11, the outer mesenchymal layer attracts haematopoietic progenitors as the first part of a two-step thymus seeding process, preceding their movement from the mesenchyme into the epithelial core (Itoi et al., 2001). Mesenchymal cells penetrate the epithelial core of the thymus from the outer capsule at around E13 or earlier.

The mechanisms by which mesenchymal cells affect thymus development are poorly understood. Fibroblast growth factors (FGF) 7 and FGF10, produced by thymic mesenchyme, and their receptor FGFR2-IIb, expressed on the epithelial component, are thought to be involved in epithelial expansion at around E14. FGF10 has also

been reported to maintain the proliferative capacity of epithelial progenitor cells in the pancreas (Bhushan et al., 2001). Addition of these factors in place of mesenchyme in vitro can induce thymic epithelial proliferation (Jenkinson et al., 2003, Revest et al., 2001), as can the addition of epidermal growth factor (EGF) (Shinohara and Honjo, 1996). It also has been reported that, at E12, Insulin-like growth factors (IGF) 1 and IGF2 are expressed by thymic mesenchyme, with the receptor IGF1R being expressed on epithelial cells - correlating with an absence of FGF7 and FGF10 at this stage (Jenkinson et al., 2007). Implication of a role for IGF/IGFR signalling in thymus growth would seem to agree with a study where over-expression of human IGF2 in mice resulted in an enlarged thymus (van Buul-Offers et al., 1995). Mesenchyme may also be required in maturation of thymic epithelial cells, for example in inducing the expression of MHC class II (Itoi et al., 2007, Shinohara and Honjo, 1997, Itoi and Amagai, 1998).

1.2.3.4. Thymic vascular development

During the early stages of thymus development, endothelial cells migrate into the thymus and proliferate, probably driven by angiogenic stimuli such as vascular endothelial growth factor (VEGF) (Leung et al., 1989). VEGF is a permeability-enhancing factor and an endothelial cell mitogen, and is expressed by both the TEC and mesenchymal cells of the developing thymus (Brooks et al., 1998, Muller et al., 2005). Since pericytes have been demonstrated to be a source of VEGF, it is possible that these migrate into the thymus ahead of endothelial cells and guide the sprouting process (Ozerdem and Stallcup, 2003).

Endothelial cells are known to express platelet derived growth factor (PDGF) β, which attract PDGF receptor (PDGFR) β^+ perivascular mesenchyme (Lindahl et al., 1997). These cells – pericytes and smooth muscle cells – then proceed to wrap around certain blood vessels, providing support and participating in the regulation of endothelial cell function. Perivascular mesenchyme has been shown to be of NC origin, even in adult thymus (Muller et al., 2008, Foster et al., 2008).

1.2.3.5. Lympho-epithelial crosstalk in epithelial development and differentiation

The influence of thymocytes on the development of epithelium in the thymus has been termed thymic crosstalk (van Ewijk et al., 1994). Haematopoietic progenitors (HPs) first invade the thymic rudiment at E11 – E11.5. Shortly after this, the thymus changes from a two-dimensional to a three-dimensional structure and differences in expression of certain keratin molecules (described in section 1.2.1) are observed (Itoi et al., 2001, Klug et al., 2002).

Observations using both RAG2/γ_c deficient mice (where a lack of RAG2 prevents TCR rearrangement, whilst a deficient γ_c gene precludes IL-7/IL7-R interaction) and Ikaros (a transcription factor required by HPs to commit to the lymphoid lineage) null mice showed that thymic epithelium was still able to adopt a 3-D morphology and also $K8^+K5^+$ and $K8^+K5^-$ TEC subsets seen in the wild-type at E13.5 and E15.5 (Klug et al., 2002). However, when these mice were analysed at the newborn stage, a hypoplastic thymus was observed. This showed similar TEC architecture to E13.5-15.5, with prominent central $K5^+K8^+$ clusters, and absence of organised medullary areas (Klug et al., 2002). Furthermore, when adult examples of these transgenic models were examined the thymi were seen to be severely hypoplastic, with a disorganised two-dimensional TEC compartment consisting of $K8^+K5^+$ TECs only. Similar results were observed in adult hCD3εtg26 mice (which overexpress a human CD3ε transgene), where T cell development was arrested at the $CD4^-CD8^-CD44^+CD25^-$, or DN1, immature stage (Klug et al., 2002, Wang et al., 1994). Further observations in CD3εtg26 mice showed that functional thymic epithelial differentiation could proceed in the absence of developing thymocytes until at least E15 (Jenkinson et al., 2005). Taken together, these data indicate that TEC development proceeds independently of thymocyte-derived signals until E15 - coinciding with the appearance of $CD25^+$ immature thymocytes.

Observations using a range of transgenic mice have, however, illuminated the roles of different thymocyte developmental stages in regulating a number of subsequent steps in the differentiation, maturation and maintenance of various TEC types. The transplantation of $RAG^{-/-}$ bone marrow into CD3εtg26 neonatal mice restores cortical

but not medullary development, with transplantation of WT BM leading to full restoration of the medulla also (Hollander et al., 1995, van Ewijk et al., 2000). It has subsequently been shown that, in E15 CD3εtg26 mice, cTECs cannot progress further than the immature $CD205^{+}CD40^{-}$MHC class II^{-} stage; $RAG^{-/-}$ mice, however, allow the appearance of $CD205^{+}CD40^{+}$MHC class II^{+} cTEC, demonstrating that thymocytes blocked in DN3 but not in DN1 are sufficient at this stage for normal cortex development (Shakib et al., 2009).

In medullary development, a defective phenotype lacking discrete medullary areas is observed in mice lacking TCR genes (TCRα null mouse, or the $TCR^{-/-}$ severe combined immunodeficiency (SCID) mouse) (Palmer et al., 1993, Shores et al., 1991). However, this can be rescued following addition of TCR^{+} haematopoietic cells to SCID mice (Shores et al., 1991). In further BM-reconstitution work using SCID mice, medullary foci ($MTS10^{+}$) were seen to develop in parallel with $CD4^{+}CD8^{-}$ thymocytes (Penit et al., 1996). Expansion of these initially small medullary islands at E18.5 and their maturation and maintenance is strongly correlated with the appearance of mature SP thymocytes (Irla et al., 2008). In addition, when RFTOC from E16.5 fetal thymi were grafted into $RAG2^{-/-}$/MHC class $II^{-/-}$ mice, normal thymus architecture was obtained, indicating the sufficiency of host-derived $CD3^{-}CD4^{-}CD8^{-}$ TN immature thymocytes to drive medullary formation (Rodewald et al., 2001). Further analysis of lympho-epithelial crosstalk in the medulla has revealed that initial induction of $CD80^{-}Aire^{-}$ mTECs to produce $CD80^{+}Aire^{+}$ cells may be mediated by RANK signalling from $CD4^{+}CD3^{-}$ lymphoid tissue inducer cells (Rossi et al., 2007b).

One means through which lympho-epithelial crosstalk is mediated is that of lymphotoxin β receptor (LTβR, a member of the TNF receptor family) signalling (Boehm et al., 2003). In $LT\beta R^{-/-}$ mice or aly/aly mice (which posses a mutant nuclear factor-κB-inducing kinase (Nik) that acts downstream of LTβR), components of this pathway are removed - leading to aberrant, disorganised medullary morphology. A similar pattern is acquired when LTβR ligands are blocked from interacting with their receptor following injection of WT mice with soluble LTβR (Boehm et al., 2003). Transplantation of WT BM into these

transgenic mice failed to restore normal medullary architecture, mapping the defect in signalling to the epithelial compartment. Numbers of mTEC in these altered thymi were significantly reduced when compared to WT, and accompanied by a proportional increase in $CD4^+$ and $CD8^+$ SP thymocytes (Boehm et al., 2003). Additional studies investigating other components of the lymphotoxin pathway such as RelB or NF-κB have observed decreased TRA expression in the medulla and autoimmune phenotypes (Fletcher et al., 2009, Gray et al., 2006, Seach et al., 2008, Valero et al., 2002). Together, these data show that LTβR signalling is critical for normal medullary differentiation and function.

1.2.4. Thymic epithelial lineage

1.2.4.1. Identification of thymic epithelial progenitors

Evidence suggests that epithelial cells are already specified to the thymus lineage prior to formation of the thymic rudiment, due to the ability of isolated and transplanted pharyngeal pouch endoderm to develop into a thymus, both in mammals and birds, as mentioned earlier (Gordon et al., 2004, Le Douarin and Jotereau, 1973). Various studies have investigated the nature and identity of the epithelial progenitors involved in the development of the thymus from this early stage through ontogeny.

The existence of a bipotent thymic epithelial cell (TEPC) was initially proposed on the basis of the existence of TEC expressing cTEC and mTEC markers. The markers 4F1 and IVC4, markers of cortex and medulla respectively, are co-expressed in E10.5 third pouch endoderm (Kanariou et al., 1989). Furthermore, *in vitro* culture of harvested embryonic TECs has shown consistent, small populations of cells expressing both cTEC and mTEC markers; however, these are not followed up by functional studies (Cirne-Lima et al., 1993, Ropke et al., 1995). Observations from thymic epithelial tumours (both in the mouse and the human) also lent some support to the common TEPC hypothesis, as many contain cells that predominantly co-express markers of cortical and medullary TECs in addition to containing differentiated subpopulations of each (Schluep et al., 1988, Von Gaudecker et al., 1997).

Subsequently, a rare population of $K5^+K8^+$ cells were observed in WT adult thymus (Klug et al., 1998). All TEC were $K5^+K8^+$ in the hypoplastic thymus of newborn hCD3εtg26 mice, but were able to give rise to $K5^-K8^+$ cTEC upon ectopic transplantation into $RAG^{-/-}$ mice, identifying $K5^+K8^+$ cells as a potential progenitor population, at least for cTEC (Klug et al., 1998). It was speculated that, since they co-expressed markers for the predominantly single-positive $K5^+K8^-$ mTEC and $K5^-K8^+$ cTEC compartments seen in the mature organ, $K5^+K8^+$ TECs may represent an unrestricted bipotent progenitor (Klug et al., 1998).

In the *nude* thymus rudiment, developmentally arrested TECs in a seemingly undifferentiated, progenitor state were found to stain with the monoclonal antibodies MTS20 and MTS24 (Blackburn et al., 1996). It was proposed, and subsequently shown, that these antibodies (both of which have recently been shown to recognise the same antigen – Plet-1 (Depreter et al., 2008)) identify a population of progenitor cells in the WT fetal thymus. This TEPC population is sufficient to form a fully functional thymus upon ectopic transplantation (Bennett et al., 2002, Gill et al., 2002). In the two studies that demonstrated this, dissociated $Plet1^+$ cells from either E12.5 or E15.5 thymus were isolated by flow cytometric sorting, reaggregated *in vitro*, and grafted under the kidney capsule of *nude* or congenic recipient mice respectively (Bennett et al., 2002, Gill et al., 2002). These were able to generate a functional thymus displaying normal cortical and medullary architecture and, as demonstrated in the immuno-compromised *nude* mouse transplants, support development of a full complement of T cells, both in the periphery and the thymus itself (Bennett et al., 2002). In both these studies, reaggregates made using comparable numbers of $Plet1^-$ cells were unable to reconstitute a functional thymus when subjected to identical transplantations in these studies (Bennett et al., 2002, Gill et al., 2002). Unfortunately, neither of these studies confirmed the epithelial percentage of their sorted $Plet1^-$ 'TEC' populations by using a definitive epithelial marker. Indeed, it is now realised that the majority of the sorted $Plet1^-$ cells used in the E12.5 grafting study were mesenchymal. Importantly, however, grafted $Plet1^+$ cells showed improved ability to generate functional thymus over dissociated and reaggregated whole thymus (Bennett et al., 2002). In the E15.5 study, 'TECs' were

selected on the basis of MHC class II expression, which would exclude mesenchymal cells but also a proportion of TECs (Gill et al., 2002).

Differences in the expression of certain markers suggest a phenotypic progression of the Plet1$^+$ population between E12.5 and E15.5. Lack of MHC class II expression and co-expression of K5 and K8 in TEPCs at E12.5 suggests an undifferentiated, unrestricted progenitor cell type (Bennett et al., 2002). By E15.5, most Plet1$^+$ cells are MHC class II$^+$, and co-express K5 and K8 more rarely, indicating a more mature TEPC population (Gill et al., 2002). Also at E15.5, a small subset (~5%) expressing UEA-1– a marker of a distinct mature mTEC group – is identifiable, suggesting a lineage restriction or change in potency in at least part of the TEPC population (Gill et al., 2002).

1.2.4.2. Does a common TEPC exist?

Although the above studies demonstrated the existence of a pool of thymic epithelial progenitors, it is not yet clear to what extent during fetal development these represent a homogenous population retaining the capacity to each generate cortex and medulla, or whether a mixed population is present with pre-restricted potential for cTEC and mTEC (Figure 1.4). The studies above were performed at population level, showing the potential of a group of cells, rather than at the clonal level where the potential of a single cell is examined, and co-expression of common markers cannot alone be used as evidence to support the existence of a common TEPC.

Evidence pointing toward divergence to a lineage specific progenitor, at least in the medulla, has been shown in studies using MHC-mismatched blastocyst/embryonic stem (ES) cell chimeras (Rodewald et al., 2001). At two weeks postnatally, it was observed that MTS10$^+$ medullary areas arose consisting of one or more 'clonal' islets - exhibiting either blastocyst or ES cell, but not mixed, origin. The identity of surrounding cortex was shown not to correlate with the origin of these medullary islets (Rodewald et al., 2001). The nature of fetal medullary development was also investigated, with similar results. E16.5 thymus lobes from MHC-mismatched mouse embryos were dissociated, CD45$^+$ haematopoietic cells were removed by flow cytometry and the remainder reaggregated. In contrast to reaggregated fetal thymic

organ culture (RFTOC) allowed to develop *in vitro*, grafted RFTOCs demonstrated organised medullary areas. Once again, these occurred as islets of uniform MHC class II identity, implying the ability of some E16.5 TECs to function as medullary progenitors (Rodewald et al., 2001). These experiments appear to demonstrate that, from at least E16.5, a population of medullary thymic epithelial progenitors (mTEPCs) exists with the ability to locally expand and generate areas of $MTS10^+$ medullary epithelium. However, these data do not rule out the continued existence of a common TEPC, and furthermore do not address mechanisms of generation of cortex, or of maintenance of cortex or medulla postnatally.

Recent work has shown that a discrete subset of fetal progenitor cells gives rise to Aire-expressing mTECs. These progenitors were identified as claudin (cld) $3,4^{hi}$ $UEA\text{-}1^+$ in E13.5 thymus (Hamazaki et al., 2007). Initially located at the apical layer of the E10.5 bilayered thymic rudiment, $Cld3,4^{hi}$ cells form a predominantly $MTS10^+$ central cluster by E12.5. By E13.5, expression of Cld3,4 occurs in small clusters throughout the thymus; and it is within a subpopulation of these cells that UEA-1 is first expressed. At later fetal stages, $Cld3,4^+MTS10^+$ clusters were surrounded by $CLd3,4^-MTS10^+$ TECs; and by the newborn stage, $Cld3,4^+$ TECs were $MTS10^-$, and were scattered throughout the medulla (Hamazaki et al., 2007). Reaggregation and grafting of E13.5 $Cld3,4^{hi}$ TECs has revealed a medullary-only potential, with those also expressing UEA-1 showing an ability to give rise to $Aire^+$ TECs. In contrast, the $Cld3,4^{lo}UEA\text{-}1^-$ TEC population showed bi-potential ability for cortex and for medulla, some of which were also $Aire^+$ (Hamazaki et al., 2007). It has been shown, from BrdU incorporation studies, that $Aire^+$ mTECs (mostly $K14^+K8^+$) are a post-mitotic population in the steady-state adult thymus, with a high rate of turnover (Gray et al., 2007a). Expression of p63 (required in maintaining a high proliferative potential in epithelial cells of both epidermis and thymus) and Aire have been found to be mutually exclusive in mTECs (Candi et al., 2007, Dooley et al., 2008, Senoo et al., 2007). This evidence, in conjunction with the appearance *ex vivo* of MHC class II^{hi} $Aire^+$ cells from isolated MHC class II^{lo} $Aire^-$ mTECs suggest a precursor/product relationship (Gray et al., 2007a).

A very recent study suggests that thymic cortex develop in a stepwise fashion, with a proliferating $CD205^{+}CD40^{-}$MHC class II^{-} population producing non-proliferating, $CD205^{+}CD40^{+}$MHC class II^{+} fully differentiated cells. CD205 expression was detected as early as E12, with CD40 expression acquired at around E14-15 (Shakib et al., 2009).

Whilst the work in this thesis was in progress, two studies were published that have used lineage-tracing analysis to address the question of whether a common thymic progenitor exists. The first of these examined the potential of TEPCs from embryonic thymus (Rossi et al., 2006). E12.5 thymus lobes from mice constitutively expressing yellow fluorescent protein (eYFP) were dissociated, and TECs were isolated by flow cytometric sorting on the basis of EpCAM (a pan-epithelial marker in fetal thymus) expression. Cells from this $EpCAM^{+}$, $eYFP^{+}$ population were shown to be predominantly $Plet1^{+}$. Single $eYFP^{+}$ cells were then microinjected into E12.5 thymus primordia removed from wild-type mice, and subsequently allowed to develop for 4 weeks following kidney capsule transplantation. Of 13 transplants, 4 were recovered that showed surviving $eYFP^{+}$ cells. Each of these displayed $eYFP^{+}$ mTEC ($MTS10^{+}K5^{+}$) and $eYFP^{+}$ cTEC ($Ly51^{+}K18^{+}$) (Rossi et al., 2006). This would appear to be the best evidence yet for the existence of a bipotent TEPC at E12.5, however attempts in our lab to repeat this have been unsuccessful and have only produced $eYFP^{+}$ cTECs (A. Farley, unpublished).

The second of these recent works used non-invasive lineage tracing to follow the fate of genetically marked TECs (Bleul et al., 2006). As a cellular marker, a mouse harbouring a silent eYFP gene under the control of the ubiquitous ROSA26 locus (*Rosa26R-eYFP*) was used. To achieve Cre-mediated deletion and eYFP expression, the *Rosa26R-eYFP* line was mated with *hK14::Cre-ERT2* mice. The latter enables the production of Cre-recombinase, by tamoxifen induction, in cells expressing the human keratin 14 (hK14) promoter. However, in these experiments the 'leaky' nature of Cre-ERT2 was exploited to generate a very low level of non-induced expression. Therefore, in rare cells in the neonatal thymus, eYFP was activated as a heritable marker (Bleul et al., 2006). In 58 thymus lobes taken 14 days postnatally (P14) from 29 pups, 21 clusters of $eYFP^{+}$ cells were observed. Of these, 1 was

cortex-only, 4 were medulla-only, and 16 were comprised of mTECs and cTECs spanning the CMJ. 9 singly occurring cTECs were also found. 10 newborn mice (P0) displayed no $eYFP^+$ cells, indicating that the majority of these seen in P14 mice originated in postnatal TEPC (Bleul et al., 2006). These data strongly suggest that in the postnatal thymus, active progenitor cells with bi-potent and medulla-only ability are present. It is not known, however, whether the mTEC- or cTEC-only clusters seen occurred downstream of the common TEPC, or whether they derive from a separate cell type. The sample-size of this analysis was small, and since the activity of the hK14 promoter has not been fully characterised in developing thymus and third-pouch endoderm, it is impossible to say whether recombination could have occurred in all TECs.

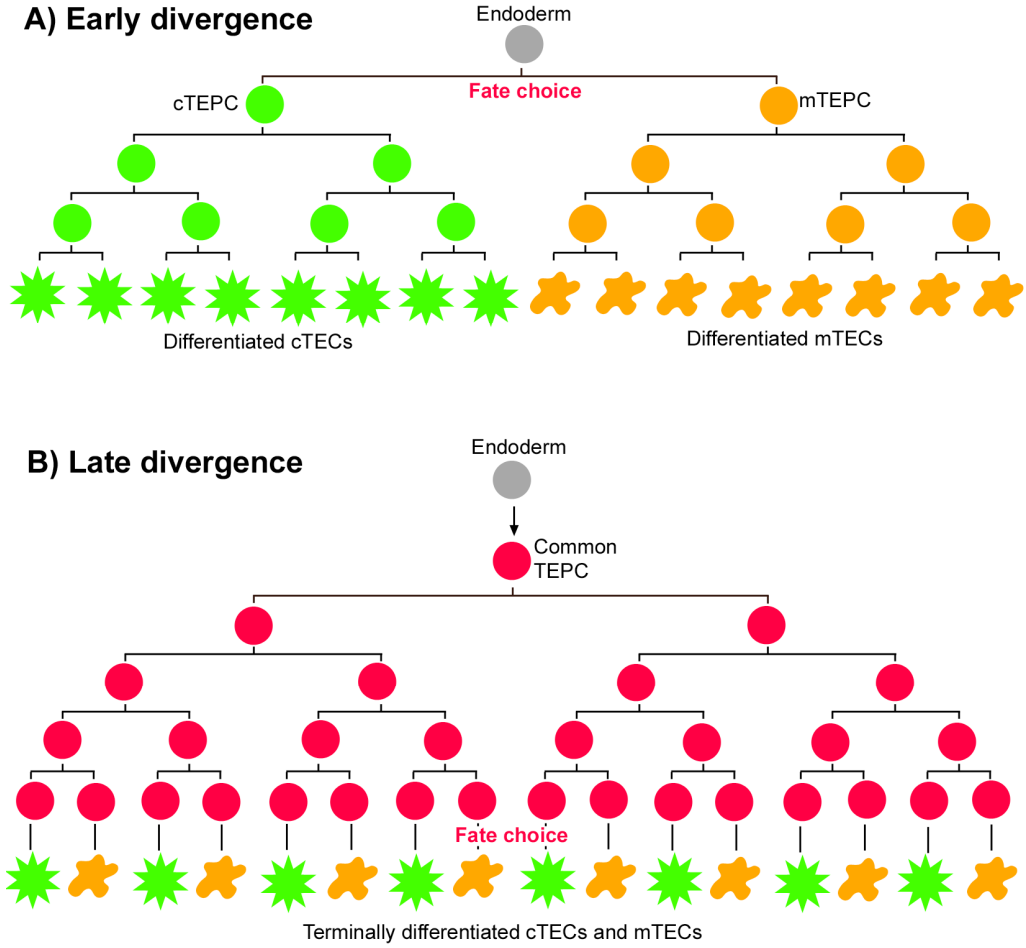

Figure 1.4 Models of thymus cortical and medullary lineage divergence

Two prospective modes of TEC lineage divergence are shown. At one extreme (**A**), thymic epithelial progenitor cell (TEPC) diverge shortly after thymic identity is assigned to cells in the early endoderm, into separate medullary (mTEPC) and cortical (cTEPC) lineages. At the other extreme (**B**), a population of common TEPCs is maintained until shortly before terminal differentiation. A likely scenario would be somewhere in between these two models - a common progenitor persists from thymus specification in the early endoderm through to early organogenesis, and subsequently gives rise to distinct mTEC and cTEC lineages.

1.3. Thymic involution and regeneration

The process of thymic involution, or atrophy, is a consequence of an ageing immune system, where profound changes in thymus anatomy lead to a progressive reduction in its size. This is due to loss of epithelial cells, and an accompanying decrease in thymopoiesis – the thymus of a 24-month-old mouse contains less than 1% of the number of thymocytes found in the newborn thymus (Taub and Longo, 2005). The aged thymus is, however, able to continue T-cell differentiation, but at a heavily reduced capacity (Sempowski et al., 2002). Thymic involution involves an organisational collapse of the cortical epithelium, loss of a distinct cortico-medullary junction, and a decline in the number and proportion of mTECs (Sutherland et al., 2005, Gray et al., 2006). This is accompanied by an increase in adipose tissue within the thymus, even though the overall size of the organ reduces (Taub and Longo, 2005). The mechanisms responsible for age-related thymic involution are poorly understood, although several reasons have been hypothesised, including: a decline in HP cells migrating into the thymus from the bone marrow; loss of certain thymic stromal cells; changes in levels of cytokines, hormones or growth factors; or alterations in productive TCR rearrangement (Taub and Longo, 2005).

It has been seen that regeneration of both structure and function can occur in the aged (18-24 month old) thymus of mice following ablation of sex steroids, either by castration or by chemical means (Gray et al., 2006, Sutherland et al., 2005). An increase in firstly MHC class II^{hi} mTECs followed by MHC class II^{lo} mTECs is observed in response to castration (Gray et al., 2006).

A recent study has demonstrated the ability of a single cell to give rise to a functional thymic microenvironment postnatally (Bleul et al., 2006). Here, a Cre-mediated re-activateable Foxn1 null allele was created (*Foxn1*^{SA2}); exhibiting a hypoplastic thymus comprised of developmentally arrested TECs (see section 1.2.2.6). This was paired with the *hK14*::Cre-ERT2 allele which, as described earlier in section 1.2.4.1, can express Cre-recombinase in epithelial cells. This strain causes a low level of deletion in the absence of tamoxifen induction of Cre. In some resultant *Foxn1*^{SA2}/*Foxn1*^{SA2}; *hK14*::Cre-ERT2 mice, single infrequent TECs were shown to

spontaneously regain Foxn1 expression and give rise to a functional thymic microenvironment with distinct cortical and medullary areas (Bleul et al., 2006). However, these cells cannot be equated with WT postnatal/adult TECs, due to the abnormal thymus development in these transgenic mice. Nor can it be conclusively proved that the TECs reactivated here in the *Foxn1*^{SA2} thymus are equivalent to those found in the embryo, prior to developmental arrest resulting from Foxn1 absence.

It may be that a thymic stem cell population, persisting even after thymic involution, occurs. A comparatively high proportion of Plet1^{+} TECs are observed in aged mice - this is seen to decrease as the number of TECs in the thymus grows following sex steroid ablation (Sutherland et al., 2005). However, these have not been functionally studied and it may be that thymic regeneration occurs via replication of differentiated cells (as has been observed in the pancreas (Dor et al., 2004)).

Confirmation and identification of a postnatal thymic stem cell population would be of great interest to medical science. If it proved possible to (re)activate these cells, either *in vivo* or after isolation, it may lead to the ability to regenerate a fully functional thymus. This would be of particular use to immuno-compromised individuals (such as the elderly, AIDS patients, or those on immunosuppressant medication) where the functional T cell repertoire would be reduced.

1.4. Aims

The primary aim of this project was to address the debate on the point of divergence of the cortical and medullary epithelial lineages, and to assess the longevity and contribution of a putative bipotent TEPC, as discussed in section 1.2.4.2. To answer these questions, various methods of developmental analysis were considered.

1.4.1. Methods of developmental analysis

A key area of study involves resolving the origins of given tissues with regard to the position and phenotype of the progenitor cells from which they are derived. Conversely, the developmental potential, proliferative capacity, and migrational abilities of an identified group of cells are also of interest. A variety of methods exist by which answers to these questions can be found experimentally.

To answer questions involving the potential of a particular area in the early embryo, such as the neural crest, somites, or central nervous system, chick/quail chimera experiments have proved successful. Sections of quail tissue can be surgically removed, grafted into the corresponding location in a chick embryo, and allowed to develop. The position of quail-derived cells can then be ascertained due to differences in staining properties in the nuclei when compared to chick cells (Le Douarin, 1974). This method has several drawbacks, however, with issues of concern including effects of wound healing following surgical intervention, and inter-species differences.

Fluorescent dyes have also been widely used to identify the contribution of different regions of cells, with a variety of applications. In the most basic approach, dye can be spotted onto a particular area of cells, whose progress during development can be followed. This method has been previously employed in thymus studies, to determine that labelled pharyngeal ectoderm did not contribute cells to the formation of thymic cortex (Gordon et al., 2004). Dye-labelling has a number of limitations. Firstly, the required embryo manipulation may disturb normal development. This particularly applies to mammals, as embryos usually must be subsequently cultured ex utero, limited to 48h or less after E6 in the mouse (Petit et al., 2005). Another

limitation of the dye-labelling method is the effect of dilution, resulting in decreased detection of labelled cells after only a small number of cell divisions.

If the population of cells being studied exhibits expression of a known unique gene, then the Cre/LoxP recombination technique can be used. A tissue-specific promoter can drive Cre recombinase production, initiating permanent heritable expression of a reporter gene such as GFP or LacZ via genetic recombination (Sauer, 1998). This method has been widely used in a variety of tissues, but has the difficulty of requiring transgenic animals to be generated. Another issue is that an identified gene expressed under a defined promoter region, and restricted to the tissue of study, is needed. Such candidates are known at the appropriate stage of development in many tissues. It is possible to temporally regulate Cre expression if the promoter of choice is expressed in different tissues at different times, enabling the investigator to have some control as to both where and when any genetic recombination occurs (Danielian et al., 1998). The Cre/LoxP system has the advantage of not requiring surgical intervention or embryo manipulation.

To unambiguously determine the properties and fate choices of individual cells within populations labelled using any of the above methods, analysis at clonal resolution is required, i.e. labelling or functional testing of a single cell. Clonal progeny can be tracked either by the injection of cellular markers, such as dye, or by genetic modification to induce expression of a reporter gene in the descendants of that cell. These methods of labelling, where the experimenter selects the initial cell, are known as prospective clonal analysis. Aside from the drawbacks of ex utero embryo manipulation mentioned above, prospective clonal analysis has the limitation of not being objective. Since the investigator selects the initial labelled cell, there is the distinct possibility that not all cells within the population being investigated will be labelled. Even if the experiment is carried out many times, certain cells may never undergo labelling due to small size, awkward position or human error.

To overcome these caveats, retrospective clonal analysis can be undertaken. This involves any single cell within the embryo or tissue being genetically labelled at random. The label is passed on to all clonal progeny from this cell, to be observed at a later stage in development. One technique uses recombinant retroviruses (RRV) to

infect embryonic cells, introducing a reporter gene that randomly integrates into the host genome (Cepko et al., 1998, Sanes et al., 1986). Due to this random integration, only a tiny number of infected cells are able to express the reporter gene – an ability that is stably transmitted to their descendants. The RRV lacks the proper machinery to enable formation of new viruses, hence does not posses the ability to cause secondary infection. This means the investigator has temporal control over any initial labelling events, for example with the timing of the intra-uterine injection of the RRV in the mouse. There is, however, potential for this injection to damage embryos. Problems involving non-uniform accessibility of all cells to the RRV, combined with an inability to infect cells that are not currently replicating, do not make this an ideal technique.

Retrospective clonal analysis can also be performed using the *laacZ* system, as described below.

1.4.2. The laacZ system

The *laacZ* system is based on expression of the *lacZ* gene from *Escherichia coli*, which encodes the β-galactosidase enzyme. Cells expressing *lacZ* can be identified histologically by addition of X-gal substrate, resulting in generation of an intracellular blue precipitate (Figure 1.5). In the *laacZ* system, this gene has been modified by duplicating an internal section of the coding sequence, resulting in the appearance of premature stop codons as shown in Figure 1.5. *LaacZ* produces a non-functional, truncated version of β-galactosidase (Bonnerot and Nicolas, 1993).

However, the ability to generate functional β-galactosidase can be regained. The DNA double stranded break repair mechanism in cells can result in intragenic homologous recombination. If a double stranded break occurs within the DNA of the duplicated region of *laacZ*, the correct open reading frame required for functional, full-length β-galactosidase production can be re-established. This recombined sequence is subsequently inherited by all descendants of the cell in which it occurred, enabling them to be traced retrospectively (Figure 1.6).

The spontaneous recombination of *laacZ* is an extremely rare event, with a constant rate of occurrence, and proportional to the size of the duplication. Ideally this will

result in a frequency where, if any $LacZ^+$ cells are observed, they can be reasonably assumed to be clonal, i.e. to originate from a single recombination event.

LaacZ retrospective clonal analysis has been successfully employed to study the development of a number of tissues, usually in combination with tissue-specific promoters. Hence, although *laacZ* recombination can happen elsewhere in the embryo, β-galactosidase expression and therefore clone visualisation occurs only in the tissue of interest. Such studies have taken place in myotome, under control of the promoter of the α subunit of the acetylcholine receptor (αAChR) (Nicolas et al., 1996), the central nervous system using a neuron-specific enolase (NSE) promoter (Mathis et al., 1997), and myocardium with the α-cardiac actin promoter (Meilhac et al., 2003). A mouse model where *laacZ* is under the control of the ROSA26 promoter has also been engineered (Tzouanacou et al., 2009). ROSA26 is constitutively expressed, therefore giving the potential for clones to be detected in any possible cell lineage during development (Friedrich and Soriano, 1991, Zambrowicz et al., 1997, Soriano, 1999). The *laacZ* gene used in these systems is preceded by a nuclear localisation sequence (NLS), allowing specific labelling of the nucleus and making resolution of individual cells easier.

Information regarding phases of cell growth can be deduced upon examination of the arrangement of cells in a clone (Figure 1.7). For example, a clone where all cells are grouped in a tight cluster points to a coherent mode of growth, whereas cells that are widely separated would indicate a phase of dispersive growth. Sometimes observation of larger clones may point to more than one distinct growth phase; for example a clone with several separated clusters could mark an initial dispersive growth phase involving older progenitors, followed by a more recent coherent growth phase. This has been observed previously, for example in myocardial cells of the embryonic mouse heart (Meilhac et al., 2003). Data on orientation of clones can reveal other characteristics of cell growth, for example isotropic growth versus orientated growth along/perpendicular to an axis.

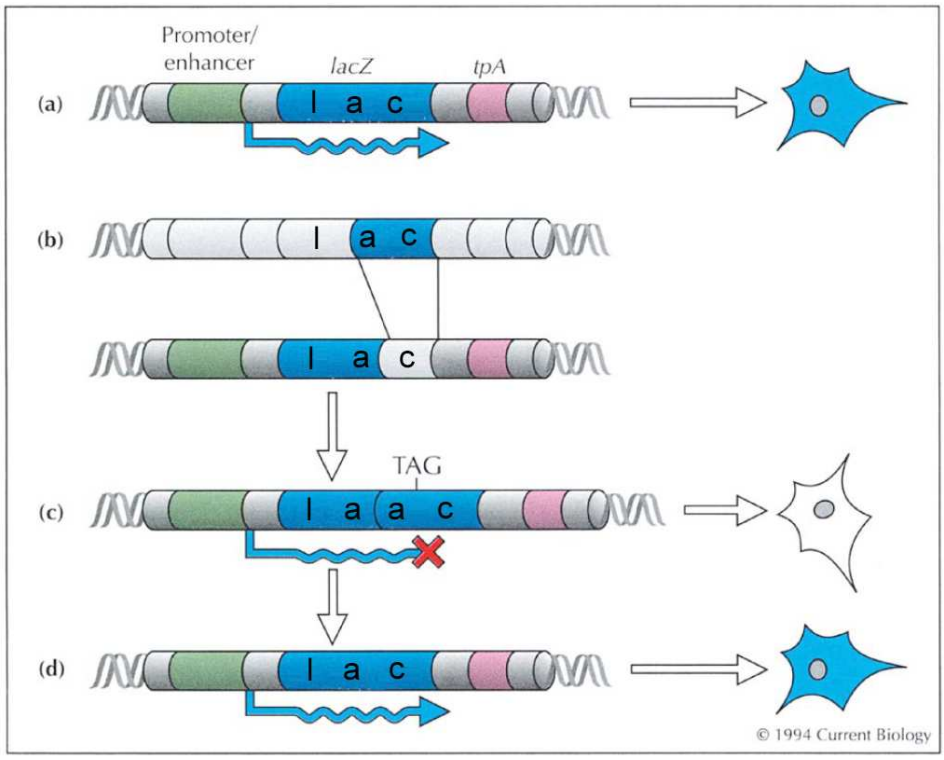

Figure 1.5 Generation and operation of the *laacZ* gene

The *lacZ* gene expresses β-galactosidase, reacting with X-gal substrate to produce a blue colour within the cell (**A**). To create the *laacZ* gene, a duplication of part of the open reading frame was created (**B**). This results in a premature stop codon, and a truncated, non-functional version of β-galactosidase that cannot process X-gal (**C**). A rare homologous recombination event can excise the duplicated segment, restoring functional activity of lacZ (**D**). (Picture from Sanes, 1994).

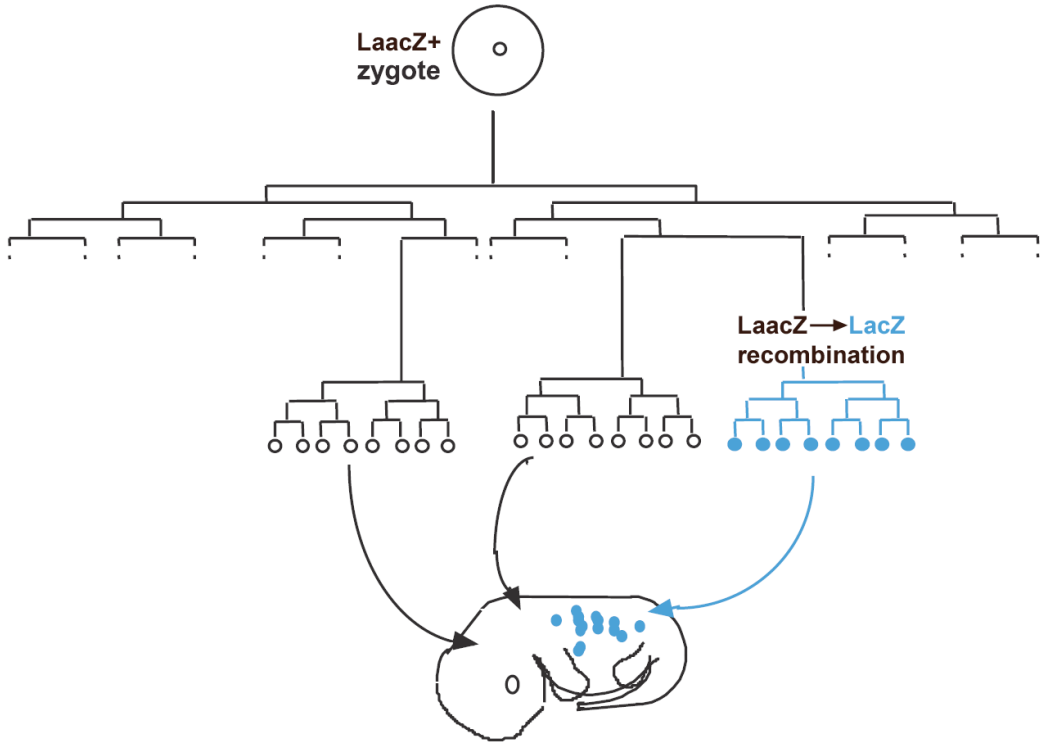

Figure 1.6 Inheritance in the *laacZ* labelling system

All cells in all lineages harbour the silent *laacZ* reporter gene. Spontaneous homologous recombination can occur at any stage during development, with those occurring earlier in development having the potential to label a larger population (long clone) than those occurring later (short clone). Upon examination of the embryo, histological staining determines the size and location of the clone, enabling information on lineage to be deduced. (Picture modified from Petit et al., 2005).

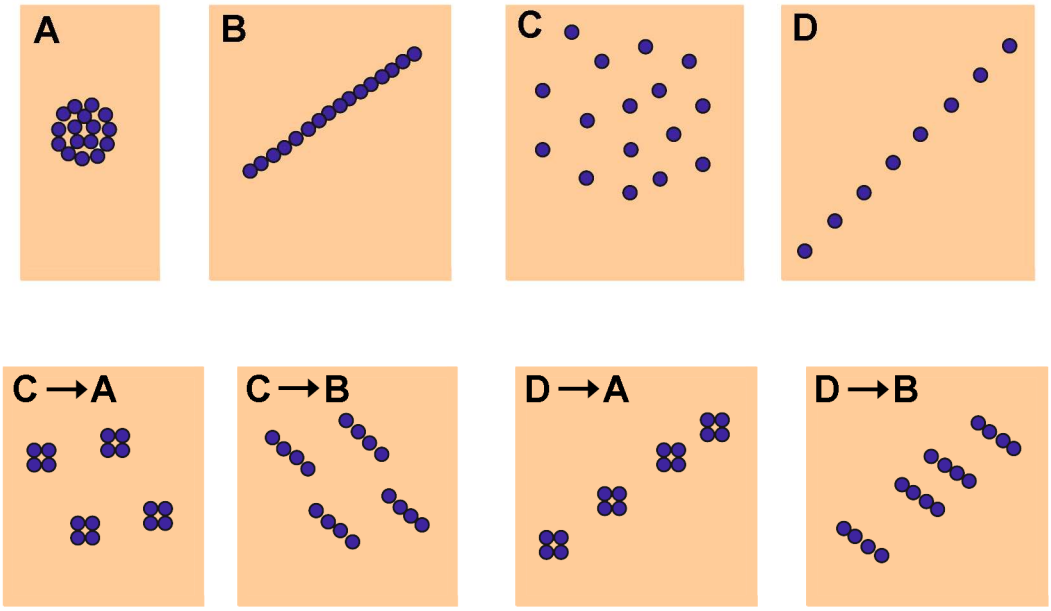

Figure 1.7 Clonal modes of growth

The growth of a structure generally combines several growth behaviours (clonal modes). Top line: Elementary clonal modes. **A**) Isotropic-coherent growth. **B**) Oriented-coherent growth. **C**) Isotropic-dispersive growth. **D**) Oriented-dispersive growth. Bottom line: Examples of growth patterns where different clonal modes occur in succession. Adapted from Petit et al, 2005.

1.4.3. Project strategy

In this project, it was decided to use *laacZ* retrospective clonal analysis to gain information on fate decision, during thymic epithelial lineage development. As stated above, *laacZ-lacZ* recombination, and thus clone generation, occurs at a known frequency. Two variants of the *laacZ* gene have been constructed, containing different intragenic duplication sizes and therefore different recombination frequencies. Ideally, the *laacZ* system should be optimised such that there is a low likelihood of multiple clones occurring in a single tissue sample and thus confusing cellular relationships. This likelihood can be calculated if the number of cells in the tissue of study is known, along with the *laacZ* recombination frequency.

Thus, determination of TEC numbers throughout ontogeny would enable calculation of the number of TEC clones likely to occur in a single thymus lobe, enabling me to choose an appropriate combination of *laacZ* duplication size and thymic developmental stage.

In Chapter Three, therefore, I determined the size of the TEC (lin^-EpCAM^+) population from E12.5 until E17.5. Due to the lack of quantitative data on all thymic cell populations, I also determined the absolute number of haematopoietic ($CD45^+$), mesenchymal ($lin^-PDGFR\alpha^+$ and/or $lin^-PDGFR\beta^+$) and endothelial (lin^-CD31^+) cells present.

In Chapter Four, I went on to examine the TEC population in more detail, focussing on the developmental kinetics of the $Plet1^+$ population. I determined the absolute number of $Plet1^+$ TECs from E12.5 to E17.5, and examine modes of proliferation in these cells. From these collective data, I proposed a model for the role of the $Plet1^+$ population in thymus development.

In Chapter Five, I outline strategies to analyse and interpret the library of prospective TEC clones. I calculated the number of TEC $lacZ^+$ clones expected to be present throughout thymus ontogeny for each *laacZ* mouse genotype, selecting an appropriate developmental stage/duplication size combination for analysis. I attempted to compile a library of thymus epithelial clones, from an extensive analysis of fetal thymic lobes. However, although I observed several clones of apparent

mesenchymal origin, supporting a single origin for intrathymic and capsular mesenchyme at E15.5, I observed no TEC clones. I describe my extensive attempts to optimise the sensitivity of detection of *lacZ*$^{+}$ cells, and conclude that the *ROSA26laacZ* system is unsuited to clonal analysis of the thymic epithelium, at least in the stages of development under examination. The CpG content of the ROSA26 promoter suggests a possibility of methylation-induced silencing brought about by *de novo* methylation of the *lacZ* reporter gene.

Chapter 2. Materials and Methods

2.1. Materials and solutions

Unless stated otherwise, all materials used in this thesis were obtained from Sigma, Invitrogen, Gibco or BDH.

Thymus dissociation mixture:

1.4 mg/ml hyaluronidase

0.7 mg/ml collagenase

0.05 mg/ml deoxyribonuclease I

Made up in PBS

FACS wash (100 ml):

5 ml foetal calf serum

95 ml PBS

1xDPBS (1 L):

0.2 g KCl

0.2 g KH_2PO_4

8.0 g NaCl

2.16 g $Na_2HPO_4 \bullet 7H_2O$ (pH 7.2 - 7.4)

X-gal-wash:

0.1 M phosphate buffer (pH 7.3)

2 mM $MgCl_2$

0.1% sodium desoxycholate

0.02% NP-40

0.05% BSA

X-gal-stain:

Made up in X-gal wash mixed with:

0.024% spermidine

5 mM $K_3FE(CN)_6$

5 mM $K_4FE(CN)_6$

0.0014% NaCl

2.5 mM X-gal

0.1% DMF

X-gal-fix:

0.1 M phosphate buffer (pH 7.3)

0.2% glutaraldehyde

2 mM $MgCl_2$

5 mM EGTA

2.2. Mice

Animals were housed within the Division of Biological Sciences Animal Facility at the University of Edinburgh under conditions outlined in the Animals (Scientific Procedures) Act 1986. Mice were housed in a stabilised environment with a 12-hour light/dark cycle and supplied with food and water *ad libitum*. Adult mice were sacrificed by the schedule 1 method of cervical dislocation.

2.2.1. Embryonic thymus collection

For timed matings, male and female mice were placed together overnight, and females were examined the following morning for the presence of a vaginal plug. This was taken as time point E0.5. Females were sacrificed at the desired stage of pregnancy, whereupon the uterine horns were removed and placed in PBS. Embryos were subsequently removed from the uterus and transferred to clean PBS, where they were sacrificed by decapitation. Thymus lobes were then removed from embryos and dissected of excess extrathymic tissue with the aid of a microscope.

In results Chapter Three, wild-type embryos were from crosses between males of the CBA strain and females of the C57BL/6 strain.

In results Chapter Five, all mice were kindly supplied by the lab of Val Wilson (Institute for Stem Cell Research, University of Edinburgh). *R26laacZ0.3* and *R26lacZ* mice were created by Elena Tzounacou at this location. *R26laacZ1.1* mice were also created by Elena Tzounacou, in the lab of Jean-François Nicolas (Pasteur Institute, Paris).

2.3. Flow cytometry

2.3.1. Cell Preparation

Embryonic thymus lobes were completely dissociated by incubation in dissociation mixture (DM) (see section 2.1) at 37°C, followed by 0.025% trypsin at37°C, for the minimum time required to produce a single cell suspension. Lobes in DM were gently pipetted up and down using a 1 ml tip every 5 minutes. E15.5 - E17.5 lobes were incubated for 15 minutes in DM, followed by 5 minutes in 0.025% trypsin. E13.5 & E14.5 lobes were incubated in DM for 10 mins in DM & 3 mins in trypsin. E12.5 lobes were incubated in DM for 10 mins and trypsin for 1 minute. Cells were pelleted by spinning at 1200rpm for 5 mins in a chilled (4ºC) benchtop centrifuge [Heraeus Labofuge 400R] and resuspended in FACS wash, before being counted using a haemacytometer.

2.3.2. Antibody staining

Cells in a suitable volume of FACS wash were incubated on ice with primary antibody for 20 min, in 5ml FACS tubes [Falcon]. Cells were washed in FACS wash and then incubated for 20 min with secondary antibody if required. Where intracellular antigens were analysed, cells were fixed and permeabilised using Fix and Perm kit [Caltag Laboratories] prior to incubation with antibodies. Following staining, cells were pelleted and resuspended in FACS wash, containing 1:25 7AAD [BD Bioscience] or 1:2000 ToPro3 [Molecular Probes] as viability markers if required. All antibodies used are detailed in Table 2.1.

2.3.3. Isotype controls

Isotype controls were used where stated. These are non-specific antibodies of the same class as the primary antibody used (e.g. IgM, IgG2a), and raised in the same species (e.g. rat, donkey), as listed in Table 2.1. Isotype controls correspond to whether a primary antibody/fluorophore direct conjugate, a biotinylated primary antibody, or an unlabelled primary antibody in combination with a fluorescently labelled secondary antibody were used. All isotype control antibodies were purchased from BD Pharmingen, apart from Rabbit IgG [Zymed].

2.3.4. Flow cytometric cell sorting and analysis

Cell sorting was performed on a MoFlo [Dakocytomation] into ice-cold FACS wash, using isotonic sheath fluid. Cell analysis data was acquired on a FACSCalibur [BD Bioscience] using CellQuest software [BD Bioscience]. Combinations of single-stained and fluorescence-minus-one (FMO) controls were used to set up cross-channel compensation. Downstream sample analysis was performed using FlowJo software [Treestar Inc]. Where isotype controls are used to set positive/negative fluorescence thresholds, gates are set to give 1% positive staining on isotypes.

2.4. Immunofluorescence

2.4.1. Frozen section preparation

Tissue was embedded in OCT compound [Tissue Tek, Miles Inc., USA], snap frozen on dry ice and stored at -80°C. Prior to sectioning, frozen tissue in OCT blocks was placed in the cryostat chamber [Leica CM1900] and allowed to equilibrate to -20°C for 30 mins. Sections were cut at 7µm and collected onto poly-L-lysine coated glass slides [VWR International]. Sections were air-dried at RT for 20 mins, fixed in 100% acetone at -20°C for 2 mins and air-dried for a further 20 mins. Slides were then stored at -80°C prior to use.

2.4.2. Cytospin Preparation

5-10,000 cells suspended in 100µl of PBS were loaded into a cytospin chamber including a poly-L-lysine coated glass slide [VWR International] and a filter card [Thermo]. Samples were centrifuged at 1,000rpm [Cytospin 3, Shandon] for 5 mins at RT. Slides were removed from the cytospin chamber and air-dried for 2 mins, then fixed in 100% acetone at -20°C for 2 mins. Following fixation, slides were air-dried for a further 2 mins and stored at -80°C prior to use.

2.4.3. Antibody staining of slides

Frozen, fixed samples on slides were allowed to air-dry for 5 mins. The area immediately surrounding each section was marked using a PAP pen [Daido Sangyo]. Slides were then rinsed briefly in PBS, prior to blocking for 15 mins with 5% serum in PBS. The species from which the serum was obtained was the same in which the

secondary antibody was raised, in order to minimise non-specific antibody binding. Slides were then incubated with primary antibody in PBS, for 1 hour at RT, followed by 3 x 5 minute washes in PBS containing 0.1% Tween 20 (PBST). This was followed by incubation with fluorophore-conjugated secondary antibody and DAPI, in PBS, for 30 mins at RT in the dark. A further 3 x 5 washes in PBST were performed, also in the dark, before rinsing with water and mounting in either glycerol/water or Vectashield Hardset mounting medium [Vector Labs]. To check for non-specific staining, isotype controls were used (see section 2.3.3). Sources and isotypes of antibodies used are detailed in Table 2.1.

2.4.4. Imaging

For immunofluorescence detection and image capture, slides were examined using a Leica AOBS confocal microscope under the excitation conditions appropriate to the fluorophores used. Images were subsequently processed with Adobe Photoshop CS.

Table 2.1 Antibody clones, isotype and source

Name	Source	Clone	Conjugate	Isotype
Primary antibodies				
anti-β-gal 1	Cortex Biochem	CR7001RP2	n	Rabbit IgG
anti-β-gal 2	Europa	1010702	n	Mouse
anti-β-gal 3	DSHB	40-1a	n	Mouse IgG1
anti-pancytokeratin	Dako	polyclonal anti-keratin	n	Rabbit IgG
anti-keratin 5	Covance Research Products	polyclonal anti-keratin 5	n	Rabbit IgG
anti-keratin 8	DSHB	Troma1	n	Rat IgG2a
anti-CD45	BD PharMingen	30-F11	n, FITC, APC, biot	Rat IgG2b
anti-TER119	BD PharMingen	TER119	n, FITC, APC, biot	Rat IgG2b
anti-EpCAM	DSHB	G8.8	n, biot*	Rat IgG2a
anti-PDGFRα	BD PharMingen	APA5	n	Rat IgG2a
anti-PDGFRβ	BD PharMingen	APB5	n, biot	Rat IgG2a
anti-CD31	BD PharMingen	MEC13.3	n, FITC	Rat IgG2a
anti-Plet1	From R.L. Boyd, Monash University Medical School, Australia	MTS20	n	Rat IgM
anti-Plet1	From R.L. Boyd, Monash University Medical School, Australia	MTS24	n	Rat IgG2a
anti-ERTR7	From W van Ewijk, University of Leiden	ERTR7	n	Rat IgG2a
UEA-1	Vector Labs	-	biot	Lectin
Secondary antibodies				
anti-Rat IgM	BD PharMingen	-	PE	-
anti-Rat IgG2a	BD PharMingen	-	FITC, APC	-
	Invitrogen	-	A488, A647	-
anti-Rat IgG2b	BD PharMingen	-	FITC, APC	-
	Invitrogen	-	A488, A647	-
Anti-Rabbit IgG	Invitrogen	-	A488, A647	-
Streptavadin	BD PharMingen	-	PE, APC, Cy5	-

List of primary and secondary antibodies used in this thesis, including source, isotype and clone identity (where relevant). 'Conjugated' column details fluorophores or other molecules used in antibody identification, abbreviations are as follows: n – non-conjugated; PE – phycoerythrin; FITC - fluorescein isothiocyanate; APC – allophycocyanin; Cy5 – cyanine 5; biot – biotinylated; A488 – Alexa Flour 488; A647 – Alexa Flour 647. * biotinylated using Molecular Probes FluoReporter kit.

2.5. S phase labelling with halogenated thymidine analogues

BrdU labelling was performed using a BrdU Flow Kit [BD Pharmingen]. Mice were given 100-200 µl intraperitoneal injections of 10 mg/ml BrdU in Dulbecco's phosphate buffered saline (DPBS) as supplied with this kit, or DPBS alone.

IdU and CldU labelling/staining protocols used were obtained from S. Tajbakhsh and P. Rocheteau, Pasteur Institute, Paris. IdU [MP Biomedicals] was made up to a concentration of 10 mg/ml (in 9 g/L NaCl, 0.2N NaOH) and i.p. injected into mice to give a 57.5 mg/kg dose. CldU [Sigma] was also made up to 10 mg/ml (in 9g/L NaCl), and injected to give a 42.5 mg/kg dose. Doses were calculated to take into account differences in molecular weight of the two analogues.

Following thymidine analogue pulses, mice were sacrificed and processed as described in sections 2.2 and 2.3. Antibodies used to detect IdU and CldU were mouse anti-BrdU [BD Pharmingen, 34780] and rat anti-BrdU [Accurate, OBT-0030], respectively.

2.6. X-gal staining

2.6.1. Pre-stain tissue fixation

The effects of three fixative solutions on X-gal staining were examined.

1) 10% formalin (a 1:10 dilution of 37% formaldehyde solution [Fisher Chemicals] in PBS).
2) 4% PFA (a 4% solution of paraformaldehyde in PBS, heated to 60^{o}C for 1 hour or until fully dissolved).
3) 'Old embryo fix' (OEF). The following were used to make 10ml of OEF: 250µl 37% formaldehyde solution [Fisher Chemicals], 80µl 25% glutaraldehyde [Sigma-Aldrich], 20µl 1M $MgCl_2$ [Fisher Chemicals], 200µl 250mM EGTA [Fisher Chemicals], 20µl 10% NP-40 [Fisher Bioreagents], 9.4ml PBS.

Following dissection and washing in PBS of tissue, fixatives were applied at 4^{o}C for varying lengths of time as detailed in results chapter.

2.6.2. X-gal staining of intact tissue

Fixed tissue was washed for 3 x 10 mins with X-gal-wash at RT before being stained with X-gal-stain in an incubator (for 48 h at 25°C ± 1°C, or as described in results chapter). It was washed again with PBS, in preparation for fixation (with X-gal-fix for 24 h at 4°C, or as detailed in results chapter). Tissue was now washed once with PBS.

2.6.3. Visualisation and recording of clones

X-gal stained tissue was cleared using serial concentrations of glycerol [Sigma-Aldrich] in PBS. Tissue was left in 30%, 50% and 80% glycerol respectively, for 24 hours in each at 4^oC. Tissue was stored in 80% glycerol at 4^oC.

Examination of stained tissue in 80% glycerol was performed under a light microscope. Any resultant β-gal$^+$ clones discovered were digitally photographed with a Zeiss Stemi SV11 microscope using Openlab v3.0 software [Improvision].

2.6.4. Tissue embedding for cryo-sectioning

Fresh or fixed tissue was embedded either in OCT compound as described in section 2.4.1, or in sucrose/gelatine.

For sucrose/gelatine embedding, pre-fixed tissue was incubated in 15% sucrose [BDH AnalaR] for 4 hours at 37^oC, as a cryo-protectant. Tissue was subsequently placed in a mould containing 15% sucrose/7% gelatine [BDH Biochemicals] for 3 hours at 37^oC. Tissue was then positioned in the orientation required for freezing and the mould was transferred to ice to allow the gelatine to set, followed by snap freezing in liquid nitrogen. Frozen blocks were stored at -80^oC prior to sectioning.

2.6.5. Sectioning of tissue

Tissues used in X-gal staining (either prior too or after sectioning) were cut at a thickness of 12-14µm on a cryostat [Leica CM1900], at -23^oC. These were thicker than normal cryosections (usually 6-7µm) - both in an attempt to show darker staining of β-gal$^+$ cells, and to reduce the number of sections that would have to be cut in order to section through a complete thymus lobe. Sections were placed on poly-L-lysine coated glass slides [VWR International], air-dried for 20 minutes and stored at -80^oC.

2.6.6. Alkaline treatment following X-gal incubation

For intact thymus lobes, X-gal staining solution was removed from staining receptacle by pipette and replaced with 1M Na_2CO_3. Lobes were incubated for 20 minutes at room temperature, before being washed in PBS for 10 minutes and embedded in OCT for freezing and sectioning.

Alkaline treatment was also performed on tissue sections stained by X-gal whilst on slides. X-gal was poured of slides, and 100µl of 1M Na_2CO_3 was immediately added to each tissue section. After 20 minutes at room temperature, Na_2CO_3 was poured off and slides were washed for 10 min in PBS. Slides were then mounted with glycerol/water and sealed with nail varnish.

Chapter 3. Results: Cellular composition of fetal thymus between E12.5 and E17.5

3.1. Introduction

Prior to undertaking retrospective clonal analysis, it was important to select a thymic developmental stage that could provide sufficient information on epithelial cell lineage divergence, without a high likelihood of multiple clones occurring within the epithelial compartment of a single thymus lobe. The developmental stages examined were at embryonic gestational day 12.5 (E12.5), E13.5, E14.5, E15.5, E16.5 and E17.5.

In order for the number of potential epithelial clones in a single lobe from an embryo of a given developmental stage to be calculated, the number of TECs present at that age needed to be ascertained. The number of somatic *laacZ* to *lacZ* recombination events expected could then be calculated within a population of a known size, since the expected recombination frequency of the *laacZ* allele is already known.

Due to the lack of quantitative data on the composition of the embryonic thymus, all other major cell types known to be present during thymus ontogeny were also analysed.

To do this, foetal thymic lobes were dissected from multiple litters of mice at the same embryonic stage, and pooled. Thymus lobes then underwent enzymatic dissociation into a single cell suspension, whereupon they were incubated with various monoclonal antibodies in order to identify specific intrathymic cell populations. Results were obtained using flow cytometry, which enabled the relative proportions of different cell types in the thymus to be found. These figures were then applied to the total number of cells per thymus lobe, to enable calculation of the actual number of each of the major cell types present in the thymus at these stages, and are detailed in this chapter.

Resultant calculations of clone frequency are detailed in Chapter 5.

3.2. Results

3.2.1. Total thymus cellularity

The total number of cells per thymus lobe was calculated for each time point. To do this, a known number of age-matched thymus lobes (from several litters of mice) were pooled and dissociated. The number of cells per ml in the resultant 1ml single-cell suspension was then counted using a haemocytometer. The total number of cells present in the sample was then divided by the number of thymus lobes used, giving the mean number of cells in 1 thymus lobe (Figure 3.1, Table 3.1). At E12.5, each lobe is comprised of $1.67x10^4 \pm 6.7x10^3$ cells, although this may be an overestimate due to the difficulty in cleanly separating the E12.5 thymus from surrounding tissue when dissecting. At E13.5, the thymus has a size of around $2.82x10^4 \pm 1.34x10^3$ cells, before undergoing a three-fold expansion to around $8.64x10^4 \pm 2.99x10^4$ at E14.5. Another three-fold increase in cell number to $2.36x10^5 \pm 9.26x10^4$ occurs between E14.5 and E15.5, whereupon the thymus continues to increase by a factor of 3.7 during the following 24 hours, giving a total cellularity at E16.5 of around $9.79x10^5 \pm 2.60x10^5$. At the final point of study, E17.5, the total number of cells per lobe was found to be $2.24x10^6 \pm 4.72x10^5$, 2.5 times the number of cells seen at E16.5.

The remainder of this chapter uses immuno-staining in combination with flow cytometry to define cellular composition in terms of known cell types. In all subsequent flow cytometric analyses shown, all events were gated to select only viable cells. This was done in two steps; firstly as shown in Figure 3.2A, events corresponding to single cells were selected on the basis of size (using forward-scatter (FSC-H)) and density (side-scatter (SSC-H)). These cells were then analysed in a second step, where the DNA-binding viability stain 7AAD was used as a marker of dead cells. Only 7AAD-negative cells are selected, as shown in Figure 3.2B. Any events passing these two criteria were regarded as viable cells, and it is these that are shown in all subsequent flow cytometric analysis in this thesis, unless stated otherwise.

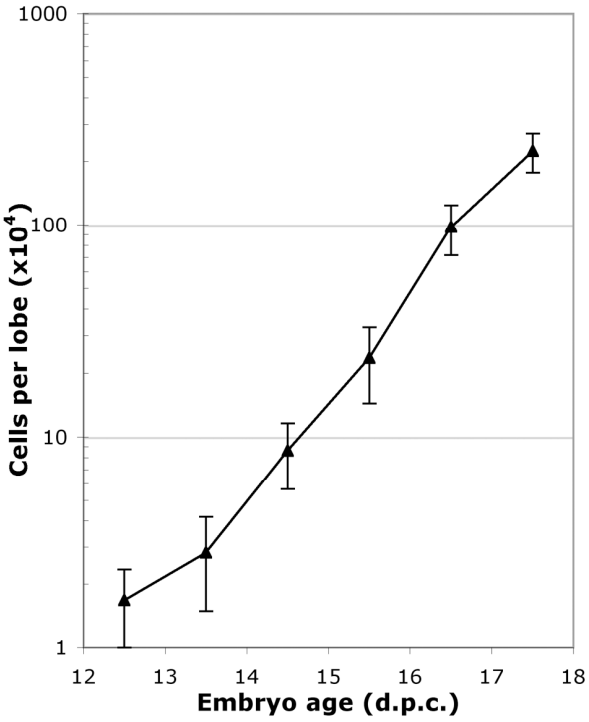

Figure 3.1 Total thymus cellularity between E12.5 and E17.5

After undergoing enzymatic dissociation, cells from pooled thymus lobes were counted by haemocytometer. Data points represent the mean and standard deviation of at least 5 independent experiments.

Table 3.1 Total cells in the embryonic thymus from E12.5 to E17.5

Embryo age (d.p.c.)	Total cells/lobe ($x10^4$)	±SD ($x10^4$)
12.5	1.67	0.67
13.5	2.82	1.34
14.5	8.64	2.99
15.5	23.6	9.26
16.5	97.9	26.0
17.5	224.5	47.2

Absolute number of cells per thymus lobe, values correspond to data points on graph in Figure 3.1 above.

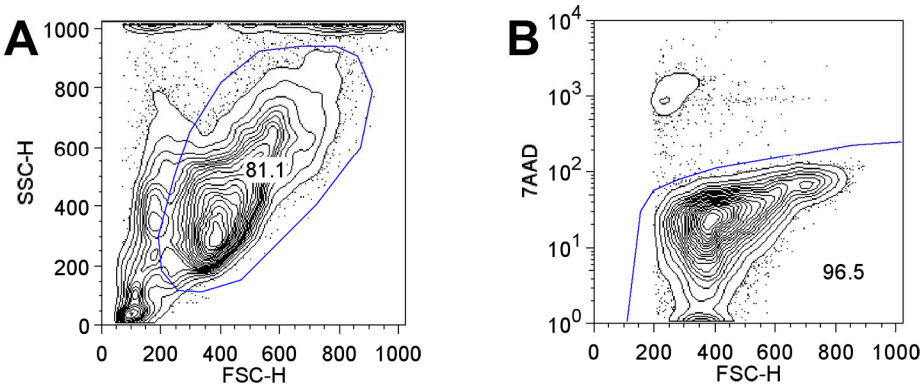

Figure 3.2 Flow cytometric gating strategy for live cells

Events regarded as cells were gated on the basis of forward-scatter (FSC-H), to determine size; and side-scatter (SSC-H), to determine density (**A**). Within this population, the intercalating dye 7-aminoactinomycin D (7AAD) was used as viability stain to identify dead cells (**B**). Only 7AAD negative cells were included in any subsequent flow cytometric analysis shown in this thesis, unless stated otherwise.

3.2.2. Haematopoietic cells

In the mature thymus, over 99% of thymic cellularity is composed of haematopoietic cells. The cell surface marker CD45 can be used to identify all haematopoietic cells apart from erythrocytes, which are a very minor presence in the embryonic thymus and were therefore not included. To define the proportion and number of $CD45^+$ cells in the developing thymus, an anti-CD45 monoclonal antibody (mAb) was used to identify haematopoietic cells by flow cytometry, as shown in Figure 3.3. At E12.5 only around 20% of thymic cells were $CD45^+$. By E13.5 just over 40% of cells in the thymus are $CD45^+$, 65% by E14.5 and by E15.5 this figure has increased to 80% of total cellularity. Haematopoietic cells account for around 85% and 95% of total cells per thymus lobe by E16.5 and E17.5 respectively (Figure 3.3, Table 3.2).

These data were applied to the total number of cells per lobe (individually for separate experiments) to give the actual number of haematopoietic cells per thymus lobe (Figure 3.4A). At E12.5 approximately $4.26x10^3$ $\pm1.64x10^3$ $CD45^+$ cells are present in a single lobe. These have penetrated through the mesenchyme into the epithelium (Itoi et al., 2001), having been attracted by chemotactic factors, and represent the first 'wave' of colonisation. At E13.5 the thymus was found to have an average of $1.37x10^4$ $\pm2.35x10^3$ $CD45^+$ cells per lobe, representing a three-fold increase within 24 hours. By E14.5 there were seen to be around $6.29x10^4$ $\pm8.92x10^3$ haematopoietic cells – an increase of $4.9x10^4$ cells from the previous day. This influx represents the second wave of thymocytes that arrive at E13.5-E14.5, probably carried by the blood vessels that are now present around the outside of the thymus. By E15.5 there are now on average $2.29x10^5$ $\pm1.97x10^4$ $CD45^+$ cells within the thymus, having increased by a factor of 3.5 since E14.5. The establishment of intrathymic vasculature, which continues to supply prospective T-cell precursors, accounts for this 'third wave'. Thus, a 3.5-fold increase leads to a total of $7.86x10^5$ $\pm2.96x10^4$ $CD45^+$ cells at E16.5, and by E17.5 there are now $2.25x10^6$ $\pm3.38x10^4$ haematopoietic cells within the stroma of each thymus lobe, giving a population proportionally similar to that seen in the mature organ.

The non-haematopoietic fraction of the thymic stroma also increases in terms of cell number during embryonic development, albeit at a rate that is not comparable to that of $CD45^+$ cells (Figure 3.4B, Table 3.2). At E12.5 around $1.54x10^4$ $\pm 2.16x10^3$ $CD45^-$ cells were shown to be present. A large number of these would be expected to be extrathymic mesenchyme, due to difficulties in completely removing the tissue that surrounds the thymus at this stage. The number of non-haematopoietic stromal cells increases to around $1.73x10^4$ $\pm 2.51x10^3$ by E13.5, and this doubles by E14.5 to give approximately $3.66x10^4$ $\pm 7.44x10^3$. By E15.5, $6.17x10^4$ $\pm 1.47x10^4$ cells that do not express CD45 are seen, by E16.5 this figure rises to $1.20x10^5$ $\pm 1.01x10^4$, and by E17.5 there are around $1.65x10^5$ $\pm 3.19x10^4$ $CD45^-$ cells within the thymic stroma – effectively showing a 2.5-fold increase during the final 48 hours investigated in this study.

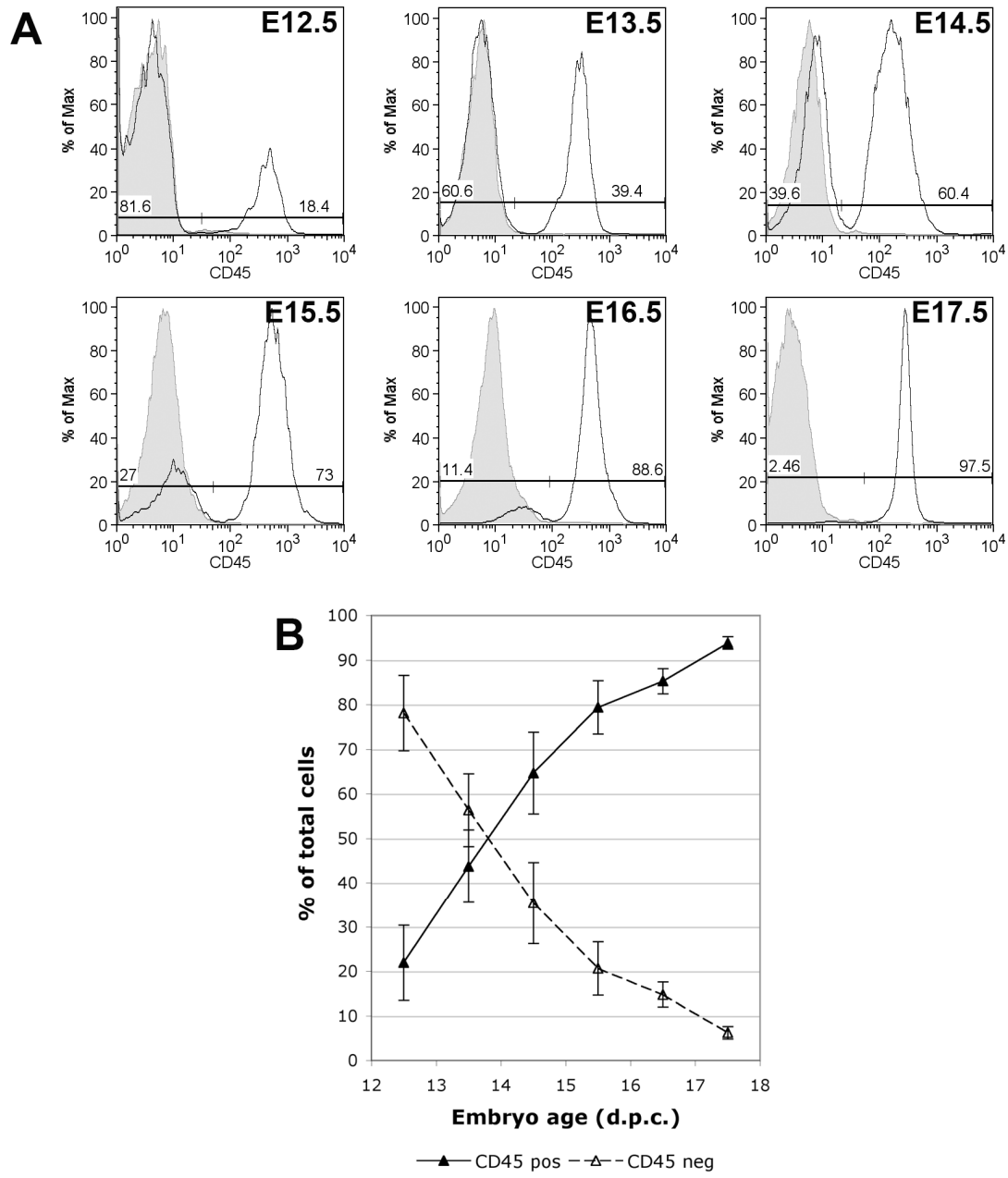

Figure 3.3 Haematopoietic proportion of thymus between E12.5 and E17.5

Dissected thymus lobes underwent enzymatic dissociation, followed by incubation with anti-CD45 monoclonal antibody. $CD45^+$ haematopoietic cells were identified by flow cytometric analysis (**A**). Histograms represent at least 5 independent experiments.

Shown in **B** are the relative percentages of $CD45^+$ (solid line) vs. $CD45^-$ (dotted line) cells within the developing thymus from day 12.5 to day 17.5. Data points represent the mean and standard deviation from at least 5 independent experiments.

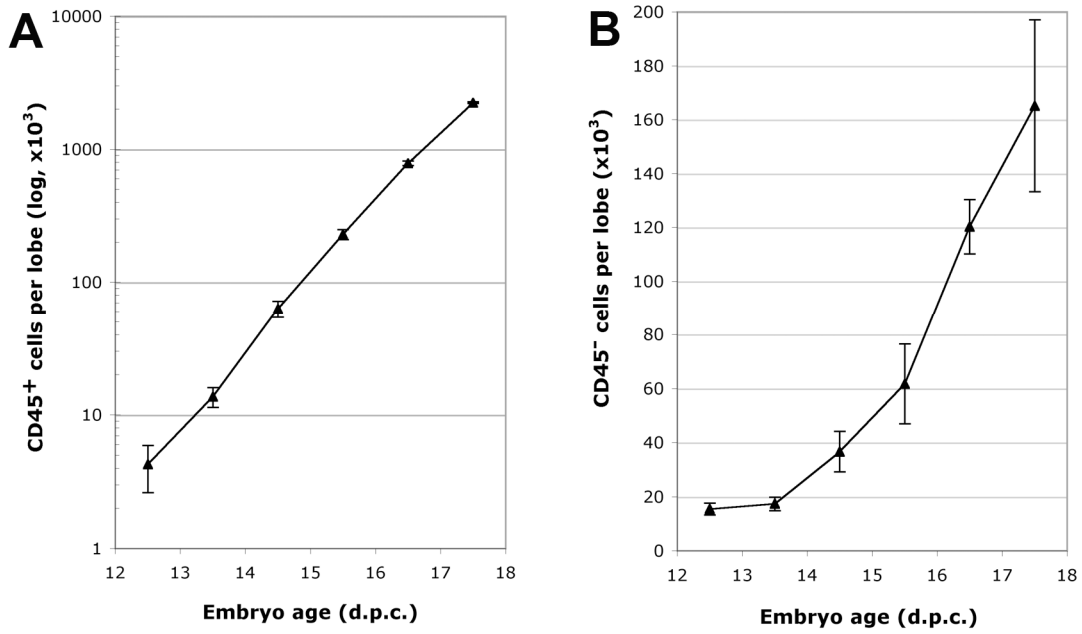

Figure 3.4 Actual numbers of haematopoietic and non-haematopoietic cells in the foetal thymus

The percentage of total cells showing $CD45^+$ staining by flow cytometry (Figure 3.3) was applied to the total number of cells per thymus lobe (Figure 3.1). These parameters were calculated for each experiment individually. Each data point represents the mean and standard deviation of at least 5 independent experiments.

These data show an exponential increase in $CD45^+$ haematopoietic cells (**A**). A more modest, but still substantial increase is shown in the $CD45^-$ non-haematopoietic fraction of the thymus (**B**).

Table 3.2 Proportion and number of haematopoietic vs. non-haematopoietic cells in the embryonic thymus from E12.5 to E17.5

Embryo age (d.p.c.)	$CD45^+$% of total thymus	$CD45^-$% of total thymus	±SD	No. $CD45^+$ cell/lobe lobe ($x10^3$)	±SD ($x10^3$)	No. $CD45^-$ cells/lobe lobe ($x10^3$)	±SD ($x10^3$)
12.5	21.9	78.1	8.4	4.26	1.64	15.4	2.16
13.5	43.7	56.3	8.1	13.7	2.35	17.3	2.51
14.5	64.6	35.4	9.2	62.9	8.92	36.6	7.44
15.5	79.4	20.6	6.0	229	19.7	61.7	14.7
16.5	85.2	14.8	2.8	786	29.6	120	10.1
17.5	93.8	6.2	1.4	2245	33.8	165	31.9

Summary of flow cytometric analysis, counting the percentage and number of $CD45^+$ haematopoietic cells within the developing thymus, from Figure 3.3 and Figure 3.4.

3.2.3. Thymic mesenchyme

Mesenchymal cells are a major component of the non-haematopoietic thymic stroma, and can be identified by immunohistochemistry using the monoclonal antibody ERTR7 (Van Vliet et al., 1984). However, ERTR7 recognises an unknown intracellular determinant of fibroblasts that has proved to be undetectable by flow cytometry, and therefore unsuitable for the purpose of quantifying mesenchymal cell numbers. During embryogenesis, derivatives of neural crest (NC), including that which surrounds the thymus, have been shown to express platelet-derived growth factor receptor alpha (PDGFRα) (Takakura et al., 1997), as does mesoderm-derived mesenchyme in the trunk. Ligands for PDGFRα are expressed on epithelial cells that are in close proximity to PDGFRα-expressing embryonic mesenchyme (Orr-Urtreger and Lonai, 1992). In *patch* (*ph*) mice - which are defective for PDGFRα expression - the proliferation, migration to within the thymus lobe, and provision of FGF growth factors by encapsulating mesenchyme appears to be substantially reduced (Itoi et al., 2007). Examination of PDGFRα expression in the developing thymus was undertaken to assess its suitability as a marker of mesenchyme for flow cytometry. Platelet-derived growth factor receptor beta (PDGFRβ) expression was also examined, in an attempt to identify the perivascular mesenchyme indicated by ERTR7 staining. PDGFRβ is expressed on mesenchymal vascular smooth muscle (VSM) and pericytes in other organs. These cells are recruited by endothelium expressing the ligand PDGFB during angiogenesis (Lindahl et al., 1997, Lindblom et al., 2003, Kaminski et al., 2001). PDGFRβ is also expressed on mesenchyme in the craniofacial and urogenital regions (Betsholtz, 2003).

At E13.5, shown in Figure 3.5, ERTR7^{+} mesenchyme can be seen to surround the thymus lobe in a thick layer, with some sections invading inward. PDGFRβ is expressed in a very similar fashion at this stage. In contrast, PDGFRα appears only to be expressed in the capsular area around the outside of the organ (Figure 3.5L). At E15.5, ERTR7^{+} cells are seen extensively within the interior of the thymus lobe, as shown in Figure 3.6. Although (as shown in Figure 3.5) these cells are negative for PDGFRα, the staining pattern for PDGFRβ (Figure 3.6E-H) shows a high

similarity in both proportion and morphology to ERTR7. By E17.5, ERTR7$^+$ cells are seen both in the capsule, albeit in a thinner layer than in earlier organogenesis, and as an extensive network throughout the organ (Figure 3.7A-D). The ERTR7$^+$ cells of the capsule are non-epithelial, shown by pan-cytokeratin staining in Figure 3.7E-I, with the capsule and sub-capsular epithelium appearing to by separated by a continuous basement membrane (Figure 3.7I). At this stage, PDGFRα expression appears to be further reduced even in the capsule (Figure 3.7J-M), with only infrequent PDGFRα$^+$ cells appearing around the outside of the thymus (Figure 3.7M, white arrowheads).

Following these immunofluorescence experiments, flow cytometry analysis was used to calculate the proportions of stromal cells expressing PDGFRα and/or PDGFRβ from E12.5 through to E17.5. The results of this analysis are shown in Figure 3.8. In A, representative flow cytometry plots of NH cells show a shift over time from a predominantly PDGFRα$^+$β$^+$ mesenchymal phenotype at E12.5 to increased PDGFRα$^-$β$^+$ at E13.5 (correlating with the observation that inward migration of mesenchyme from the capsule has now begun, Figure 3.5). This trend continues until, at E16.5, less than a tenth of the PDGFRβ$^+$ cells continue to show PDGFRα expression.

Just under half of all NH cells are mesenchymal at E12.5 (Figure 3.8B). Between E12.5 and E14.5 there is a rapid decrease on the proportion of mesenchymal cells making up the non-haematopoietic stroma. This matches the high rate of epithelial cell proliferation at this stage, addressed in the following chapter of this thesis. Between E14.5 and E17.5 the mesenchymal proportion of the NH thymus component appears to remain at between 10-15%, however the proportion of PDGFRα$^+$ cells has significantly decreased to less than 1%.

These data were applied to the total number of non-haematopoietic (NH) cells previously found to be in each thymus lobe (Figure 3.4). Thus, the absolute number of mesenchymal cells present at each time point was calculated (Table 3.3, Figure 3.9). The large number of mesenchymal cells (specifically PDGFRα$^+$β$^+$ cells), and relatively large standard deviation observed at E12.5, may be explained by the fact

that, when dissecting large numbers of these early thymus lobes, it is difficult to completely trim off all surrounding pharyngeal mesenchyme. It is interesting to note that the number of PDGFR$\alpha^{+}\beta^{-}$ and PDGFR$\alpha^{+}\beta^{+}$ cells remains constant from E13.5 to E17.5, whilst it is only PDGFR$\alpha^{-}\beta^{+}$ cells that substantially increase in number during thymus development – particularly between E15.5 and E16.5. This may be a result of proliferation induced by endothelial cells, with PDGFRβ^{+} perivascular VSM and pericytes undergoing recruitment by the nascent intrathymic vascular network as mentioned earlier in this section.

Figure 3.5 Staining of selected mesenchyme markers at E13.5

Following page

Immunofluorescence staining of E13.5 thymus, showing effectiveness of different markers in identifying thymic mesenchyme. ERTR7 (panels **A-D**) is a general marker of thymic fibroblasts. In **D**, fibroblasts invading the epithelial interior of the organ from the capsule can clearly be seen (white arrowheads), and there is a clear population fibroblast population already visible deep inside the lobe (white arrows). A very similar pattern is seen with PDGFRβ staining (panels **E-H**), upon staining a different section from the same E13.5 lobe, with PDGFRβ$^+$ cells visible in the thymic interior (white arrows), and invading from the capsule (white arrowheads). Conversely, PDGFRα$^+$ cells only appeared in the capsule (panels **I-L**). Scale bars are 100 μm.

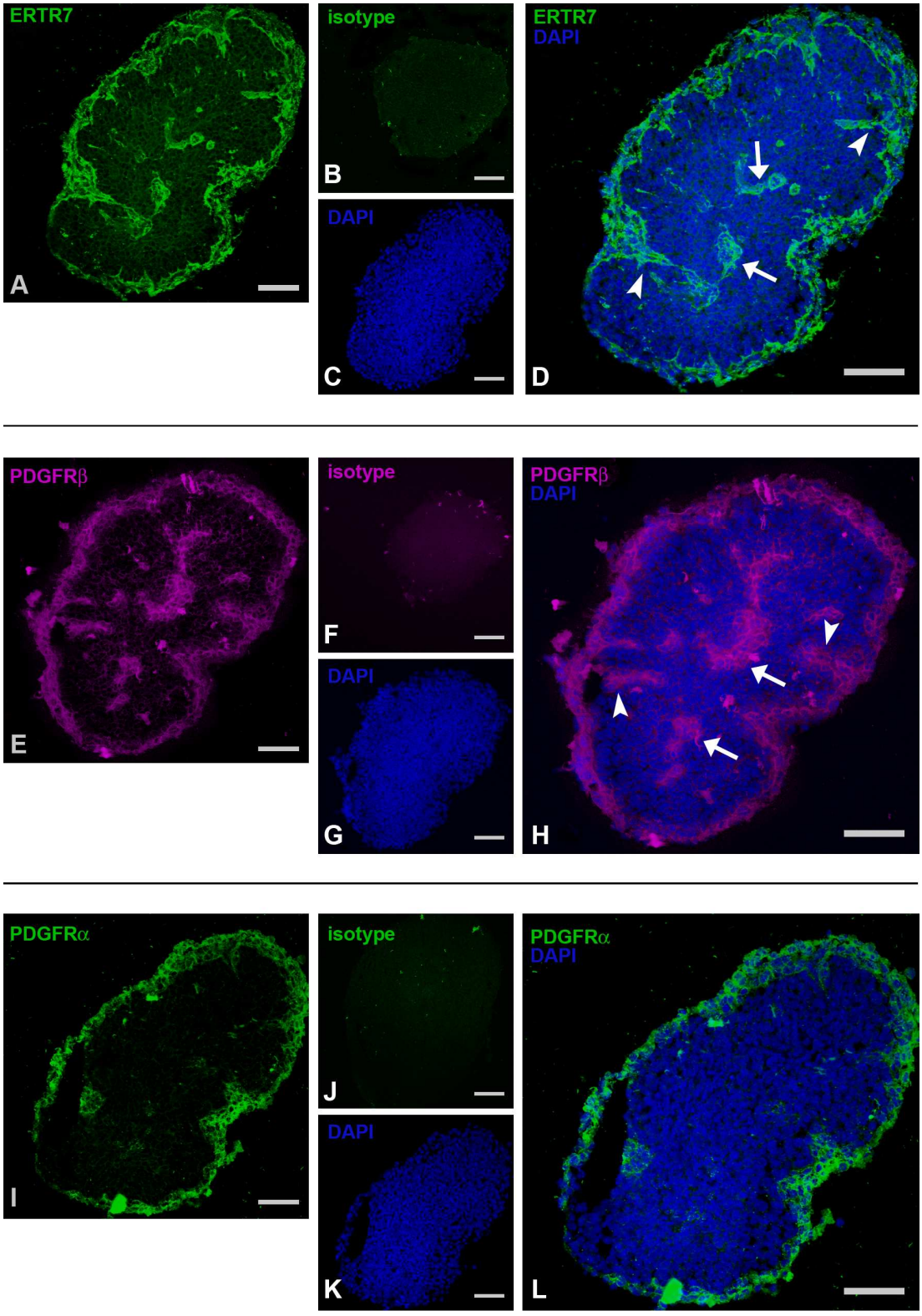

Figure 3.5 Staining of selected mesenchyme markers at E13.5

For legend, see previous page.

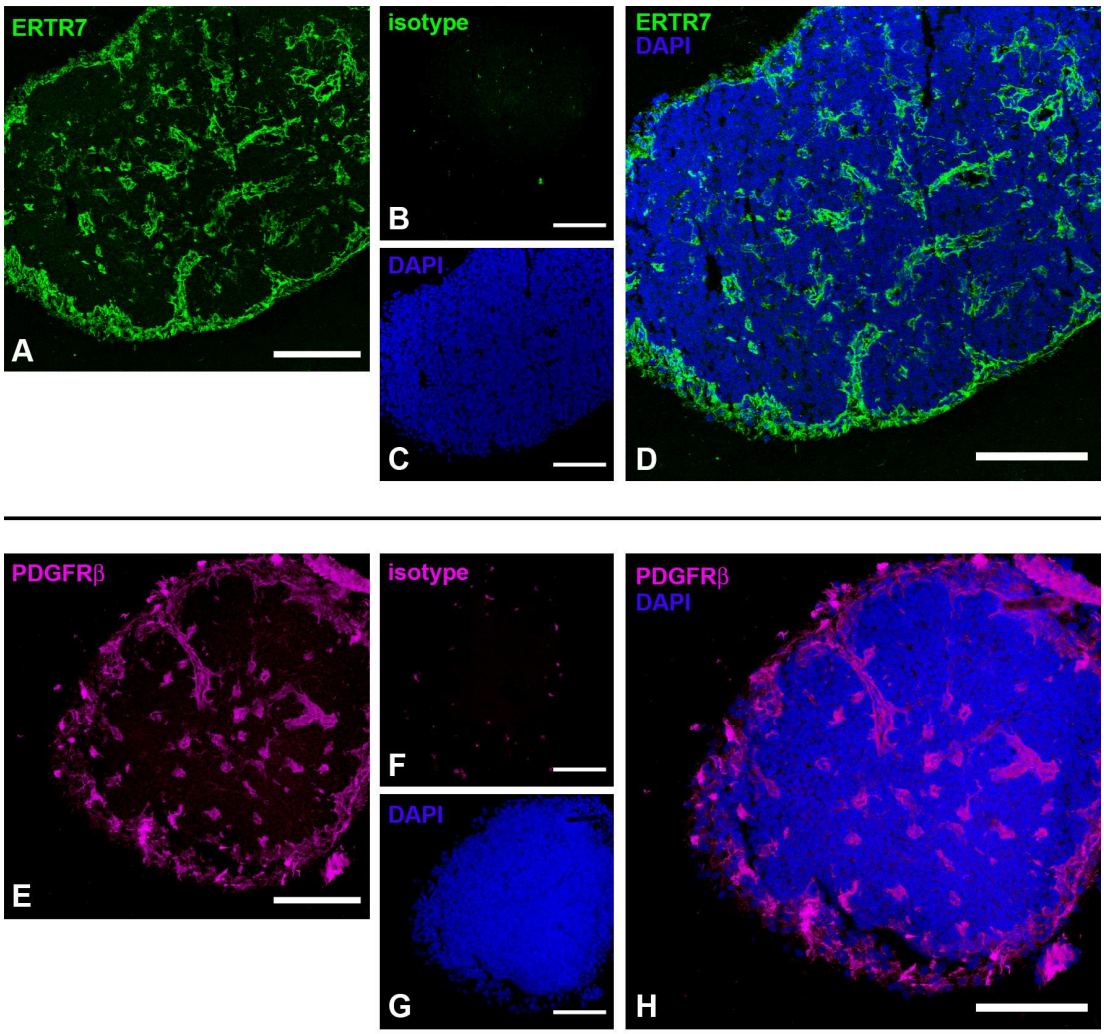

Figure 3.6 PDGFRβ continues to mark mesenchyme during at E15.5

Immunofluorescence staining of E15.5 thymus sections. ERTR7 (**A-D**) shows mesenchyme surrounding the outside of the thymus, with extensive areas present within the interior of the lobe. PDGFRβ (**E-H**) displays a similar pattern. Scale bars are 200μm.

Figure 3.7 Non-epithelial, ERTR7^{+} mesenchymal cells are predominantly PDGFRα^{-} by E17.5

Following page

Immunofluorescence staining of E17.5 thymus. Thymic mesenchyme, staining for ERTR7, (**A-D**) is observed in the capsule, and scattered throughout the interior of the thymus. These cells are non-epithelial, as they do not stain with PanK (**E-I**). At E17.5 only a small number of cells, located in the capsule, appear to stain with PDGFRα (**J-M**, marked by arrowheads in **M**) Scale bars in **A-D** and **J-M** are 100µm, in **E-I** are 50µm.

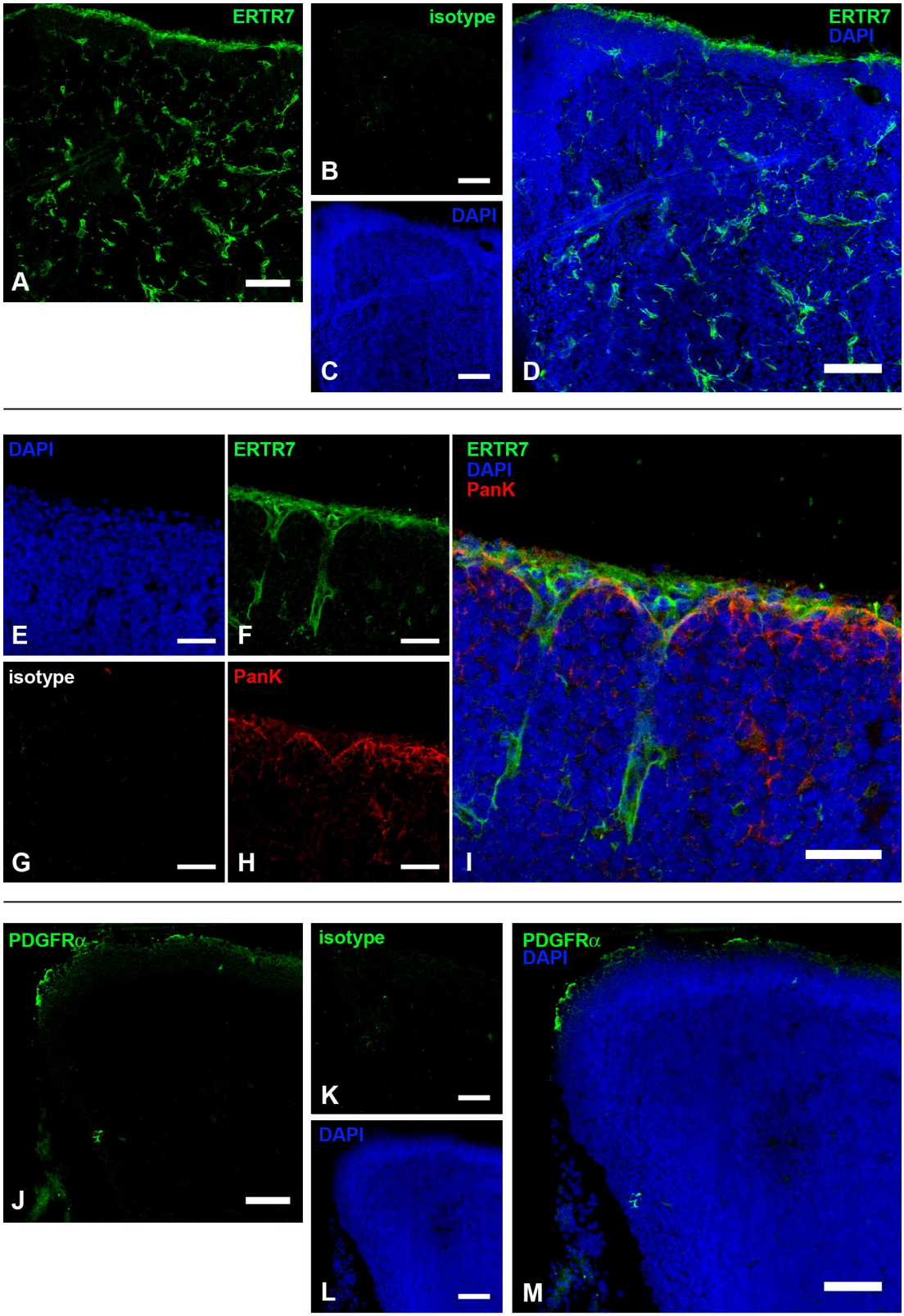

Figure 3.7 Non-epithelial, ERTR7^{+} mesenchymal cells are predominantly PDGFRα^{-} by E17.5. *For legend, see previous page.*

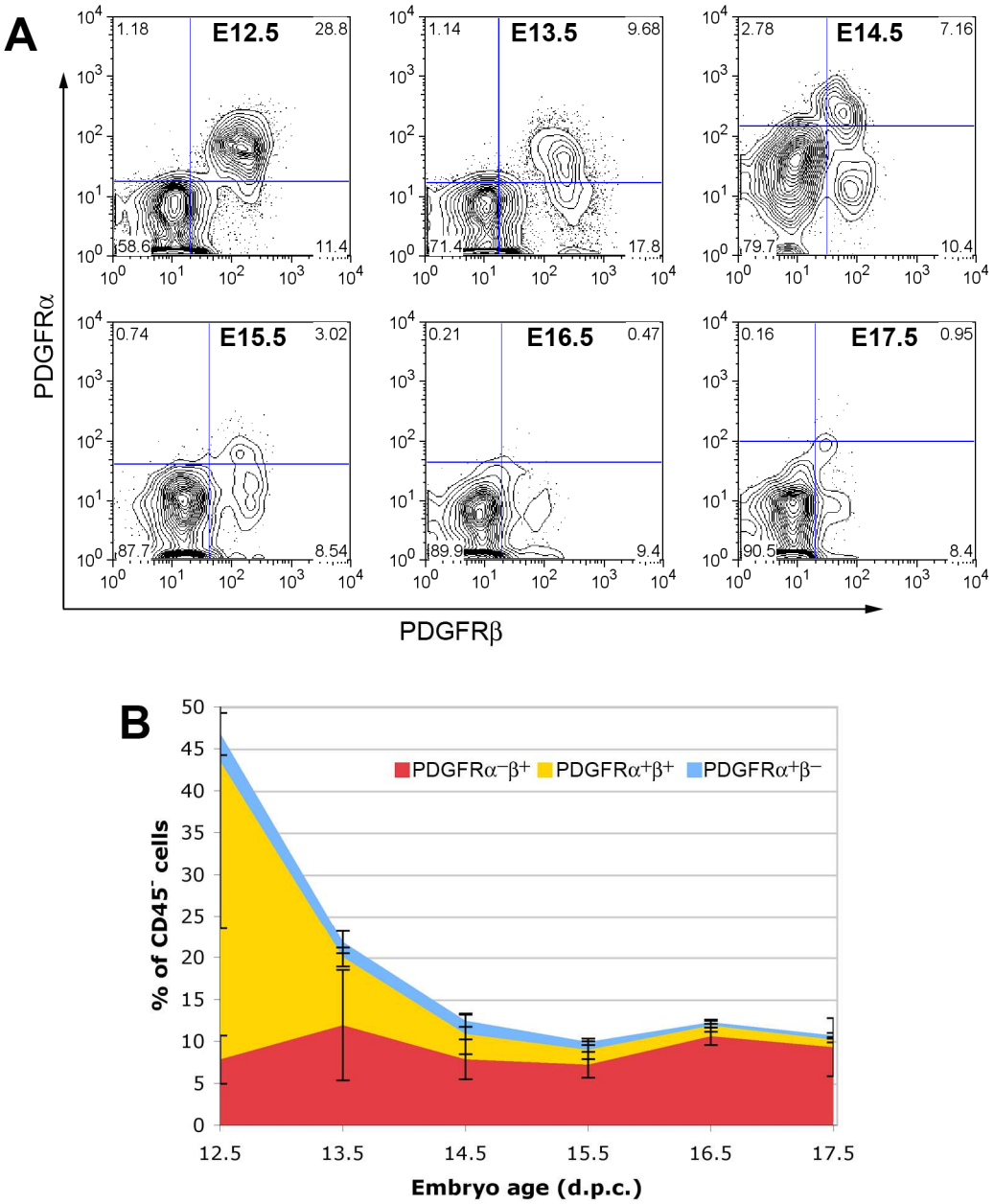

Figure 3.8 Flow cytometric analysis of PDGFRα vs. PDGFRβ expression

Data show proportions of non-haematopoietic cells from dissociated thymic lobes staining for PDGFRα and/or PDGFRβ. **A**, representative flow cytometric analyses of $CD45^-TER119^-$ cells incubated with mAbs for PDGFRα and PDGFRβ. Quadrants are set on isotype controls, also using $CD45^-TER119^-$ cells. Plots are representative of at least 3 independent experiments.

In **B**, the percentage of $CD45^-TER119^-$ cells that are $PDGFR\alpha^+\beta^-$ (blue) $PDGFR\alpha^+\beta^+$ (yellow), or $PDGFR\alpha^-\beta^+$ (red) at each time point is shown. Data points represent the mean for at least 3 independent experiments. ±standard deviation is shown.

Table 3.3 Number of cells expressing PDGFRα and/or PDGFRβ

Embryo age (d.p.c.)	No. $\alpha^+\beta^-$ per lobe	±SD	No. $\alpha^-\beta^+$ per lobe	±SD	No. $\alpha^+\beta^+$ per lobe	±SD	Total mesen. cells/lobe	±SD
12.5	510	389	1,207	444	5,494	3,076	6,876	2,923
13.5	314	233	2,069	1,145	1,408	195	3,712	855
14.5	573	263	2,873	873	1,114	890	5,208	1,812
15.5	609	239	4,439	944	1,080	653	8,071	3,446
16.5	497	214	12,748	1,256	1,535	865	14,780	2,329
17.5	820	570	15,365	5,697	1,442	511	17,628	5,945

Flow cytometric data regarding proportions of $CD45^-TER119^-$ cells expressing PDGFRα and/or PDGFRβ (Figure 3.8) were applied to the number of $CD45^-TER119^-$ cells present in a single thymus lobe, from E12.5 to E17.5, to calculate absolute mesenchymal cell numbers. Calculations were performed separately for each experimental replicate, with data here representing the mean and standard deviation for at least 3 independent experiments.

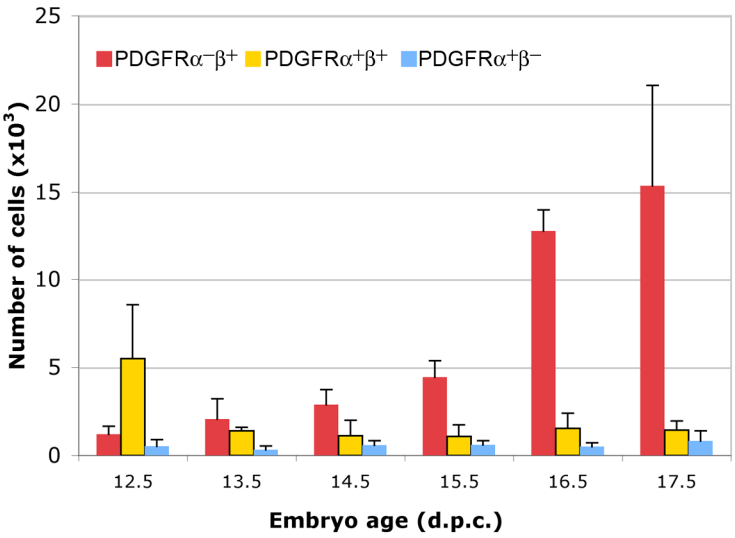

Figure 3.9 Actual numbers of mesenchyme cells in the foetal thymus

Flow cytometric data regarding proportions of $CD45^-TER119^-$ cells expressing PDGFRα and/or PDGFRβ (Figure 3.8) were applied to the number of $CD45^-TER119^-$ cells present in a single thymus lobe, from E12.5 to E17.5, to calculate absolute mesenchymal cell numbers. Values are given in Table 3.3. Blue bars represent $PDGFR\alpha^+\beta^-$, yellow represents $PDGFR\alpha^+\beta^+$, and $PDGFR\alpha^-\beta^+$ cells are represented by red. Data represents the mean and standard deviation for at least 3 independent experiments. Calculations were performed separately for each experimental replicate.

3.2.4. Thymic endothelium

In order to analyse thymic endothelial cells by flow cytometry, a MAb recognising platelet endothelial cell adhesion molecule-1 (PECAM-1, a.k.a. CD31) was used on dissociated thymus, as previously documented (Gray et al., 2002, Muller et al., 2005). At E12.5, just under 5% of all non-haematopoietic cells in the thymus showed CD31 expression, with this proportion very gradually decreasing to marginally over 3% at E17.5, as shown in Figure 3.10A and Table 3.4. If these values are translated into actual numbers of $CD31^+$ cells at each time point (Figure 3.10B, Table 3.4), it becomes apparent that this population grows slowly between E12.5 and E15.5 – doubling from just under 750 to approximately 1500 cells. Between E15.5 and E16.5, however, the number of $CD31^+$ cells present appears to double again, to almost 3400, and at E17.5 has increased to just over 5300 cells. The sharp increase in number from E15.5 is mirrored by the observed increase in $PDGFR\beta^+$ mesenchyme – a cell type known to be associated with endothelium – pointing to an elevated generation of intrathymic vasculature at this stage. It cannot be ruled out that $CD31^+$ cells are still being recruited from outside the thymus at this stage. However, this seems less likely due to the thymic capsule forming a barrier around the organ, and it is probable that the increase in $CD31^+$ cells from E15.5 marks an increase in proliferation of endothelial cells or their precursors. This may well be mediated by VEGF, an endothelial cell mitogen expressed by both TECs and thymic mesenchyme (Muller et al., 2005).

Table 3.4 Thymic endothelial cells from E12.5 to E17.5

Embryo age (d.p.c.)	$CD31^+$% of $CD45^-TER119^-$	±SD	No. $CD31^+$ cells/lobe	±SD
12.5	4.78	1.30	736	201
13.5	4.59	0.52	796	90
14.5	2.95	0.52	1,081	191
15.5	2.48	0.23	1,530	140
16.5	2.82	0.53	3,387	638
17.5	3.23	1.24	5,335	2,044

Number of $CD31^+$ endothelial cells in the embryonic thymus between E12.5 and E17.5, calculated from flow cytometry results. Number of cells calculated separately for each experimental replicate, values stated above are mean and standard deviation of at least 3 independent experiments.

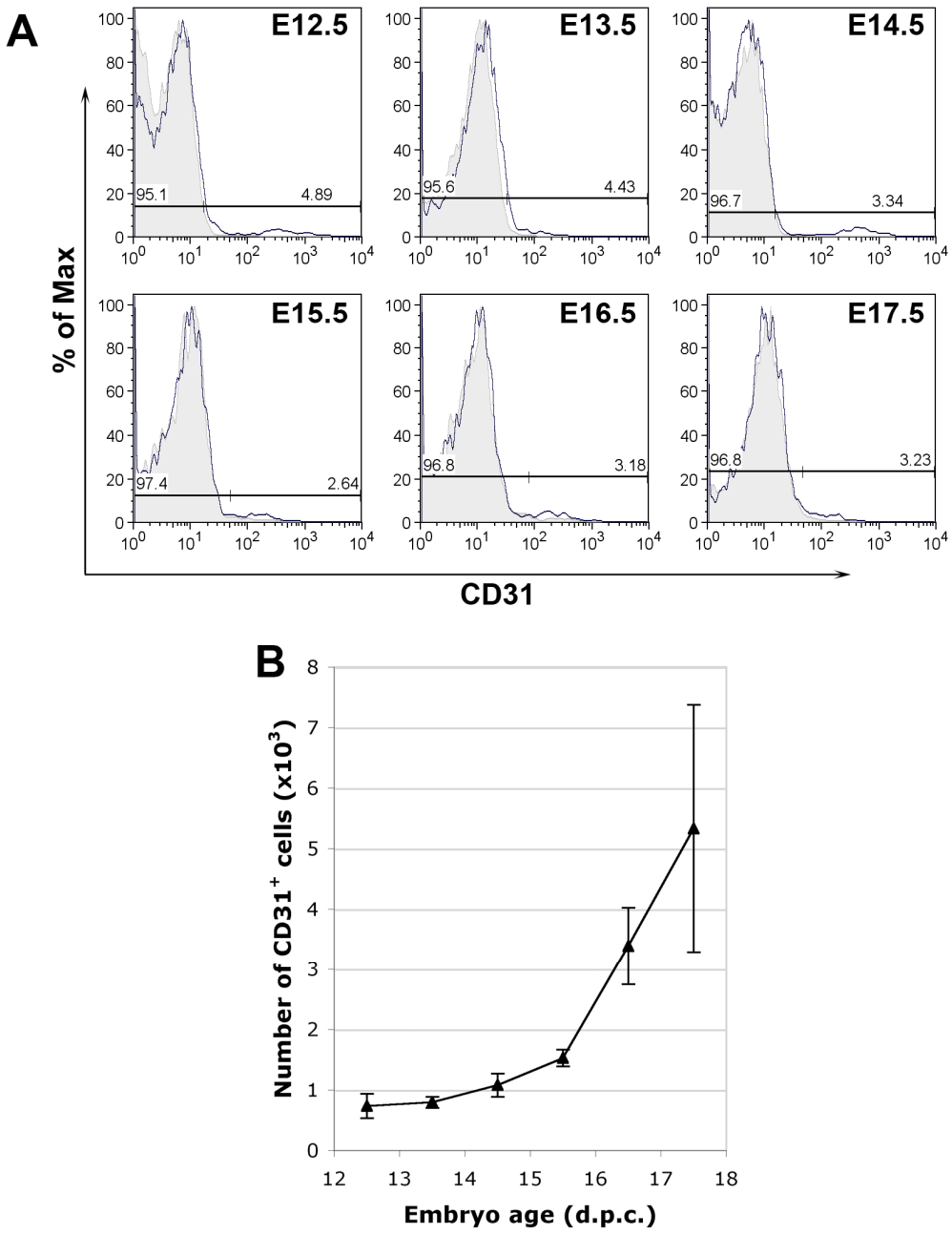

Figure 3.10 Number of CD31$^+$ endothelial cells from E12.5 to E17.5

Flow cytometric analysis for CD31, on cells gated as being CD45$^-$TER119$^-$ (**A**). Gates were set on isotype-matched controls, shown in grey. Histogram plots are representative of at least 3 independent experiments.

The absolute number of CD31$^+$ cells per thymus lobe was calculated by multiplying the CD31$^+$ percentage of the NH population by the number of NH cells per lobe at each time point (**B**), exact values are given in Table 3.4.

3.2.5. Thymic epithelium

Thymic epithelial cells are keratin$^+$, however the intracellular nature of keratin means that it cannot be used in conjunction with many other cell-surface markers. In order to more easily identify TECs by flow cytometry, I used the extracellular marker EpCAM.

EpCAM expression on TECs was confirmed by co-staining with a pan-cytokeratin antibody on cytospins (Figure 3.11). To do this, dissociated cells were sorted by flow cytometry - excluding those positive for CD45, TER119, PDGFRα or CD31. Since low levels of EpCAM have also been observed on CD4$^-$CD8$^-$ and CD4$^+$CD8$^+$ thymocytes, and also some dendritic cells, it must be used in conjunction with a means to distinguish haematopoietic versus non-haematopoietic cells (Borkowski et al., 1996, Nelson et al., 1996). The remaining cells were collected and spun onto glass slides, fixed in acetone, and air-dried. Labelling with anti-EpCAM and pan-cytokeratin antibodies was then performed, and slides were analysed by fluorescent confocal microscopy. In all samples from E12.5 to E17.5, 99% (± 2%) of EpCAM$^+$ cells were seen to show keratin$^+$ staining (Figure 3.11), confirming EpCAM's suitability as a marker of foetal thymic epithelium at the time points under investigation.

Flow cytometric analysis of the epithelial proportion of the thymus during development was carried out, with the epithelial component identified as being EpCAM$^+$CD45$^-$TER119$^-$ (Figure 3.12A). As a fraction of total dissociated thymus, epithelial cells are around 40% at E12.5 and E13.5, dropping quickly as the haematopoietic cell population undergoes massive influx into, and proliferation within, the thymic primordium until only around 2.5% of cells in the organ are epithelial at E17.5 – close to the proportion observed in the mature organ. As a proportion of NH cells, however, epithelial cells rise from around 55% at E12.5 to 80% at E13.5. This increases to about 85% at E14.5, and appears to remain the case until at least E17.5 (Figure 3.12B, Table 3.5).

When these data are translated into actual number of epithelial cells per lobe, a steady increase is apparent (Figure 3.12C, Table 3.5). Roughly, a doubling in total

epithelial cells present is observed in each 24-hour period between E12.5 and E14.5. The rate of increase of the epithelial population then falls slightly, showing a 1.5-fold increase between E14.5 and E15.5 to around $5.1x10^4$. The number of epithelial cells per lobe rises to $1x10^5$ at E16.5 and about $1.4x10^5$ at E17.5.

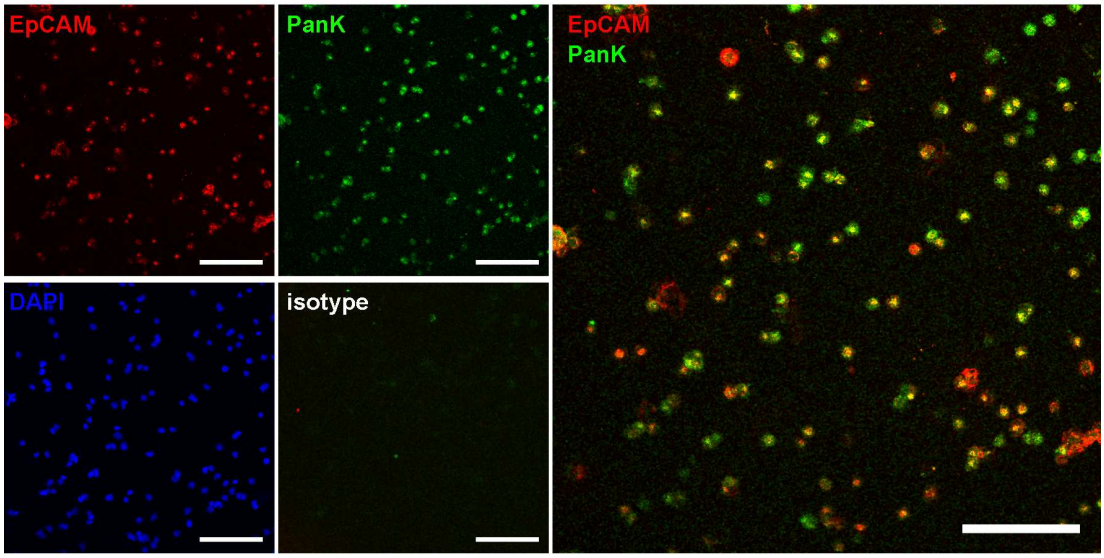

Figure 3.11 EpCAM marks all foetal thymic epithelial cells

Dissociated thymus was sorted by flow cytometry to remove any cells expressing CD45, TER119, PDGFRα or CD31. Remaining cells were collected and spun onto glass slides and fixed with acetone. Slides were stained with pan-cytokeratin (PanK) antibody and anti-EpCAM-1 antibody. Results showed 99% (±2%) of PanK positive cells staining for EpCAM, at all time points from E12.5 to E17.5. The above example is from E14.5 thymus, but representative of all time points examined. Scale bars are 100µm.

Figure 3.12 Increase in EpCAM$^+$ thymic epithelium from E12.5 to E17.5

See following page.

A, representative flow cytometric analysis of total dissociated thymus shows a decrease of EpCAM$^+$CD45$^-$TER119$^-$ negative thymic epithelium as a proportion of the entire thymus. **B**, EpCAM$^+$ cells increase as a fraction of the non-haematopoietic component of the thymus. **C** shows the total number of EpCAM$^+$ cells per lobe, calculated as:

(Number of NH cells per lobe) x (percentage of EpCAM$^+$ cells in NH population)

Values were calculated separately for each experimental replicate. Values on graphs are means of at least 3 independent experiments and error bars show ± standard deviation.

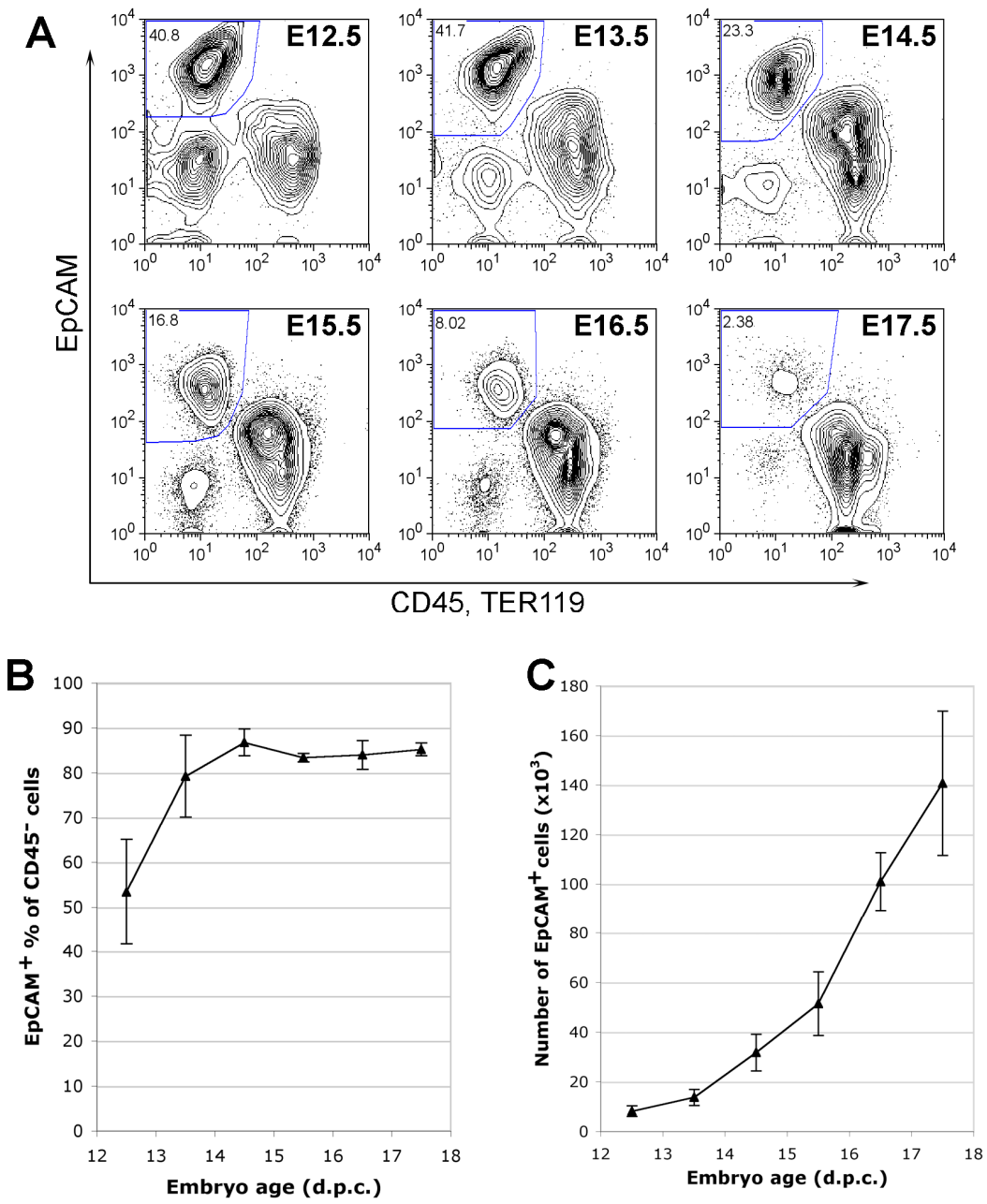

Figure 3.12 Increase in EpCAM+ thymic epithelium from E12.5 to E17.5

Table 3.5 Proportion and number of TECs in the embryonic thymus between E12.5 and E17.5

Embryo Age (d.p.c.)	$EpCAM^+lin^-$ % of total cells	±SD	$EpCAM^+$% of $CD45^-TER119^-$ cells	±SD	Total TEC number ($x10^3$)	±SD ($x10^3$)
12.5	39.9	9.4	53.4	11.7	8.23	2.12
13.5	40.4	11.0	79.2	9.1	13.7	3.24
14.5	29.7	6.1	86.8	3.0	31.8	7.40
15.5	16.2	4.1	83.4	1.0	51.4	12.8
16.5	8.8	2.4	84.0	3.2	101.0	11.7
17.5	2.5	0.7	85.2	1.4	140.7	29.2

Summary of flow cytometric analysis from Figure 3.12. Values were calculated separately for each experimental replicate. Data here show the mean and ± standard deviation for at least 3 independent experiments.

3.3. Discussion

These data provide a numerical picture of thymus ontogeny. The major cell type present in the mature organ – the haematopoietic population – shows a phenomenal increase in number between E12.5 and E17.5 when compared to the non-lymphoid component, as shown in Figure 3.4. When considered without haematopoietic cells, the largest change in total number is seen in the epithelial cell population, which shows a 17-fold increase in cell number between E12.5 and E17.5 as seen in Figure 3.13. Mesenchymal and vascular cell numbers increase between E12.5 and E17.5 by a factor of around 3 and 6 respectively (Figure 3.13). By E17.5, the number of epithelial cells present in the thymus is approximately 6 times larger than the total number of mesenchymal cells and vascular cells combined (Figure 3.13).

With regard to relative proportions of each cell type within the non-lymphoid stroma, mesenchyme appears to be the major cell type at E12.5 but is quickly overtaken by epithelium by E13.5, and by E14.5 then the relative contribution seems to be constant through to E17.5, as shown in Table 3.6. Epithelial cells make up around 85%, mesenchyme around 12%, and vascular cells 3%.

Since this work was undertaken, a number of studies have been published that support some of the data in this chapter. Work by Gray et al. shows comparative numbers of total cells per lobe, and numbers of $CD45^-$ cells, from E14 through to E18 (Gray et al., 2006). Furthermore, data from Hamazaki and colleagues also provide a very close match to my assessment of $CD45^-$ cell numbers from E13.5 to E17.5 (Hamazaki et al., 2007). A study by Jenkinson et al., examining $PDGFR\alpha^+$ thymic mesenchyme, supports my finding that this cell type reduces as a proportion of the non-haematopoietic population during thymus ontogeny (Jenkinson et al., 2007). A more recent study, analysing the expression of PDGFRα and PDGFRβ, supports my observation that whilst PDGFRα expression is reduced during thymus ontogeny, and becomes confined to the capsule, $PDGFR\beta^+$ cells remain throughout the organ during embryonic development (Foster et al., 2008). This study also shows that by E13.5, neural crest-derived cells have begun to differentiate into cells of a perivascular phenotype, and that NC derived mesenchyme persists into the adult

thymus (Foster et al., 2008). In addition, experiments in which the size of the TEC population was calculated at E12 and E15 also give near-identical data those calculated in this chapter (Jenkinson et al., 2008).

There are some caveats to this analysis, the first of which is cell dissociation technique. The times used in enzymatic incubations are different for thymus lobes at different stages of embryonic development, with incubation times reduced to the minimum duration required to produce a single-cell suspension. This was done in order to minimise exposure of cells to potentially harmful conditions, or enzymes that may have an effect on certain antigens expressed by the cell surface (i.e. trypsin). As a result, in later embryonic stages, it may be that there is increased cell death in certain subsets, or reduced ability to detect certain antigens due to increased cleavage of specific cell-surface markers. None of these issues have been obvious from my work, however this could be examined by increasing dissociation times for early embryonic tissue and examining relative frequency of specific cell types or detection levels of certain cellular markers.

Secondly, dead cells are not accounted for in haemacytometer counts, which will have introduced some degree of error in the calculation of total cell numbers as relative cell frequencies have been assessed on viable, 7AAD negative cells. A viability dye such as trypan blue could have added in order to visualise dead cells when counting by eye.

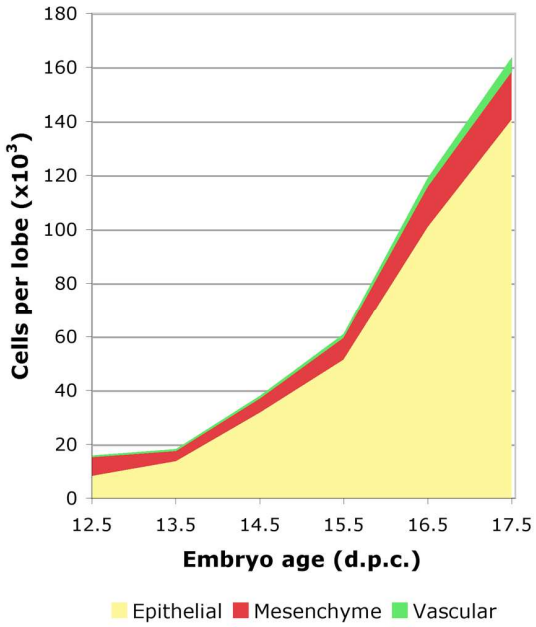

Figure 3.13 Summary of non-haematopoietic cell numbers

The above figure summarizes the number of cells present at each time point for each of the major non-haematopoietic cell types - epithelial, mesenchymal and vascular. Their relative proportion in the non-lymphoid stroma is summarized in Table 3.6 below.

Table 3.6 Summary of contribution of major cell types to the non-haematopoietic component of the embryonic thymus

Embryo age (d.p.c.)	Non-CD45$^+$		EpCAM$^+$		PDGFRα$^+$ and/ or PDGFRβ$^+$		CD31$^+$	
	% of total thymus	No. (x10^3)	% of CD45$^-$	No. (x10^3)	% of CD45$^-$	No. (x10^3)	% of CD45$^-$	No. (x10^3)
12.5	78.1	15.6	53.4	8.22	44.6	6.88	4.8	0.74
13.5	56.3	17.3	79.2	13.7	21.4	3.71	4.6	0.80
14.5	35.4	36.6	86.8	31.8	14.2	5.21	3.0	1.08
15.5	20.6	61.6	83.4	51.4	13.1	8.07	2.5	1.53
16.5	14.8	120.2	84.0	101.0	12.3	14.8	2.8	3.39
17.5	6.2	165.1	85.2	140.7	10.7	17.6	3.2	5.34

Compilation of data calculated in this chapter, giving the stromal (non-haematopoietic) proportion of the embryonic thymus, the relative composition of the stroma, and the absolute numbers of the main non-haematopoietic cell types present from E12.5 until E17.5. For standard deviation error values, refer to cell-specific sections of this chapter.

Chapter 4. Results: Modelling of thymic epithelial proliferation

4.1. Introduction

Following the work described in Chapter Three, the thymic epithelial compartment was analysed in more detail.

The Plet1$^+$ thymic epithelial progenitor cell (TEPC) population (identified with the monoclonal antibodies MTS20 and MTS24) can give rise to a properly organised and functional thymus equivalent, when isolated from E12.5 and E15.5 mouse thymi and ectopically transplanted *in vivo* (Bennett et al., 2002, Gill et al., 2002).

In Chapter Four, I investigate the numbers of Plet1$^+$ thymic epithelial cells present throughout E12.5 to E17.5 of fetal thymus development. I also examine levels of apoptosis and participation in the cell cycle in Plet1$^+$ vs. Plet1$^-$ cells, in order to look at possible models of TEC kinetics and proliferation.

In combination with data from Chapter Three, these analyses would also assist in interpreting any data from TEC clones generated by the laacZ labelling system in Chapter Five.

4.2. Results

4.2.1. Proportion of thymic epithelial cells showing Plet1 staining between E12.5 and E17.5

Flow cytometry was used to assess the proportion of Plet1$^+$ vs. Plet1$^-$ thymic epithelial cells (TECs) present as thymus organogenesis proceeds from E12.5 to E17.5. TECs were identified as being non-haematopoietic (negative for CD45 and TER119) but showing positive staining for EpCAM, as shown in Figure 4.1A. The proportion of TECs showing staining with MTS20 antibody was then ascertained, with examples for each age of study shown in Figure 4.1B. At E12.5, it was seen that almost 90% of TECs showed Plet1$^+$ staining. This proportion reduces to around 66% at E13.5, and sharply decreases again to approximately 23% at E14.5. A further

steady reduction in the proportion of Plet1$^+$ TECs continued to E17.5, where an average of just 6.5% was seen. These data are summarised in Table 4.1.

4.2.2. Absolute numbers of Plet1$^+$ and Plet1$^-$ thymic epithelial cells from E12.5 to E17.5

In order to ascertain the changes in size of the Plet1$^+$ and Plet1$^-$ populations during thymus development, absolute numbers of Plet1$^+$ or Plet1$^-$ TECs were calculated. For each experiment, the number of TECs per lobe was first calculated – by multiplying the percentage of EpCAM$^+$CD45$^-$TER119$^-$ cells in the sample by the total number of cells per lobe known to be present at the particular age of study. This figure was then applied to the percentage of Plet1$^+$ or Plet1$^-$ TECs already known to occur in that sample (from Figure 4.1), to give the absolute number of Plet1$^+$ or Plet1$^-$ TECs present. These data are summarised in Table 4.1, and represented graphically in Figure 4.2. It can be seen that numbers of Plet1$^-$ TECs increase massively on a daily basis, effectively doubling every 24 hours. Conversely, no significant difference was observed in the size of the Plet1$^+$ TEC population through all stages of organogenesis investigated here, numbering roughly 6,000-7,000 cells throughout. To ascertain whether variations in the number of Plet1$^+$ TECs at different developmental stages were significant, a one-way ANOVA test was used. This test is based on a Gaussian distribution of results, something that would be expected (but not proved, due to a small number of replicates, e.g. n=4 for each group of results). The P-value was found to be 0.662, so it was therefore considered that the difference between the numbers of Plet1$^+$ TEC was insignificant Table 4.2.

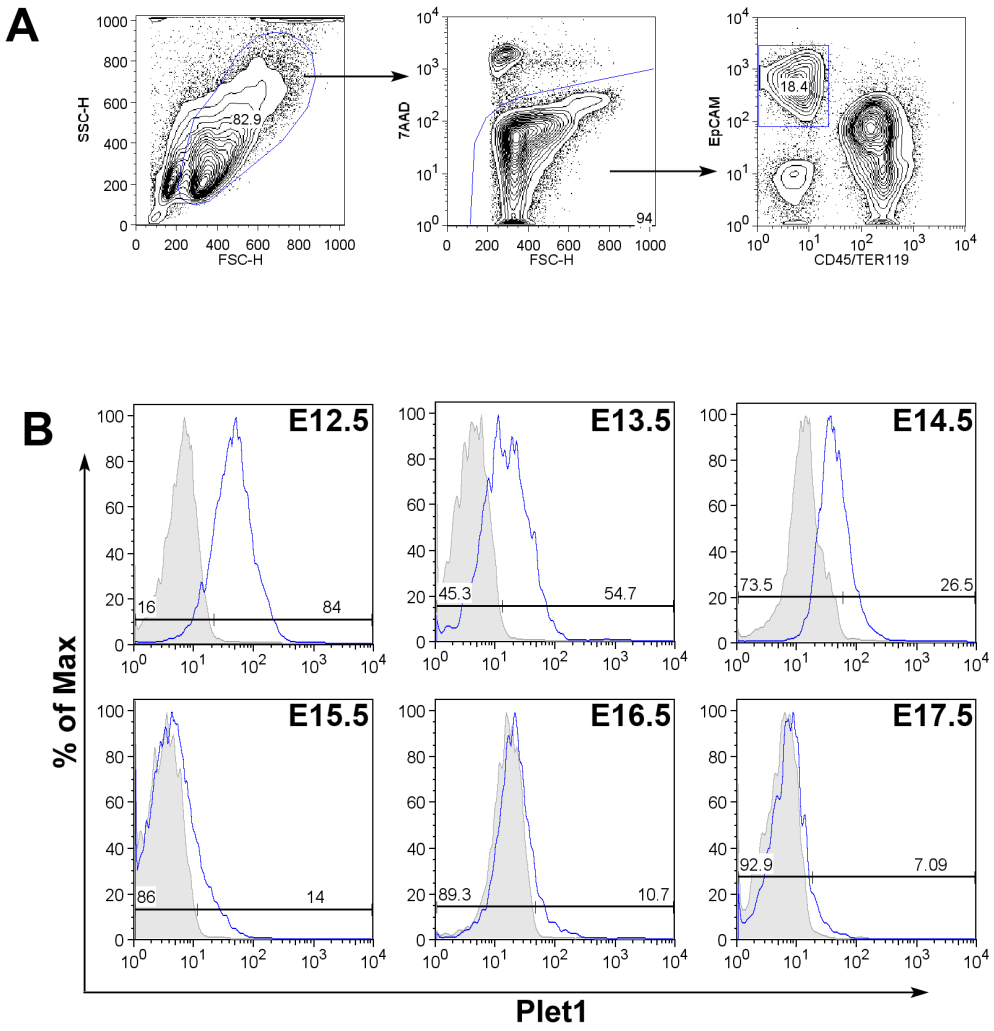

Figure 4.1 Proportion of TECs showing Plet1$^+$ staining

FACS analysis of antibody staining. In **A**, an analysis of E15.5 thymus is used to demonstrate gating procedure. Cells were selected on the basis of size and density (left), live cells were 7AAD$^-$ (centre), and TECs were identified as being EpCAM$^+$/CD45$^-$/TER119$^-$ (right) (**A**). Panel **B** shows Plet1 (MTS20) staining for E12.5 to E17.5 TECs, compared to isotype-matched controls (shown in grey). Examples are representative of at least 3 independent experiments.

Table 4.1 Proportion and number of Plet1$^+$ and Plet1$^-$ thymic epithelial cells from E12.5 to E17.5

Embryo Age	Plet1$^+$ % of TEC	SD±	Plet1 status	Number of TEC (x10^3)	±SD (x10^3)
12.5	88.7	4.1	+	5.9	0.5
			-	1.1	0.1
13.5	66.2	15.6	+	7.1	1.3
			-	6.5	0.7
14.5	23.3	6.1	+	6.6	1.1
			-	20.0	4.7
15.5	18.1	4.2	+	7.1	1.2
			-	35.8	2.8
16.5	12.8	3.6	+	7.1	1.4
			-	65.2	9.7
17.5	6.5	0.8	+	7.2	2.0
			-	121.8	5.8

Dissociated thymus lobes were stained with antibodies against CD45, TER119, EpCAM and Plet1 (MTS20), and analysed by flow cytometry. For gating, see Figure 4.1. Data and standard deviation (±SD) represents at least 3 independent experiments.

Table 4.2 No significant difference in Plet1$^+$ population size

Source of Variation	df	SS	MS	F	P-value
Between Groups	5	5,129,907	1,025,981	0.655	0.662
Within Groups	18	28,212,756	1,567,375		
Total	23	33,342,664			

One-way ANOVA analysis of Plet1$^+$ TEC number between E12.5 and E17.5, using data summarised in Table 4.1. df = degrees of freedom; SS = sum of squares; MS = mean square (SS/df); F = *F* ratio (MS between groups/MS within groups). P-value = probability of significant difference between groups (<0.05 is significant). Calculated using Microsoft Excel.

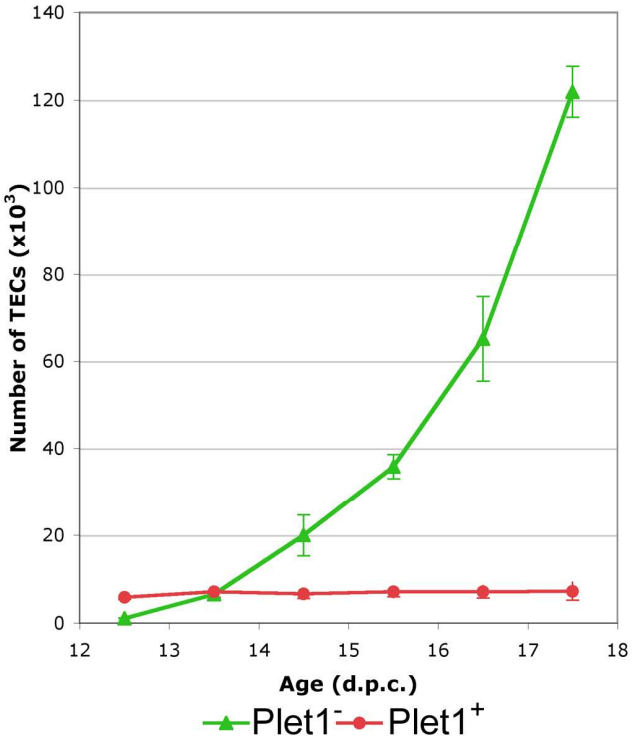

Figure 4.2 Actual numbers of Plet1$^+$ vs. Plet1$^-$ TECS from E12.5 to E17.5

Cell numbers were calculated by applying the percentage of Plet1$^+$ or Plet1$^-$ TECs to the number of TECs (EpCAM$^+$CD45$^-$TER119$^-$) per lobe for each separate experiment. Plet1$^+$ TECs represented by red circles, Plet1$^-$ TECs represented by green triangles. Error bars represent standard deviation.

4.2.3. Analysis of apoptosis in foetal thymic epithelial cells

Before an attempt at dissecting the kinetics of TEC proliferation could be made, levels of apoptosis needed to be examined. This was necessary because an under-estimate of cell proliferation would be made if significant apoptosis was present within the developing TEC population, but not taken into account.

Fluorescently conjugated Annexin V (AV) protein was used, in combination with 7AAD, to detect apoptotic cells. Phosphatidylserine (PS), a negatively charged phospholipid, is normally present in the inner, cytoplasmic leaflet of the plasma membrane (Op den Kamp, 1979). In dying cells, PS is translocated to the outer, external layer of the membrane (Fadok et al., 1992). AV binds to PS, in a Ca^{2+}-dependent manner (Andree et al., 1990).

Use of an intercalating dye (7AAD in this instance) enables distinction between apoptotic and necrotic cells. Translocation of PS to the cell surface marks one of the first stages of apoptosis, during which time the plasma membrane is still intact and can exclude 7AAD. Necrosis, however, involves an early loss of integrity in the plasma membrane and results in the inability to exclude this dye. Therefore, cells in early apoptosis are $AV^{+}7AAD^{-}$, whilst necrotic/dead cells are $AV^{+}7AAD^{+}$ (Vermes et al., 1995).

The proportion of TECs involved in apoptosis was examined at 24h intervals from E12.5 until E17.5, as described in Figure 4.3. The results are summarised in Table 4.3. It was seen that the level of apoptosis within the TEC population remained low throughout the period of thymus ontogeny. Between 2.6% and 5.8% of TEC were seen to be in the early stages of apoptosis at each time point, with a mean of 4.3%. This degree of apoptosis was judged as insufficient to be taken into account when modelling the growth of the TEC compartment. Necrotic/dead cells were approximately the same between experiments, and were attributed to the enzymatic digestion and mechanical dissociation processes used here to give a single-cell suspension for flow cytometry.

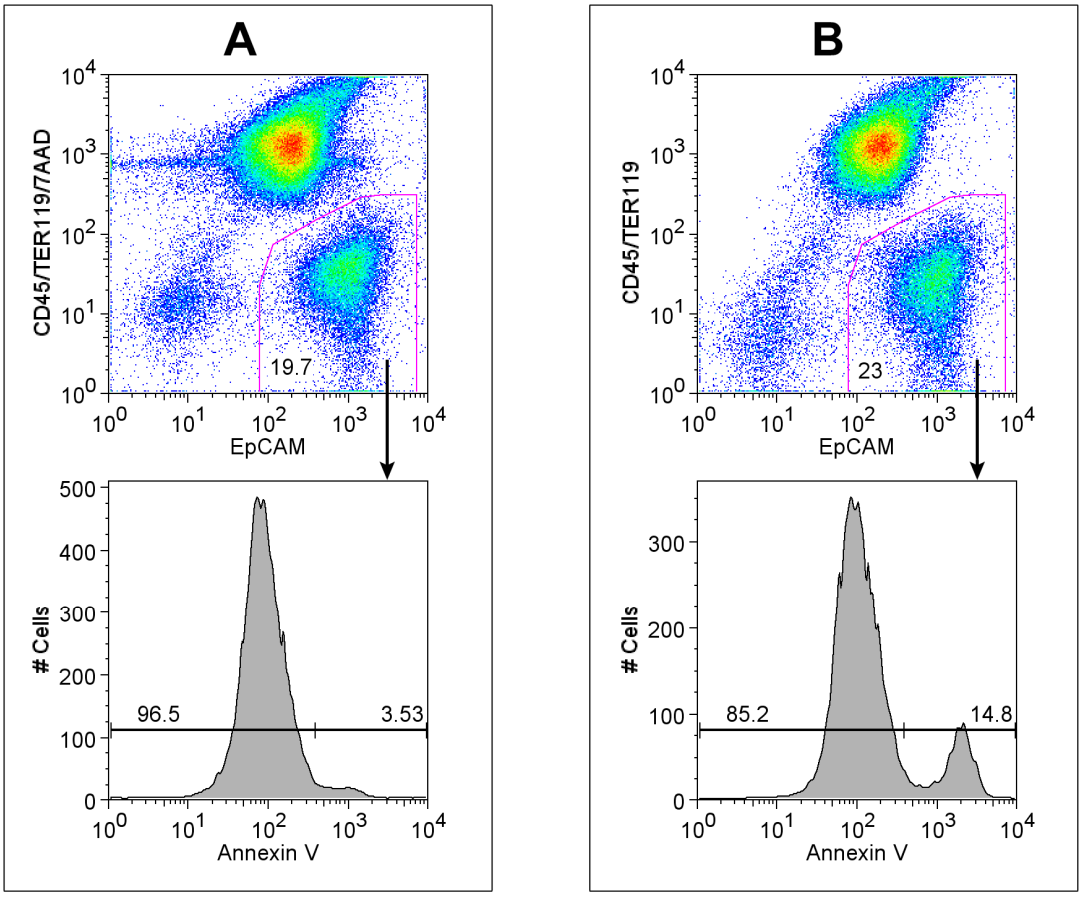

Figure 4.3 Apoptosis within TEC population

Flow cytometric analysis of epithelial cells undergoing apoptosis and necrosis. This figure shows a typical experiment, using E15.5 thymus as an example.

TEC were gated as $EpCAM^{+}CD45^{-}TER119^{-}$. 7AAD is in the same detection channel as CD45/TER119, enabling necrotic/dead cells to be excluded at the same time as these markers (**A**, top panel). Viable TEC were then examined for Annexin V (AV) staining (**A**, bottom panel).

As a positive control to confirm the position of AV^{+} cells, $EpCAM^{+}CD45^{-}TER119^{-}$ TECs were selected without the addition of 7AAD (**B**, top panel). This allows the inclusion of AV^{+} necrotic/dead cells in the gated TEC population. Consequently, a larger AV^{+} peak appears on the histogram in **B** - confirming that the gate in **A** is in the correct position to identify cells in early apoptosis.

Table 4.3 Proportion of TEC undergoing apoptosis from E12.5 – E17.5

Embryo Age	Repeats (n)	Mean AV^+ % of TEC
12.5	2	4.9
13.5	2	2.6
14.5	2	4.6
15.5	2	3.6
16.5	1	4.2
17.5	1	5.8
	Mean	4.3
	±SD	1.1

Dissociated thymus lobes were stained with antibodies for EpCAM, CD45 and TER119. Cell viability and apoptosis were detected using 7AAD and fluorescently conjugated Annexin V. Cells analysed by flow cytometry, for gating procedure see Figure 4.3.

4.2.4. Analysis of DNA content to investigate proportions of Plet1$^+$ and Plet1$^-$ TECs involved in proliferation

In order to further examine the kinetics underlying thymic epithelial proliferation and expansion, it was decided to investigate the proportions of the Plet1$^+$ TEC and Plet1$^-$ TEC populations that were actively involved in cell proliferation – achieved by analysing cellular DNA content. Cells were sorted by flow cytometry, whereupon Plet1$^+$ and Plet1$^-$ non-haematopoietic populations were separated and collected (Figure 4.4A-C). Sorted cells were subsequently fixed and permeabilized. Within these samples, epithelial cells were identified as those showing staining with a pan-cytokeratin (PanK) antibody (Figure 4.4D). Samples were incubated with 7AAD intercalating dye, in order to quantify the amount of DNA present in each cell. Flow cytometric analysis then allowed an estimation of the proportion of cells in G_1/G_0 phase, S phase, or G_2/M phases of the cell cycle (Figure 4.5). Cells found to be in either S phase or G_2/M phases were grouped together as '$S/G_2/M$', i.e. actively proliferating. These data are summarised in Table 4.4, and graphically in Figure 4.6. It was seen that the proportion of cells in $S/G_2/M$ phases ('proliferating') was significantly higher in the Plet1$^+$ TEC population than in the Plet1$^-$ TEC population, from E12.5 to E15.5. In Plet1$^+$ TECs, around 40% of cells were seen to be in $S/G_2/M$ at E12.5. This increased to a peak of 53% at E13.5, followed by a decrease to 50%, 35% then 18% at E14.5, E15.5 and E16.5 respectively. In Plet1$^-$ TECs, the proportion of $S/G_2/M$ cells also peaked at E13.5 (around 44%) after an increase from 30% at E12.5. As in Plet1$^+$ TECs, a decrease in the proportion of $S/G_2/M$ cells was observed – to 33% at E14.5 and 21% at E15.5. By E16.5, the proportion of $S/G_2/M$ cells was equivalent in both Plet1$^+$ and Plet1$^-$ TEC populations (around 17-18%). This continued to be the case at E17.5, where a similar proportion of $S/G_2/M$ cells were observed (16-17%).

One caveat of this analysis is that cells in either G_1 or G_0 are indistinguishable from each other. This means that any cells in G_1 gap phase are not taken into account by these experiments. Consequently, it can be considered that in every sample, by a similar degree, there is a higher proportion of cells in cycle than might be obvious from this assay. However, the main point of this analysis was to allow differences

between samples to be detected – something that would not be duly affected by this issue.

Figure 4.4 Strategy used to purify Plet1$^+$ TECs and Plet1$^-$ TECs by flow cytometric sorting

See following page.

Cells from dissociated whole thymus were stained with antibodies and sorted using flow cytometry. Live cells were gated on the basis of size and 7AAD uptake; from these, non-haematopoietic (NH) cells were gated as being CD45$^-$/TER119$^-$ (**A**). Gates were then set to separate NH cells into Plet1$^+$ and Plet1$^-$ populations, using MTS20 antibody and an isotype matched control (**B**). These NH Plet1$^+$ and Plet1$^-$ populations were sorted and collected, then analysed to check purity was above 95% (**C**). Collected cells were fixed and permeabilized, whereupon TECs were identified by further staining for pan-cytokeratin (PanK), in comparison to an isotype control (**D**). E14.5 cells are used here as a demonstration of procedure.

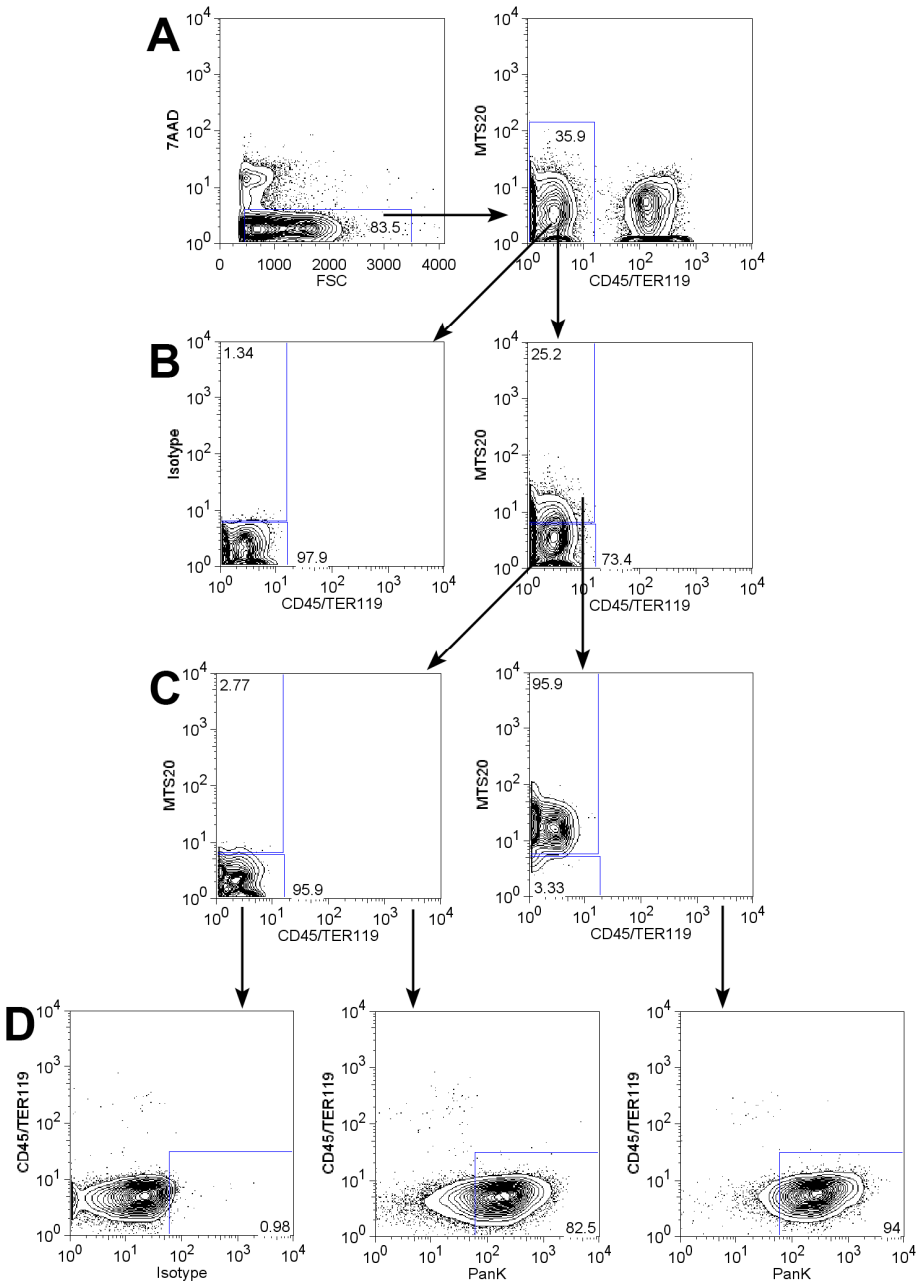

Figure 4.4 Strategy used to purify Plet1^{+} TECs and Plet1^{-} TECs by flow cytometric sorting

For legend, see previous page.

Figure 4.5 Cell-cycle analysis of purified Plet1$^+$ and Plet1$^-$ TECs using quantification of DNA content

See following page.

Sorted Plet1$^+$ or Plet1$^-$ TECs (for sort criteria, see Figure 4.4) were fixed, permeabilized and incubated with 7AAD, so as to quantify DNA content by flow cytometry. A cell cycle analysis platform in FlowJo (Treestar inc.) software was used to determine proportion of cells in G_1/G_0, S, or G_2/M phases of the cell cycle.

Representative examples of at least 3 independent experiments are shown for each time point. Red (Plet1$^+$) or green (Plet1$^-$) histograms indicate the actual levels of 7AAD detected by flow cytometry. Blue overlaid peaks on each graph represent different phases in the cell cycle, calculated by the software, as indicated in the top left panel (E12.5, Plet1$^+$). '%G1' marks cells in G_1/G_0 phases, '%S' marks cells in S phase and '%G2' marks cells in G_2/M phases.

Cell cycle analysis using quantification of DNA content

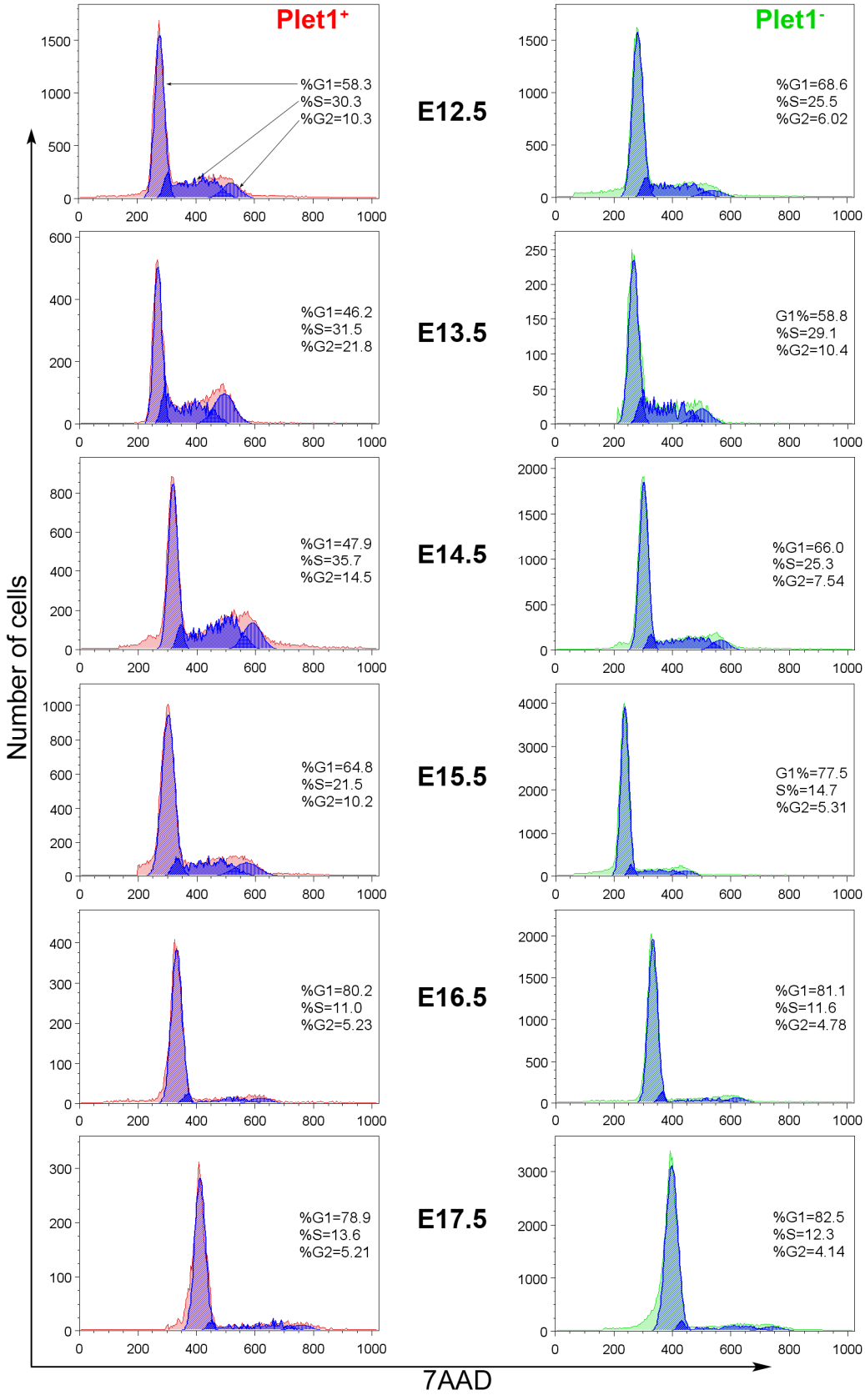

Table 4.4 Proportion of Plet1$^+$ and Plet1$^-$ TECs in different phases of the cell cycle

		Plet1$^+$ TEC				Plet1$^-$ TEC				
Age	**Statistic**	**% in G_1/G_0**	**% in S**	**% in G_2/M**	**% in S/G_2/M**	**% in G_1/G_0**	**% in S**	**% in G_2/M**	**% in S/G_2/M**	**P=**
12.5	Mean	58.2	29.9	11.3	41.2	70.5	22.1	7.3	29.4	0.001
	SD±	2.1	1.3	1.1	2.1	3.1	3.0	1.3	3.2	**
13.5	Mean	44.2	35.6	19.6	53.4	55.5	32.2	11.5	43.7	0.003
	SD±	4.7	3.2	4.7	2.8	3.2	2.7	1.7	3.6	**
14.5	Mean	49.2	33.5	15.4	48.9	67.2	24.0	8.7	32.7	0.000
	SD±	3.3	3.7	1.3	2.8	2.7	1.8	1.7	1.6	**
15.5	Mean	65.4	24.6	10.8	35.4	79.4	15.5	5.6	21.1	0.000
	SD±	4.1	3.0	1.7	3.0	4.4	2.3	1.0	2.4	**
16.5	Mean	82.7	12.0	6.1	18.1	82.2	12.4	5.0	17.4	0.644
	SD±	1.6	0.8	1.4	2.0	1.0	1.3	0.2	1.3	
17.5	Mean	80.6	10.9	5.9	16.8	83.4	11.4	4.5	15.9	0.601
	SD±	3.6	2.6	1.0	2.9	2.5	1.0	0.4	0.7	

Dissociated thymus lobes were stained with antibodies against CD45, TER119 and Plet1 (MTS20) and sorted by flow cytometry (Figure 4.4). Sorted cells were stained with anti-pan-cytokeratin and 7AAD. DNA content of cells was ascertained by flow cytometry, cell cycle phase proportions calculated by FlowJo software (Figure 4.5). Data are representative of at least 3 independent experiments. P values were calculated from the percentages of cells in S/G_2/M, using a non-paired, 2-tailed *t* test. Values were expected to have a normal distribution, although small sample size (n=3 to 7) prevented this from being proved. Highly significant differences, where $P<0.01$ are indicated by asterisks (**).

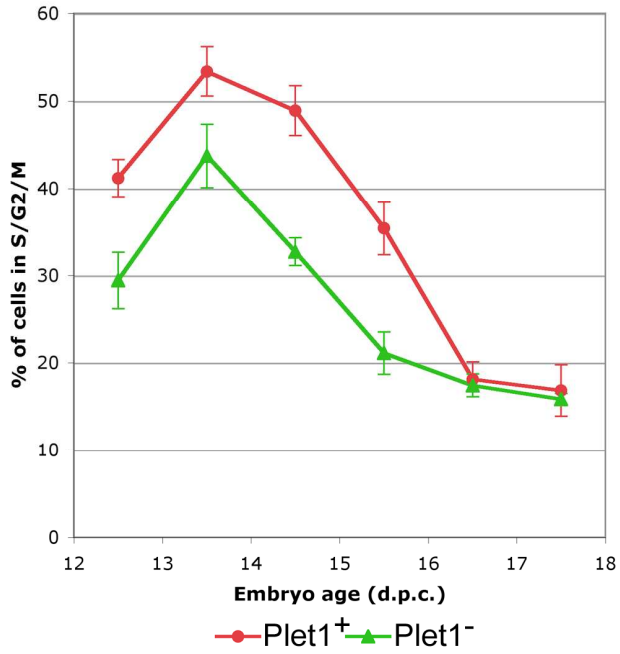

Figure 4.6 A consistently higher proportion of Plet1$^+$ than Plet1$^-$ cells are involved in cell cycle from E12.5 until E15.5

Compiled results of DNA content analysis, as described in Figure 4.5 and summarised in Table 4.4. This graph displays the percentage of TECs that were calculated to be in the S, G_2 or M phases of the cell cycle. Plet1$^+$ TECs are represented by red circles, Plet1$^-$ TECs by green triangles. Data points represent the mean of at least 4 independent experiments. Error bars represent ± standard deviation.

4.2.5. Absolute numbers of S/G_2/M Plet1$^+$ and Plet1$^-$ thymic epithelial cells

The data obtained from DNA content analysis was subsequently used to ascertain the absolute numbers of Plet1$^+$ or Plet1$^-$ TECs that were in S/G_2/M or G_1/G_0. To calculate these figures, the absolute numbers of Plet1$^+$ or Plet1$^-$ TECs calculated to be in the thymus (Table 4.1) were applied to the proportion of Plet1$^+$ or Plet1$^-$ TECs that were adjudged to be in either G_1/G_0 phase ('non-proliferating') or S/G_2/M phases ('proliferating') (Table 4.4). Results are summarised in Table 4.5, and represented graphically in Figure 4.7. Strikingly, the number of S/G_2/M Plet1$^+$ cells appears to reduce from a peak of around 4,000 per lobe at E13.5 to less than 1,300 at E16.5. This is accompanied by an increase in the number of G_1/G_0 Plet1$^+$ TECs, from a basal level in the region of 3,300 ±160 cells at E12.5-E14.5 up to over 5,800 by E16.5. As expected, by far the greatest increase during the developmental stages examined was in G_1/G_0 Plet1$^-$ TECs, most of which can be deemed as post-mitotic, and upon the path to terminal differentiation. Interestingly, however, there was also a large increase in the number of Plet1$^-$ TECs in S/G_2/M. From initially only around 300 at E12.5, the number of S/G_2/M Plet1$^-$ TECs sees a near ten-fold increase to just under 2,900 by E13.5. This population doubles in the next 24 hours to over 6,500 cells, and again in the next 48 hours to around 11,000. By E17.5 there were seen to be approximately 20,000 S/G_2/M Plet1$^-$ epithelial cells in each thymus lobe – accounting for almost 94% of 'proliferating' TECs.

As stated earlier in this chapter, due to the inability to distinguish between G_1 and G_0 cells by this method, the number of 'proliferating' TECs will be an underestimate, and the number of 'non-proliferating' TECs will be an overestimate.

Table 4.5 Actual numbers of Plet1$^+$ or Plet1$^-$ TECs in G_1/G_0 or $S/G_2/M$ phases of the cell cycle

Embryo age	Plet1 status	Mean % G_1/G_0 (1)	SD±	Mean % $S/G_2/M$ (2)	SD±	Absolute # TEC (x10^3) (3)	±SD (x10^3)	Absolute # TEC in G_1/G_0 (x10^3) (1x3)	±SD (x10^3)	Absolute # TEC in $S/G_2/M$ (x10^3) (2x3)	±SD (x10^3)
12.5	+	58.2	2.1	41.2	2.1	5.90	0.50	3.43	0.36	2.43	0.26
	-	70.5	3.1	29.4	3.2	1.08	0.06	0.76	0.07	0.32	0.03
13.5	+	44.2	4.7	53.4	2.8	7.11	1.26	3.14	0.70	3.79	0.78
	-	55.5	3.2	43.7	3.6	6.51	0.69	3.62	0.50	2.85	0.41
14.5	+	49.2	3.3	48.9	2.8	6.61	1.06	3.25	0.63	3.23	0.61
	-	67.2	2.7	32.7	1.6	19.97	4.66	13.43	3.50	6.53	1.63
15.5	+	65.4	4.1	35.4	3.0	7.12	1.17	4.65	0.96	2.52	0.49
	-	79.4	4.4	21.1	2.4	35.83	2.77	28.46	3.46	7.56	0.77
16.5	+	82.7	1.6	18.1	2.0	7.08	1.40	5.85	1.25	1.28	0.28
	-	82.2	1.0	17.4	1.3	65.15	9.71	53.53	8.50	11.35	1.84
17.5	+	80.6	3.6	16.8	2.9	7.23	2.04	5.83	1.86	1.22	0.38
	-	83.4	2.5	15.9	0.7	121.85	5.79	101.66	7.41	19.32	1.05

Dissociated thymus lobes were stained with antibodies to identify numbers of Plet1$^+$ and Plet1$^-$ thymic epithelial cells present at daily intervals from E12.5 to E17.5 (from Table 4.1). These data were combined with DNA content analysis (from Table 4.4) to calculate the number of Plet1$^+$ and Plet1$^-$ TECs that were either in the G_1/G_0 or $S/G_2/M$ phases of the cell cycle, as indicated by column numbers in parenthesis. Errors were calculated by adding the proportional standard deviations (±SD) from both sets of data.

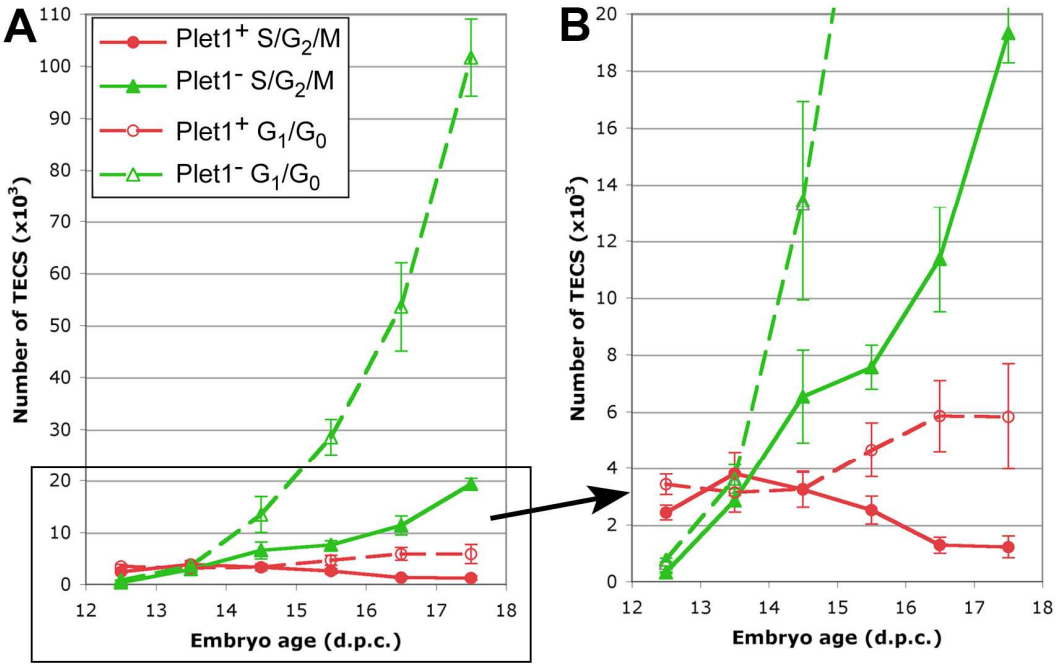

Figure 4.7 Absolute numbers of Plet1$^+$ vs. Plet1$^-$ TECs involved in cell cycle between E12.5 and E15.5

Graphs display values calculated in

Table 4.5, where flow cytometric data for the absolute number of Plet1$^+$ and Plet1$^-$ TECs were combined with data on the proportion of either population adjudged to be involved in the cell cycle.

Graph **B** is a close-up of the boxed area of graph **A**, included in order to show a clearer view of the differences between the Plet1$^+$ G_1/G_0, Plet1$^+$ $S/G_2/M$ and Plet1$^-$ $S/G_2/M$ populations.

Plet1$^+$ cells in G_1/G_0 represented by red, filled circles and solid line. Plet1$^+$ cells in $S/G_2/M$ represented by red, open circles and dotted line. Plet1$^-$ cells in G_1/G_0 represented by green, filled triangles and solid line. Plet1$^-$ cells in $S/G_2/M$ represented by green, open triangles and dotted line. All data points are representative of at least 3 independent experiments. Error bars represent ± standard deviation.

4.2.6. Possible modes of Plet1$^+$ TEC proliferation and cell cycle kinetics

Because it is known that the number of Plet1$^+$ cells in the thymus remains constant between E12.5 and E17.5 (Figure 4.2), that at least a proportion of these are proliferating at any one time (Figure 4.6), and that apoptotic cell death is minimal (Figure 4.3), possible modes of Plet1$^+$ TEC proliferation can be examined. The basic choice to be made between models is whether a Plet1$^+$ cell divides in a symmetric or an asymmetric manner (Figure 4.8). In symmetric division, a Plet1$^+$ TEC would give two Plet1$^+$ progeny. If asymmetric division were to occur, one Plet1$^+$ daughter and one Plet1$^-$ daughter would be produced. The main difference between these models is how the fate of the two daughter cells is decided.

Since the number of Plet1$^+$ cells remains constant throughout the stages of development examined, it follows that an average of half of all Plet1$^+$ daughter cells produced must switch to a Plet1$^-$ lineage for the symmetrically dividing model to be true (Figure 4.8A). If both daughter cells are identical after mitosis of their parent, this lineage decision must be regulated by external factors – in effect, the 'niche' in which the cells now find themselves. In a 3-dimensional, unpolarized stroma such as the developing thymus, it is difficult to imagine how this phenotypic switch could be controlled with sufficient accuracy as to maintain a constant number of Plet1$^+$ cells.

Conversely, if Plet1$^+$ TECs divide in an asymmetric fashion, then a mechanism to regulate the number of Plet1$^+$ cells is already in place (Figure 4.8B). The result of this model is self-renewal, whereby every dividing Plet1$^+$ parent cell will produce one Plet1$^+$ daughter identical to itself, and one Plet1$^-$ cell.

Consequently, it seems much more likely that Plet1$^+$ cells divide in an asymmetric, self-renewing manner as this provides the best explanation of how a consistently sized population of these TECs may be maintained.

Assuming that asymmetrical Plet1$^+$ TEC division does indeed occur, two different scenarios can be envisaged with respect to cell cycle kinetics. These must fit with the data on proportions of Plet1$^+$ TEC in S/G_2/M (Figure 4.6).

In the first scenario, (Figure 4.9A), an increasing proportion of the Plet1$^+$ population enters quiescence as thymus ontogeny proceeds - leaving a smaller and smaller number of actively proliferating Plet1$^+$ cells ('non-uniform' proliferation).

In a second scenario (Figure 4.9B), most Plet1$^+$ cells continue to proliferate during thymus ontogeny, but the period between divisions increases such that a smaller proportion of cells are in S/G_2/M at any one time ('uniform' proliferation).

4.2.7. Analysis of embryonic TEC division using labelled nucleotides

To distinguish between the two possible models of Plet1$^+$ cell cycle kinetics mentioned above (i.e. uniform vs. non-uniform proliferation, Figure 4.9), an *in vivo* DNA double-labelling technique using pulses of halogenated thymidine analogues was attempted. Pulse labelling allows identification of any cells undergoing DNA replication during a specific time window, in contrast to the 'snapshot' of proliferative activity provided by 7AAD staining alone in Section 4.2.4.

In double labelling, a pulse of 5-iodo-2'deoxyuridine (IdU) is followed by a pulse of 5-chloro-2'deoxyuridine (CldU). IdU was used in the primary labelling since it is less genotoxic than CldU (S. Tajbakhsh and P. Rocheteau, Pasteur Institute, Paris; personal communication). IdU and CldU can be distinguished by two anti-BrdU antibodies; one of which also has high affinity for IdU but not CldU, and the other vice versa (Aten et al., 1992, Bakker et al., 1991).

Double labelling occurs where a cell participates in S phase during the first (IdU) and the second (CldU) pulses. In the non-uniform proliferation model, shown in Figure 4.9A, a large number of Plet1$^+$ cells bearing the first label but not the second would be expected, with these cells having entered quiescence. A smaller number of Plet1$^+$ TEC would continue to proliferate through to the second pulse, with these bearing both first and second labels.

In the uniform proliferation model (Figure 4.9B), it would be expected that all or most Plet1$^+$ TEC would be double-labelled. However, this would be dependent on the second pulse being long enough to catch all cells of the proliferative compartment in S phase.

It was decided to time the first pulse to finish at E14.5, as the proportion of $Plet1^+$ TEC proliferating at any one moment was seen to sharply decrease with time from thereon (Figure 4.6). To find the optimum labelling duration (the minimum pulse time required to give the maximum proportion of labelled cells) leading up to E14.5, a series of 5-bromo-2'deoxyuridine (BrdU) pulses of differing lengths was examined (BrdU was used in place of IdU in this experiment, as it was cheaper, and already stocked in the lab). BrdU was dissolved in DPBS ('carrier'), and applied by *in vivo* injection to pregnant female mice. Pregnant mice were given a series of 5 intra-peritoneal (i.p.) injections, beginning at E12.5, of BrdU or carrier only at 12-hour intervals (see Table 4.6). Mice were sacrificed 2 hours after the final injection.

Analysis of embryos was carried out at E14.5. In all cases, embryonic thymi were dissociated and stained with antibodies, whereupon $Plet1^+$ TECs and $Plet1^-$ TECs were collected using flow cytometric sorting (see Figure 4.4). These were fixed, permeabilized and analysed for BrdU uptake (using an anti-BrdU antibody), and total DNA content (using 7AAD). Optimum pulse duration was seen to be 26 hours (3 BrdU injections), as shown in Figure 4.10, since longer pulses (38 or 50 hours, using 4 or 5 BrdU injections respectively) did not appear to increase the fraction of labelled cells.

I planned to follow up this work with IdU/CldU double labelling experiments. Unfortunately, repeated attempts to identify IdU^+ or $CldU^+$ cells with two anti-BrdU antibodies of different specificity, one reportedly IdU-specific ('anti-IdU') and one CldU-specific ('anti-CldU'), were problematic.

To test the specificity of these antibodies, equimolar concentrations of either IdU or CldU only, IdU and CldU together, or saline carrier only (negative control) were i.p. injected into pregnant wild type female mice. These animals were sacrificed 4 hours post-injection, when embryos were at the E14.5 stage.

Embryonic thymi were removed and cells dissociated, whereupon cells were fixed, permeabilized, and tested for reactivity with anti-IdU or anti-CldU antibodies by flow cytometry. However, even after careful titration the former did not appear to bind to either, whilst the latter showed non-specific binding in all samples (including

carrier-only negative control samples). Due to time constraints, it was decided not to proceed with these experiments.

However, some inferences about the proliferative behaviour of $Plet1^+$ TECs prior to E14.5 can still be made from Figure 4.10. It appears from examining the proportion of cells in the $BrdU^-$ population that between 8.48% and 17.9% of E14.5 $Plet1^+$ TEC have not proliferated since before E12.5, and remain in G_0 through to E13.5 and E14.5. In addition, it is apparent from the 26-hour BrdU pulse that around 90% of $Plet1^+$ TEC have been involved in S phase between E13.5 and E14.5.

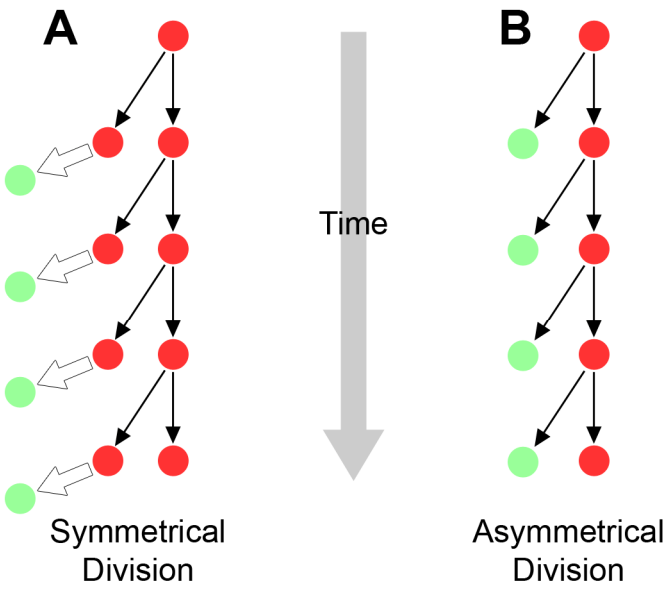

Figure 4.8 Symmetrical vs. asymmetrical division of Plet1$^+$ cells

Cartoon depicting two contrasting types of Plet1$^+$ TEC division. Red circles represent Plet1$^+$ TECs. Green circles represent Plet1$^-$ TECs. Thin black arrows show parent/daughter relationships of cells, thick white arrows represent a phenotypic change in a single cell.

If symmetrical division of Plet1$^+$ TECs were to occur (**A**), an average of half of all resulting daughter cells must switch to a Plet1$^-$ phenotype in order for the number of Plet1$^+$ cells in the thymus to remain constant.

If Plet1$^+$ TECs divide asymmetrically (**B**), the number of Plet1$^+$ cells would automatically be maintained in a self-renewing fashion.

This figure does not speculate on the behaviour of Plet1$^-$ cells once Plet1 expression has been lost.

Figure 4.9 Uniform vs. non-uniform Plet1+ TEC proliferative behaviour

See following page

Cartoon demonstrating two possible models of embryonic $Plet1^+$ TEC proliferative behaviour change. Either could explain the observation from Figure 4.6 that, as time (*t*) progresses from E12.5 to E17.5, a smaller proportion of $Plet1^+$ TEC are in S, G_2 or M phases of the cell cycle at any one moment.

Red circles indicate a representative random group of $Plet1^+$ TEC, with the cell cycle status of each cell shown to proceed in the direction of arrows from E12.5 to E17.5. Blue arrows indicate $S/G_2/M$ phase, where cells would be identified by 7AAD analysis (Figure 4.6), black arrows indicate G_1 phase and pink arrows indicate G_0. All $Plet1^+$ TEC are here assumed to divide by self-renewal, giving rise to one $Plet1^+$ daughter and one $Plet1^-$ daughter (Figure 4.8).

In **A**, non-uniform proliferation is shown. Initially most $Plet1^+$ TEC are proliferating, but as thymus ontogeny proceeds a growing proportion enters quiescence.

B demonstrates a uniform proliferation model. Here, all $Plet1^+$ begin to enter G_0 'replication refractory' periods. These refractory periods lengthen as thymus ontogeny proceeds, resulting in individual cells proliferating less frequency.

Coloured boxes represent timings of sequential IdU (green) and CldU (orange) pulses in thymidine analogue double-labelling experiments. Gap between pulses ensures no double labelling occurs during a single S phase.

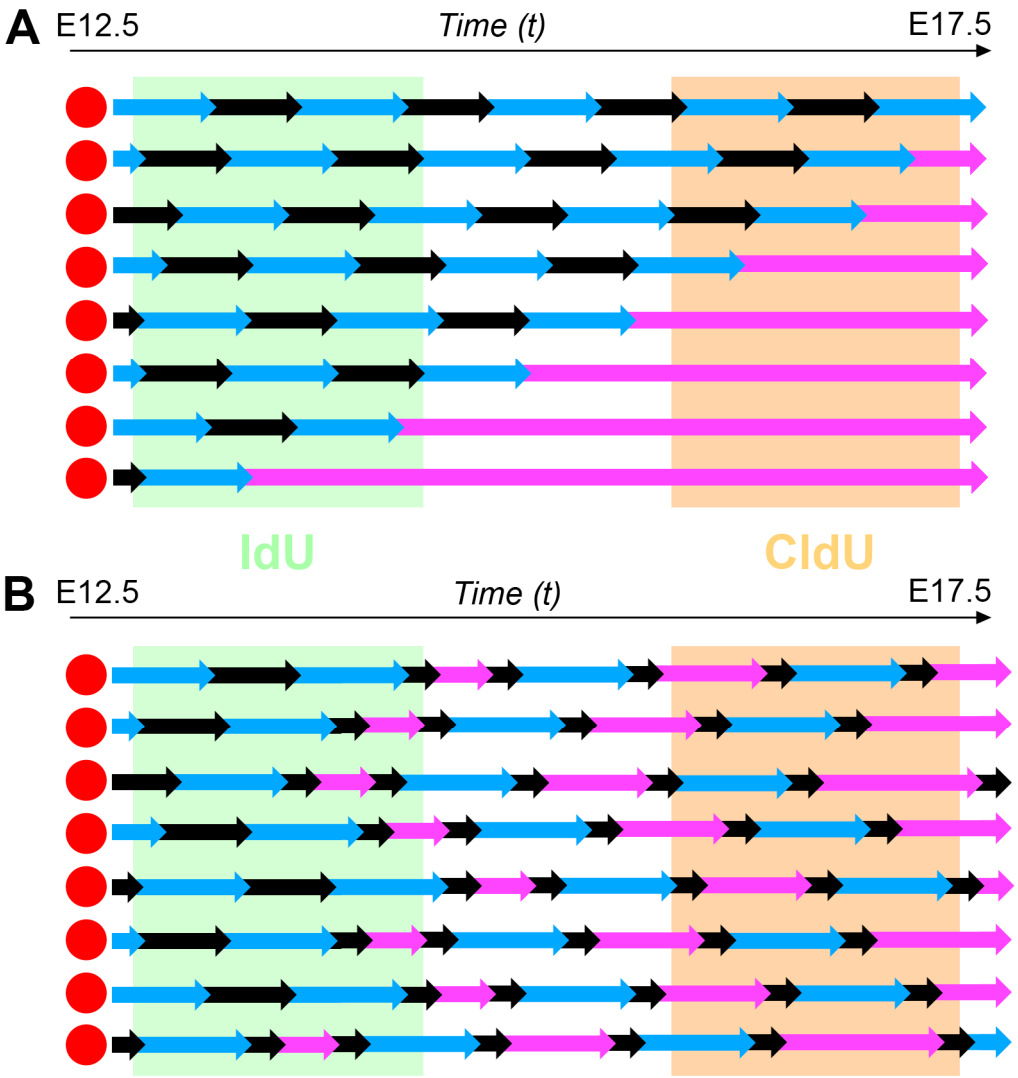

Figure 4.9 Uniform vs. non-uniform Plet1^{+} TEC proliferative behaviour

For legend, see previous page.

Table 4.6 BrdU pulse duration experimental setup

Pulse duration (h)	BrdU introduced (d.p.c.)	No. carrier only injections	No. BrdU injections
0	-	5	0
2	14.5	4	1
14	14.0	3	2
26	13.5	2	3
38	13.0	1	4
50	12.5	0	5

Groups of 3 or more pregnant mice were pulsed with BrdU for 0, 2, 14, 26, 38 or 50 hours. All groups received 5 intraperitoneal injections, beginning at E12.5 and then every 12 hours, of either carrier only, or carrier plus BrdU, as detailed above. The age at which BrdU was consequently introduced is also stated. Thymi from all embryos were harvested and processed 2 hours after final injection at E14.5. Within each group, thymi were pooled and processed in a single sample.

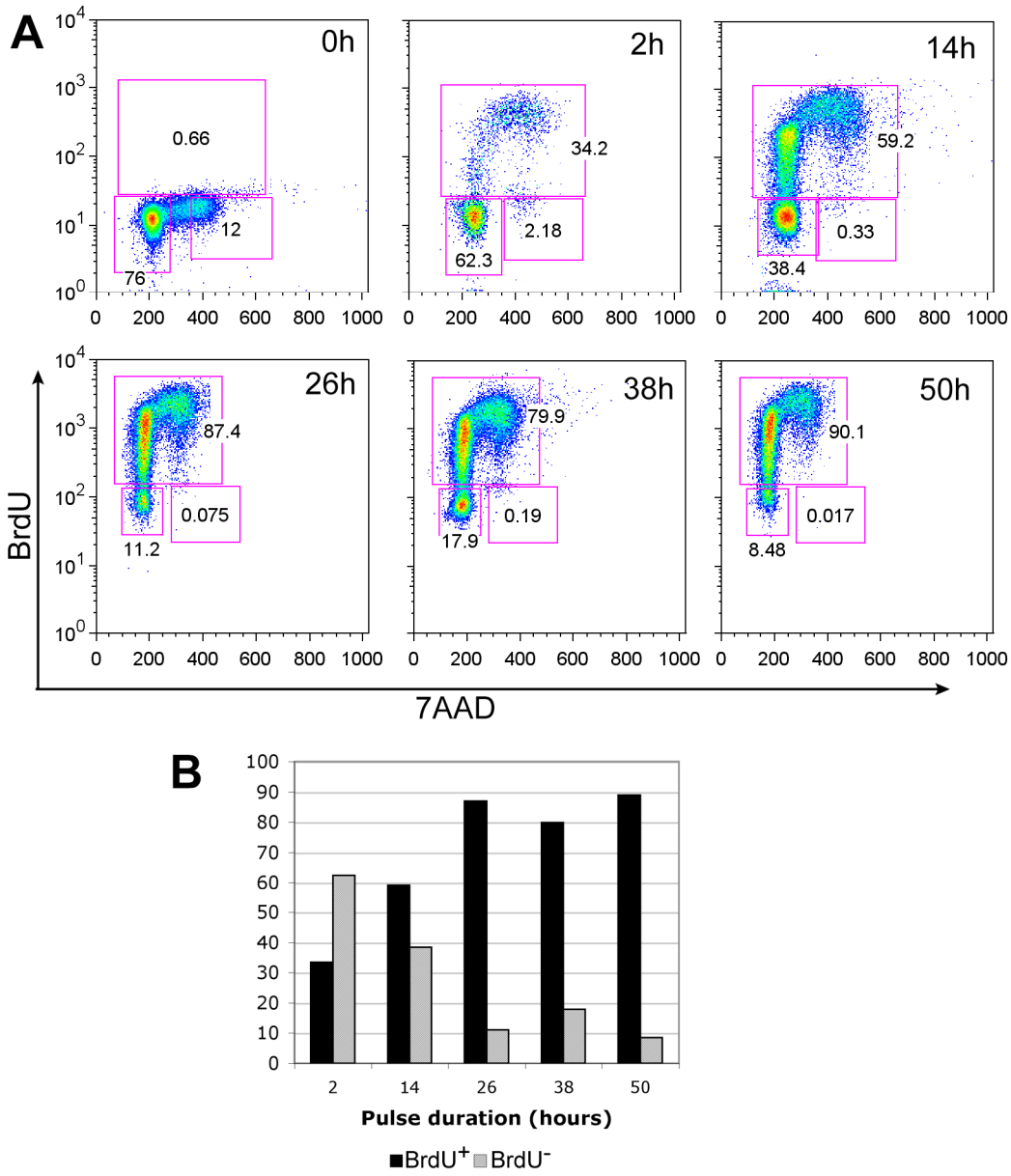

Figure 4.10 Analysis of BrdU uptake

To find the optimum pulse duration required for maximum labelling of E14.5 Plet1$^+$ TEC, intra-peritoneal injections of BrdU were given to pregnant females as detailed in Table 4.6. BrdU content was analysed in sorted Plet1$^+$ cells at E14.5.

In **A**, BrdU analysis is displayed. Cells are CD45$^-$TER119$^-$PanK$^+$MTS20$^+$ (see Figure 4.4). Data in top row (0h, 2h, 14h) and bottom row (26h, 38h, 50h) were gathered on different days.

Histogram (**B**) shows percentage of labelling achieved with each pulse duration. Black bars represent the proportion of Plet1$^+$ TEC labelled with BrdU. Grey bars indicate the proportion of Plet1$^+$ TEC that were unlabelled and remained in G_0. N=1.

4.3. Discussion

I analysed the proportion of TECs staining for Plet1, an extra-cellular antigen marking a population of foetal thymic epithelial progenitors, by flow cytometry (Figure 4.1).

Plet1$^+$ TECs were seen to comprise almost 90% of all TECs at E12.5. It had previously been reported that Plet1$^+$ TECs comprised around 50% of total thymic epithelium at E12.5 (Bennett et al., 2002, Gill et al., 2002). However, these studies did not take into account thymic mesenchyme, which makes up a substantial proportion of thymus cellularity at E12.5 (see Chapter Three of this thesis) and which would have been included in their 'total epithelial' populations.

I found the Plet1$^+$ proportion of TECs to steadily reduce on a daily basis, comprising around 18% at E15.5. Gill and colleagues reported Plet1$^+$ cells to be 25% of the total CD45$^-$ population. Although not an enormous difference, this discrepancy might be accounted for by improvements in dissociation technique. It is likely that differentiated Plet1$^-$ TECs (especially delicate, stellate cTEC) were more prone to cell death than undifferentiated Plet1$^+$ TEC during older, less refined methods of dissociation. Current methods use additional enzymes, such as hyaluronidase, to break extracellular matrix attachments, and consequently are less reliant on potentially damaging mechanical force to separate cells.

When proportional data were translated into actual numbers of Plet1$^+$ or Plet1$^-$ TECs present at each day of embryonic development from E12.5 until E17.5, it was striking to observe that the number of Plet1$^+$ cells remained constant – at approximately 6,000 – 7,000 (Table 4.1, Table 4.2).

Following this observation, I decided it was important to examine whether the Plet1$^+$ TECs either continued to divide, or dropped out of the cell cycle. TEC DNA was quantified by 7AAD staining, to ascertain the percentage of Plet1$^+$ and Plet1$^-$ cells that were in S/G_2/M phase at each time point. This revealed the proliferative peak in both Plet1$^+$ and Plet1$^-$ TECs to be around E13.5. In both Plet1$^+$ and Plet1$^-$ TECs, a

steady decrease in the proportion of cells in $S/G_2/M$ was seen in each successive 24-hour period after E13.5.

It might have been expected that a higher proportion of cells would have been dividing at E12.5 than at E13.5. One possible explanation for this result is the influence of intrathymic mesenchyme. Mesenchyme-derived growth factors, FGF7 and FGF10, are known to induce epithelial proliferation (Revest et al., 2001). Mesenchymal cells penetrate inward from the periphery of the thymus lobes from around E13, resulting in closer proximity to an increased number of TECs. This could increase the proportion of the TEC population receiving proliferation-inducing signals, resulting in a larger percentage of TECs entering the cell cycle.

A recent publication, using the proliferation marker Ki67 in keratin$^+$ thymic cells, has backed up my findings on the proportion of TECs proliferating during different stages of thymus ontogeny with very similar data (Jenkinson et al., 2007).

Since there were always some Plet1$^+$ cells proliferating at each stage of organogenesis examined, and yet the Plet1$^+$ population was found to be of a constant size, it was concluded that Plet1$^+$ TECs must continually contribute to Plet1$^-$ TEC expansion throughout thymus ontogeny. Examination of TEC apoptosis levels supported this conclusion. Minimal TEC death was observed during these stages of ontogeny (Figure 4.3), indicating that all daughter cells from Plet1$^+$ TEC divisions were still present. Taken together, these findings allowed the proposal of two contrasting modes of Plet1$^+$ TEC division (Figure 4.8).

The first model is symmetrical division, where two identical Plet1$^+$ daughter cells are produced (Figure 4.8A). In order to conform to the data showing a constant population size, a symmetric division model would require external factors to cause an average of only one daughter to remain Plet1$^+$, whilst one became Plet1$^-$. This could be the case if parent cells were fixed in position, e.g. anchored to a basement membrane, and mitosis occurred in a polarised fashion (such that one daughter would move away whilst the other would remain in the 'niche' occupied by the parent cell). This concept could easily be applied in simple stratified epithelium. In the three-dimensional stroma of the embryonic thymus, however, it is not obvious how such a

mechanism may occur. The second model is asymmetrical division, where the Plet1$^+$ population is constantly maintained through self-renewal (Figure 4.8B).

Thus, the asymmetric model provides the most logical means of maintaining Plet1$^+$ TEC number. If an asymmetrically dividing model were true, occasional symmetrical division may still occur in order for homeostatic maintenance of stem/progenitor cell numbers. This has been proposed to occur in the intestinal epithelium, where mathematical modelling suggests that around 5% of stem cell divisions occur symmetrically, resulting in an ability to adjust the number of stem cells present in a single crypt (Loeffler et al., 1997).

The data showing a proportional decrease in Plet1$^+$ cell proliferation over time were applied to the corresponding absolute number of Plet1$^+$ TEC present, for each time point. From this, it is clear that as organogenesis proceeds, a smaller number of Plet1$^+$ TECs are actively proliferating. The following scenarios can here be envisaged:

A) Non-uniform replicative behaviour. A decreasing sub-population of Plet1$^+$ cells continues to proliferate, whilst the remainder enter quiescence.

B) Uniform replicative behaviour. All/most Plet1$^+$ cells remain in the cell cycle, but become increasingly slow-cycling.

Scenario A involves a Plet1$^+$ population with heterogeneous cell cycle kinetics (Figure 4.9). Most will be actively proliferating during earlier stages of organogenesis, but over time an increased number become quiescent. If this scenario is true, quiescence may be in response to presentation or withdrawal of certain undefined external mitogenic or anti-mitogenic factors. It is likely that other cells in the thymus would provide such queues. Changes in the immediate 'niche' of a Plet1$^+$ TEC, or in its wider vicinity, during thymus development may activate the triggers involved in the decision between continued proliferation or entry into quiescence.

If scenario B were true, it may be as a result of proportional changes in length of one or more phases of the cell cycle. M phase is generally consistent (around an hour) in most mammalian cell types. However, G_2 (normally 2 to 5 hours), and particularly

G_1 and S phases can be more prone to durational variation. For example, studies on the developing rat retina have indicated an increase in cell cycle length over the course of embryonic and early postnatal development, predominantly attributable to increased S phase duration (Alexiades and Cepko, 1996). Cell cycle phase time can increase for a number of reasons. For S phase, the number of replication origins and their timing can regulate duration (Holmquist, 1987). In G_1 or G_2, cells must pass checkpoints, which are partly to ensure the cell is in a physiologically fit state and prepared to proceed with the subsequent stage. If the nutritional or energetic requirements for carrying out these tasks were met with decreased efficiency, or in a less timely manner, some phases of the cell cycle may be progressively slowed (or vice versa). In the thymus, the number of epithelial cells detected to be in $S/G_2/M$ at any one time was found to decrease as thymus ontogeny proceeds (Figure 4.6). In the context of the cell cycle, it follows that this could result from an increased (G_1/G_0):$(S/G_2/M)$ ratio, i.e. prolonged G_1/G_0 or shortened $S/G_2/M$ phases.

Another explanation for scenario B may be the existence of an increasing refractory period between divisions (G_0), as indicated in Figure 4.9B. A study on β cell expansion in the mature mouse pancreas has shown such a mechanism (Teta et al., 2007). Here, the authors labelled proliferating cell DNA *in vivo* with sequential pulses of the halogenated thymidine analogues CldU and IdU. Double labelled cells were only seen in substantial numbers following 1 month and 8 month pulses of the respective analogues, whereas 1 week of CldU followed by 4 weeks of IdU yielded very few. The study concluded that most adult β cells are not postmitotic, and eventually divide more than once, but that these divisions are limited by a replication refractory period (Teta et al., 2007). The cell cycle kinetics of $Plet1^+$ TECs could be explained by an increase in replication refractory period as thymus development proceeds, resulting in an increasingly smaller fraction of cells being in $S/G_2/M$ at any one time.

Double labelling with the halogenated thymidine analogues IdU and CldU was attempted, in order to distinguish between the two models from Figure 4.9. Unfortunately this proved unsuccessful due to detection problems. However, labelling with BrdU alone was able to reveal some information. A 26-hour pulse

from E13.5 to E14.5 showed almost 90% of Plet1$^+$ TECs proliferated during this period, whilst longer pulses indicated between 8.5% and 17.9% of Plet1$^+$ TECs had not proliferated since before E12.5 (Figure 4.10).

4.3.1. Epithelial progenitor/stem cells in other tissues

In addition to the thymus, a number of other organs exhibit epithelial turnover and renewal. The nature of stem/progenitor cells that are involved in the creation and maintenance of these organs have been studied at various levels of depth and may be helpful in suggesting the models of proliferation and differentiation which occur in thymic epithelium. Unfortunately with regards to thymus development, it is mainly observations on adult tissue stem cells that have been recorded in these studies and not progenitor/stem cells involved during initial embryonic organ development. However, I decided to examine whether any mechanisms documented within these other organs may assist in the dissection of events within thymus development.

4.3.1.1. Mammary epithelium

In the mammary gland a single stem cell is able to give rise to an entire new, functional mammary epithelial network (Shackleton et al., 2006). There are two major mammary epithelial types – myoepithelial and luminal (with ductal and alveolar subtypes). In the human, progenitor cells have been identified that are luminal-restricted, myoepithelial-restricted or bipotent when cultured *in vitro* (Eirew et al., 2008, Stingl et al., 2001). Similarly, in the mouse, separate progenitor populations with varying proliferative abilities have been identified (Stingl et al., 2006). These cell types may represent a progressive restriction of epithelial lineage.

4.3.1.2. Intestinal epithelium

Similar to the steady-state mature thymus, constant epithelial turnover occurs in the intestine. Intestinal stem cells inhabit invaginations known as crypts, with the lower part of each adult crypt holding 4-6 SC (Cai et al., 1997, Potten, 1998, Roberts and Potten, 1994). These cells self-renew, and multipotent daughters produce a transit amplifying (TA) population. Around 6 generations are produced from each first generation TA progenitor cell, culminating in terminal differentiation. In the small

intestine, commitment to one of 4 epithelial lineages (enterocyte, Goblet cell, enteroendocrine cell or Paneth cell) occurs at around the third generation of the TA population (Marshman et al., 2002). First and second generation TA cells have progressively improved DNA repair abilities, but intestinal SC preferentially undergo apoptosis rather than attempt to repair damaged DNA (Potten, 1977). The number of SC present in a single crypt may subsequently be adjusted – mathematical modelling suggests that around 5% of SC divisions occur in a symmetrical manner, producing 2 SC or two TA cells, providing a means of homeostatic maintenance (Loeffler et al., 1997). Recent work has enabled the identification of an intestinal SC population as small, $Lgr5^+$ cells interspersed between Paneth cells (Barker et al., 2007, Haegebarth and Clevers, 2009).

4.3.1.3. Pancreatic epithelium

The pancreas contains three types of epithelial-derived cells – those of the pancreatic ducts, endocrine (islet) cells, and exocrine (acinar) cells. The pancreas develops initially as small buds from the endodermal epithelium, from E9.5 - at which point the epithelial cells are morphologically similar and show staining for the transcription factor *Pdx1* (Offield et al., 1996). These buds begin extending multiple branches into the surrounding mesenchyme at around E11.5. The distal tips of the nascent branching epithelium contain $Pdx1^+Cpa1^+$ multipotent progenitor cells that leave endocrine and duct progeny in their wake (Zhou et al., 2007). At approximately E14, these multipotent cells have been observed to undergo a phenotypic transition and become restricted to the exocrine lineage (Zhou et al., 2007). In contrast to medullary islets in the thymus, neither acini nor endocrine islets in the pancreas exhibit clonal growth from single cells (Percival and Slack, 1999).

Islet β-cell mass expands continually but gradually throughout adulthood (Bock et al., 2003, Butler et al., 2003, Kushner et al., 2002). Limited regeneration can occur following injury by partial pancreatectomy. However, no new islets are formed, and it has been shown that although new β-cells can be created within existing islets, these occur by self-duplication of existing β-cells rather than differentiation from a pancreatic stem cell (Dor et al., 2004). Interestingly, however, a recent study showed

that with a different injury model – partial duct ligation - a neurogenin3 (ngn3)$^{+}$ β-cell progenitor population appears (Xu et al., 2008). This seems to be analogous to the transient ngn3^{+} progenitor population seen during embryonic development, suggesting the persistence of a β-cell stem/progenitor cell into adulthood that may be reactivated under certain conditions.

4.3.1.4. Epidermal epithelium

Patterns of epithelial stem cell growth and amplification have been reasonably well characterised in the skin. Upon culture of skin keratinocytes, populations of varying proliferative ability can be identified (Barrandon and Green, 1987). The cells with the largest clonogenic potential, so-called 'holoclones', are found predominantly in the 'bulge' region of the hair follicle, below the sebaceous glands – a region rich in label-retaining cells (LRC) (Kobayashi et al., 1993, Rochat et al., 1994, Cotsarelis et al., 1990). This region contains multipotent stem cells; capable of producing not only hair follicle cells, but also giving rise to the intrafollicular epidermis (both in expanding newborn mouse skin, and in response to wounding in adult mouse skin) (Oshima et al., 2001, Taylor et al., 2000). During homeostasis, however, continual epidermal replacement is generated solely from unipotent epidermal stem cells anchored in the innermost, basal, layer (Ito et al., 2005). These have been shown to divide in an asymmetric manner, and it is thought that most or all basal layer epithelial cells may have unipotent SC abilities (Clayton et al., 2007, Lechler and Fuchs, 2005). Sebaceous glands can also be maintained from their own resident progenitors during homeostasis (Horsley et al., 2006).

Hair follicles undergo cycles of proliferation and downward expansion into the dermis (anagen), followed by degeneration (catagen) and a period of dormancy (telogen). The lowest permanent section of the hair follicle is the bulge region. When anagen occurs, transient proliferation is seen amongst the otherwise quiescent cells of the bulge (Wilson et al., 1994b). These slow-cycling cells are specified during early morphogenesis, giving rise to the adult bulge later during skin development (Nowak et al., 2008).

The existence of an additional population of Plet1$^+$ (MTS24$^+$) cells, displaying stem/progenitor–like clonogenic properties, has been recently documented (Nijhof et al., 2006). These reside directly above the bulge region of the hair follicle, in the upper isthmus, and transplant experiments suggest they are also multipotent (Jensen et al., 2008). Their relationship to bulge SC remains to be determined.

Recent work has also identified a population of faster-cycling Lgr5$^+$ bulge stem/progenitors (Jaks et al., 2008). Although most bulge cells remain active but slow-cycling during anagen the bulge remains a constant size, as their progeny leave the bulge and contribute to the growing follicle (Blanpain et al., 2004, Oshima et al., 2001).

4.3.2. Models of TEC proliferation during ontogeny

The idea of a constant sized, continually cycling population of stem/progenitor cells has been applied to intestinal crypts and to the bulge region of the hair follicle. Although developed mainly from observations in adult tissue, and not during organ development, I have tried to relate this concept to thymus ontogeny. It is conceivable, and consistent with my experimental results, that a slowly cycling Plet1$^+$ TEC population of constant size gives rise to more rapidly dividing transit amplifying (TA) Plet1$^-$ progeny. The majority of Plet1$^+$ cells would be expected to divide asymmetrically, allowing self-renewal of the stem/progenitor population. In addition, there may be a mechanism for occasional symmetrical division – this would aid in homeostatic maintenance of stem/progenitor cell numbers, and has been noted to occur in intestinal SC (Loeffler et al., 1997).

A continual increase in the total TEC population size, coupled with a continual decrease in the rate of Plet1$^+$ proliferation, suggests that post-mitotic, fully differentiated TECs are produced from a dynamic population of Plet1$^-$ TA TECs that undergo several rounds of division.

Decreased Plet1$^+$ proliferation coincides with phenotypic changes in Plet1$^+$ cells such as increased MHC class II expression, and a decreasing number of Plet1$^+$ cells co-expressing K5 and K8. It may be that progressive lineage restriction accompanies

these phenotypic changes. Alternatively, lineage restriction may occur after a number of rounds of TA cell division (as in the intestine).

Clones generated by the *laacZ* system could potentially reveal the size of any Plet1^{-} proliferative unit (i.e. from prospective first-generation TA cells until fully differentiated cortex or medulla), and also the lineage potential within these proliferative units.

Chapter 5. Results: Retrospective clonal analysis using the *laacZ* system

5.1. Introduction

5.1.1. Application of the laacZ system in thymic epithelial cells

It is known that all TECs originate from the endoderm of the 3rd pharyngeal pouch (Gordon et al., 2004). However, at the start of this project there was no reliable information as to the relationship between mTECs and cTECs during embryonic development. Do medullary and cortical lineages diverge at an early stage during thymus development, do they share a common progenitor cell until shortly before differentiation, or does a mixture of these mechanisms operate? Compilation of a TEC clone library would definitively answer this question (Figure 5.1).

It was decided to use the *laacZ* expression model under control of the ubiquitous ROSA26 promoter, resulting in detectable clones in all possible cell lineages. Antibody staining would be used to confirm the identity of any potential TEC clones.

It is important to compile a saturated clone library as far as possible, where every potential size and variety of clone is represented at least once, and additional clones would not provide extra information. In general, tissues will exhibit the longest clones (many labelled cells) rarely and shortest clones (i.e. one labelled cell) much more frequently, due to a smaller pool of ancestral cells being present at the time when longer clones would be initiated. It might be thought that long clones would originate from more distant precursors, with smaller clones being born at a more recent point in history. However, this is not necessarily the case. Large clones may originate from a population of more recent, rapidly dividing cells. Conversely, labelling of older cells that divide slowly, become dormant, or differentiate at an early stage can give rise to clones of a much smaller size. In a saturated clone library, the ratio of different clone sizes that appear can aid in deducing the modes of cell division involved in construction of a tissue.

5.1.2. Strategies for TEC clone library analysis

Firstly, modes of TEC division can be deduced by examining the frequency at which long (many labelled cells) and short (few labelled cells) clones occur. If cells divide in a symmetrical manner (Figure 5.2A), a small number of longer, older clones would be observed, with a higher frequency of shorter, younger clones (Figure 5.2B&C). Conversely, if cells were to divide in an asymmetrical, self-renewing manner, only one extra cell is produced from each round of cell division (Figure 5.2D.) In this model, there would be an equal chance of observing a clone of any given size (apart from a single-cell clone, expected to occur in half of all labellings), as demonstrated in Figure 5.2D and E. Upon grouping clones into classes of increasing exponential size however, an increase in occurrence would be observed for each size group (Figure 5.2F).

The minimum/maximum sizes and scarcity at which clones consisting entirely of cTEC or of mTEC are seen would aid in identifying size, longevity, and proliferative potential of the putative common TEPC. In order to ascertain the point in time at which common TEPCs make the transition to mTEPCs and cTEPCs (or indeed do not), the clone library can be subjected to a variety of analyses. Two of which, *crossing index* and *dual origin coefficient*, are described below.

Crossing index is a measure of clones appearing in multiple parts of a structure that has been "divided into units either arbitrarily or on the basis of morphological markers" (Petit et al., 2005). In this case there are two units - cortex and medulla. Here, the crossing index would be created using groups of clones of the same size, i.e. those containing 4 cells, those containing 5 cells etc. The crossing index would be expressed as the percentage of that clone size group crossing the medulla/cortex divide. If a particular size group has a crossing index of 0%, one can imply that no common TEPCs were present at the stage where the initial labelling of clones of that size occurred. The minimum clone size at which the crossing index is larger than 0% will point toward the most recent point in history at which a common progenitor existed. A very high crossing index would be expected to occur at some point, in a clone size corresponding to an ancestral cell capable of giving rise to all TEC types,

even if it were to occur only at a very early stage prior to formation of the thymic rudiment.

Dual origin coefficient can be calculated in order to assess proportional contribution to medulla and cortex from clones of different sizes. I have adapted this method from the "coefficient of bilaterality" used in determining left/right contribution of clones along the mediolateral axis of the presomitic mesoderm (Eloy-Trinquet and Nicolas, 2002). In the thymus, dual origin coefficient (DOC) would be defined as (nC-nM)/(nC+nM), where nC and nM are the number of labelled cTEC and mTEC cells respectively, in any given clone. DOC values would range between -1 (a clone comprising solely of medullary epithelium) and 1 (a cortex-only clone). Clones with a DOC of 0 would contribute an equal number of cells to both lineages. DOC would be plotted against clone size, thus allowing comparison within a roughly equivalent precursor pool.

Three hypothetical examples using imaginary clones are shown below to demonstrate the outcome of DOC analysis in different developmental models. Example 1 (Table 5.1, Figure 5.3A) shows a group of clones emanating from a precursor pool containing lineage-restricted TEPCs only. DOC values of either 1 or -1 are present, ruling out a bipotent progenitor at the stage these clones were born. In example 2 (Table 5.2, Figure 5.3B), all clones exhibit a dual cortical and medullary identity. These would have originated from a pool of common TEPCs retaining the potential to give rise to both cTECs and mTECs and hence displaying DOC values anywhere between -1 and 1. Example 3 (Table 5.3, Figure 5.3C) also represents clones from a bipotent precursor pool. However, most of the precursors here gave rise exclusively to cortex, with only a small number producing medulla in addition. This bias would be seen if a default TEC phenotype existed (i.e. cortex), diverging only when induced to do so in certain cells. I have included this model based partly on the finding that medullary areas are often present as "cuffs" surrounding intermediate-sized thymic vasculature (Anderson et al., 2000). It is a possibility that these medullary areas originate by differentiating from an equipotent pool of TEPCs, upon receipt of molecular stimuli associated with certain vessels, i.e. fate choice could be 'niche-dependent'. The models described above are by no means the only

possible outcomes for DOC analysis of the thymus, however they are good examples to demonstrate the usefulness of this technique.

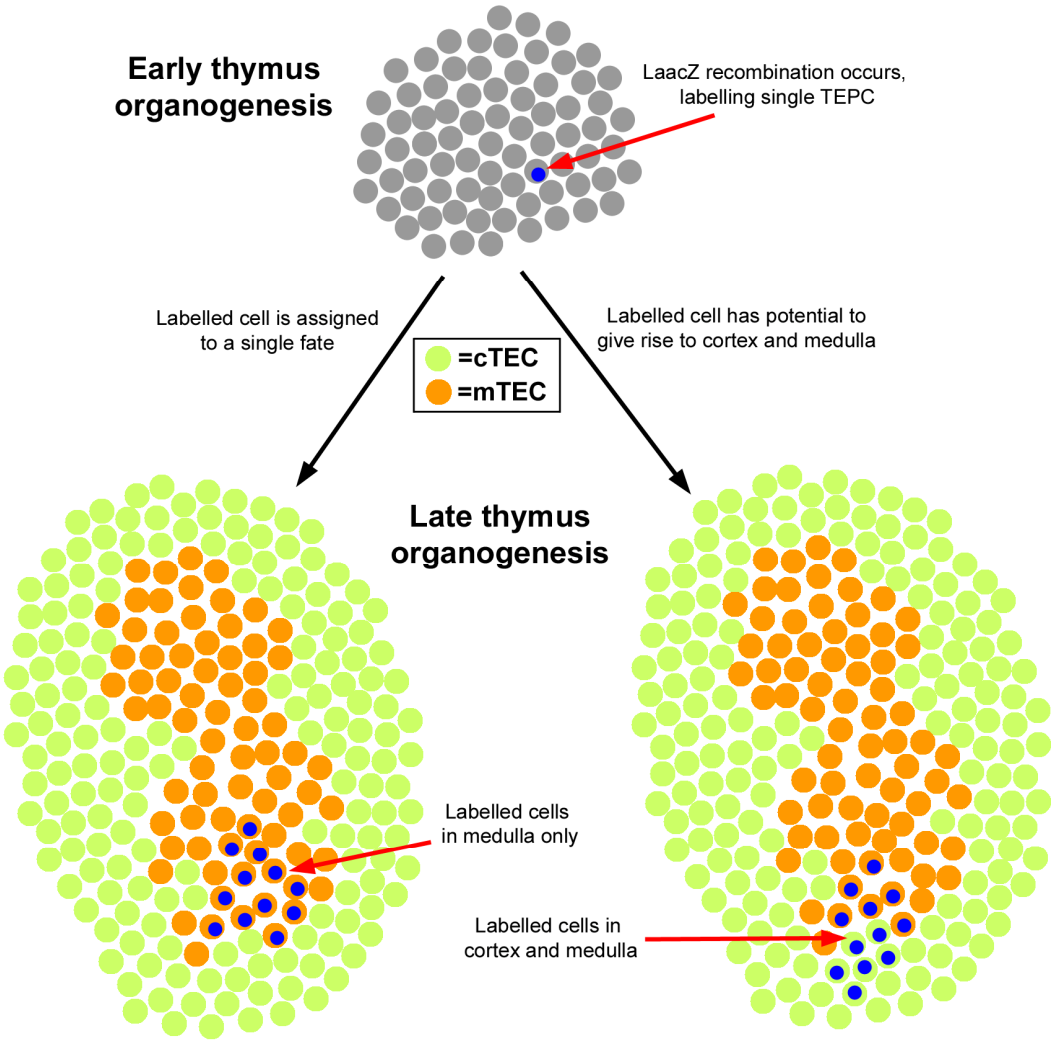

Figure 5.1 Possible outcomes of clonal analysis

Compilation of a TEC clone library would reveal the relationship between cortex and medulla. A basic example of retrospective clonal analysis is shown here. At the top, the very early thymus is represented, showing a population of epithelial progenitor cells. The developmental potential of these is unknown. A single laacZ recombination event occurs, labelling one of these TEPCs. Below are representations of two possible outcomes, following analysis of this thymus lobe at a later time point. The diagram on the left shows a clone consisting entirely of mTECs, indicating that the cell in which the laacZ recombination occurred was restricted to a medullary-only fate. Conversely, the right-hand diagram represents a clone containing both mTECs and cTECs, showing that the initial labelled cell retained the potential to give rise to medullary and cortical lineages.

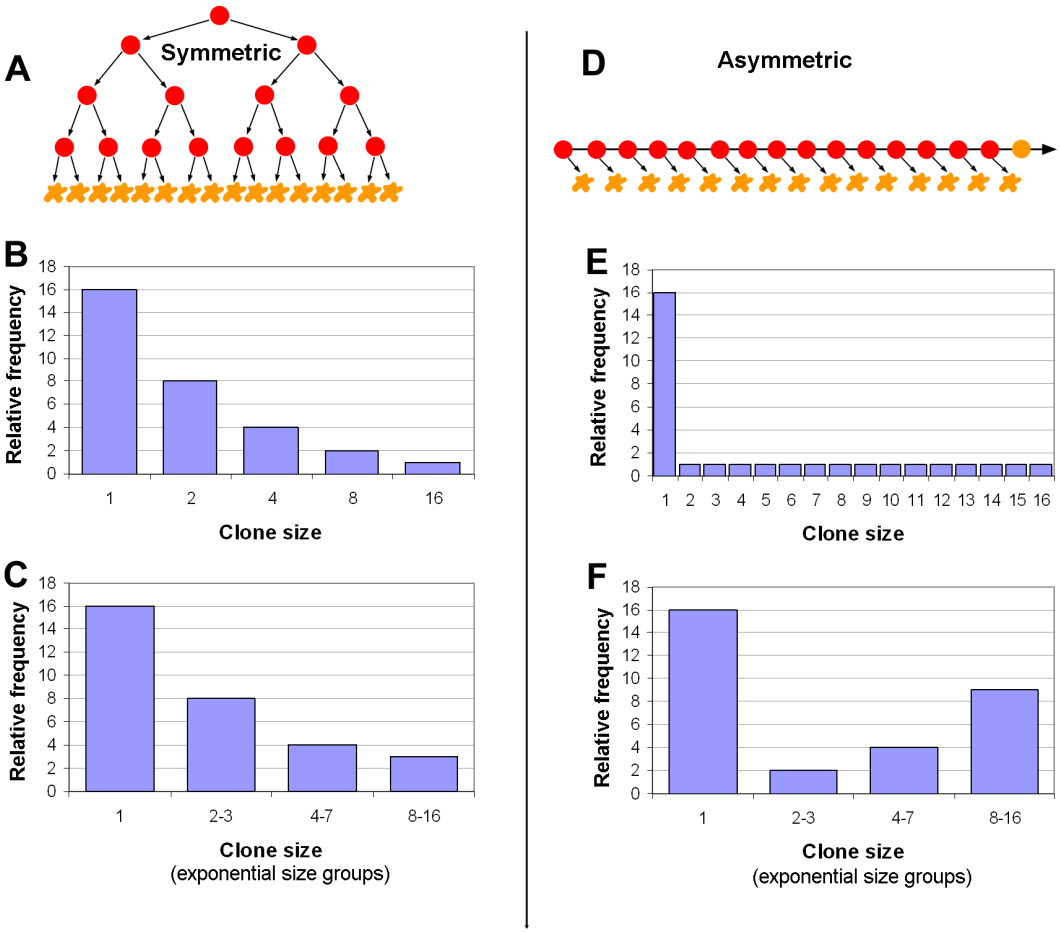

Figure 5.2 Frequency of clone sizes can indicate modes of cell division

In each of these models, imagine that a laacZ recombination has an equal chance of occurring in any cell. Cells present at the time of clone observation are shown in yellow, precursors are shown in red to indicate mode of growth. Graphs show the relative frequency expected for clones of a specified size (or group of sizes) to occur, in a population of cells with the given growth mode.

A population of progenitor cells may divide in a symmetric manner as shown in **A**. In this model, clones show a decrease in frequency as their size increases (**B**). This is seen irrespective of whether or not clones are grouped according to exponential increases in size (**C**).

In the asymmetrical model (**D**), clones comprised of one cell are most frequent; clones with more than one cell appear with lower, equal frequency (**E**). Upon grouping these clones into classes of upward exponential size however, an exponential increase in their occurrence is observed (**F**).

Table 5.1 Single lineage contribution

Table 5.2 Global dual lineage contribution

Table 5.3 Biased, occasional dual lineage contribution

See following page.

Tables show imaginary data used to demonstrate 3 outcomes of dual origin coefficient (DOC) analysis. Each table details the composition of 12 clones in a similar size group (A-L), indicating the number of cortex and medulla cells in each, and the total number of cells.

DOC values were calculated as: (nC-nM)/(nC+nM), where nC is the number of labelled cortical cells and nM the number of labelled medullary cells in that particular clone.

Table 5.1, Table 5.2, and Table 5.3 are illustrated by Graph A, Graph B and Graph C respectively in Figure 5.3.

For legend, see previous page.

Table 5.1 Single lineage contribution

Clone	Cortex (nC)	Medulla (nM)	Total	D.O.C.
A	27	0	27	1.00
B	18	0	18	1.00
C	21	0	21	1.00
D	0	16	16	-1.00
E	30	0	30	1.00
F	0	28	28	-1.00
G	0	19	19	-1.00
H	23	0	23	1.00
I	0	25	25	-1.00
J	0	22	22	-1.00
K	25	0	25	1.00
L	17	0	17	1.00

Table 5.2 Global dual lineage contribution

Clone	Cortex (nC)	Medulla (nM)	Total	D.O.C.
A	12	8	20	0.20
B	18	14	32	0.13
C	20	10	30	0.33
D	11	9	20	0.10
E	14	16	30	-0.07
F	9	16	25	-0.28
G	10	16	26	-0.23
H	16	9	25	0.28
I	16	15	31	0.03
J	10	12	22	-0.09
K	7	10	17	-0.18
L	12	12	24	0.00

Table 5.3 Biased, occasional dual lineage contribution

Clone	Cortex (nC)	Medulla (nM)	Total	D.O.C.
A	12	8	20	0.20
B	18	0	18	1.00
C	26	0	26	1.00
D	22	9	31	0.42
E	22	0	22	1.00
F	17	0	17	1.00
G	32	0	32	1.00
H	20	0	20	1.00
I	16	15	31	0.03
J	29	0	29	1.00
K	24	0	24	1.00
L	16	12	28	0.14

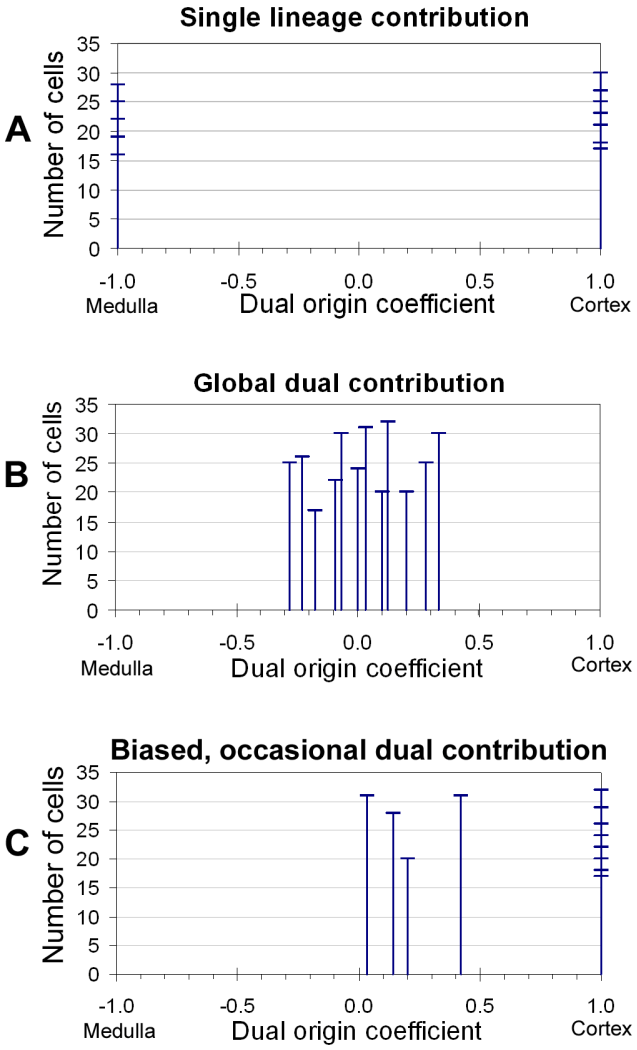

Figure 5.3 Dual origin coefficient showing three models of TEC development

A) A unipotent model is represented, using data from Table 5.1. Separate progenitor pools exist for cortex or for medulla. Clones are exclusively medullary or cortical, never both.

B) Shows data from Table 5.2. Here, clones originate from a common progenitor pool, which can and does give rise to both lineages. All clones are therefore composed of both cortex and medulla.

C) Represents Table 5.3. The precursor cells in which these labelled clones originated primarily gave rise to cortex only. However, a small number also show medullary progeny. This model might be seen if progenitors had bipotent ability, but only a fraction received an induction signal to produce medulla.

5.2. Results

5.2.1. Calculation of expected epithelial clone frequency

Two variants of the *laacZ* gene, containing different duplication sizes and therefore different recombination frequencies, have been constructed. The shorter, with an internal duplication of 289bp (*R26laacZ0.3*), shows *laacZ* recombination occurring at a rate of 1.66×10^{-6} per cell per generation in mouse embryonic stem (ES) cells in culture. The larger 1,117bp duplication (*R26laacZ1.1*) displays a higher recombination rate of 8.15×10^{-6} per cell per generation in ES cells (E. Tzouanacou, unpublished results). These two duplication sizes enable the selection of an appropriate clone generation frequency for TEC clone production.

In order to choose the correct combination of embryo age and *laacZ* duplication size, a number of factors were taken into account. Firstly, a thymus developmental stage at which sufficient numbers of differentiated cTECs and mTECs are present and identifiable was important, so that the lineage of labelled epithelial clones could be ascertained (E14 or above). Secondly, an age should be identified at which the size of the epithelial population would allow the assumption of any labelled TECs being clonal, i.e. less than one TEC *laacZ* recombination event per thymus lobe.

Recombination of *laacZ* can be analysed by the fluctuation test of Luria and Delbrück. This test was originally developed in order to distinguish between random and bacteriophage-induced mutations in *E. coli* that resulted in resistance to phage attack (Luria and Delbruck, 1943). The test predicts that for a spontaneous, random and heritably transmitted mutation (such as *laacZ* recombination), the number of genetic recombinations occurring follows a Poisson distribution, with parameter $\boldsymbol{\lambda}$. Here, $\boldsymbol{\lambda}$ is the expected mean number of recombinations per thymus lobe and can be expressed as **mNt** (where **m** is the recombination frequency, measured as number of recombinations per cell per generation, and **Nt** is the number of TECs present per lobe as calculated in Chapter 3). $\boldsymbol{\lambda}$ was calculated for each combination of *laacZ* duplication size and embryo age of study, as shown in Table 5.4. If the expected mean number of occurrences of clones in a single lobe is $\boldsymbol{\lambda}$, then the probability of exactly **N** clones occurring in a single lobe is $\boldsymbol{(\lambda^N e^{-\lambda})/(N!)}$ according to Poisson. This

enables the fraction of thymus lobes harbouring **N** independent clones to be calculated, and hence the percentage of all thymus lobes expected to carry **N** independent clones (Table 5.4).

The recombination frequencies can be increased further if *laacZ* mice are mated together i.e. a homozygous *R26laacZ1.1* cross, a homozygous *R26laacZ0.3* cross, or a heterozygous cross involving one parent from each strain. The expected recombination frequencies for these three additional options are shown in Table 5.5.

It was initially decided to use *R26laacZ0.3*$^{+/+}$ embryos, at the E16.5 stage, to perform the analysis. At E16.5 the majority of TECs display a differentiated phenotype, enabling easier classification of potential clones. This genotype would be expected to produce labelled TEC clones in approximately 26% of thymus lobes studied, providing a reasonable return for the number of lobes involved (Table 5.5). The expected probability of >1 TEC labelling event occurring in a single lobe is calculated at 3.6%. This might appear to be higher than desired, but in reality a large number of clones would consist of one cell and would therefore be very rarely detected. The likelihood of two epithelial clones of a detectable size arising in a single thymus lobe would consequently be an extremely rare event.

Table 5.4 Expected thymic epithelial recombination frequencies in heterozygous (*laacZ* x wild-type) embryos

Embryo age	**17.5**	**16.5**	**15.5**	**14.5**	**13.5**	**12.5**
TEC # (Nt)	$1.41x10^5$	$1.01x10^5$	$5.14x10^4$	$3.18x10^4$	$1.37x10^4$	$8.23x10^3$
Genotype	***R26laacZ1.1*$^{+/-}$**					
Rec. rate (m)	$8.15x10^{-6}$					
mNt (λ)	1.147	0.823	0.419	0.259	0.112	0.067
% of thymus lobes displaying N independent clones						
N=0	31.8%	43.9%	65.8%	77.2%	89.4%	93.5%
N=1	36.4%	36.1%	27.6%	20.0%	10.0%	6.3%
N=2	20.9%	14.9%	5.8%	2.6%	0.6%	0.2%
N=3	8.0%	4.1%	0.8%	0.2%	0.0%	0.0%
N=4	2.3%	0.8%	0.1%	0.0%	0.0%	0.0%
N=5	0.5%	0.1%	0.0%	0.0%	0.0%	0.0%
Total labeled (*fL*)	68.2%	56.1%	34.2%	22.8%	10.6%	6.5%
Genotype	***R26laacZ0.3*$^{+/-}$**					
Rec. rate (m)	$1.66x10^{-6}$					
mNt (λ)	0.234	0.168	0.085	0.053	0.023	0.014
% of thymus lobes displaying N independent clones						
N=0	79.2%	84.6%	91.8%	94.9%	97.7%	98.6%
N=1	18.5%	14.2%	7.8%	5.0%	2.2%	1.3%
N=2	2.2%	1.2%	0.3%	0.1%	0.0%	0.0%
N=3	0.2%	0.1%	0.0%	0.0%	0.0%	0.0%
N=4	0.0%	0.0%	0.0%	0.0%	0.0%	0.0%
N=5	0.0%	0.0%	0.0%	0.0%	0.0%	0.0%
Total labeled (*fL*)	20.8%	15.4%	8.2%	5.1%	2.3%	1.4%

0.0% = less than 0.05%

Calculation of the proportion of thymus lobes expected to contain a given number (N) of epithelial clones. To find the mean number of TEC clones per lobe (λ) at a specific embryo age, the number of epithelial cells at that age (Nt) was multiplied by the laacZ-LacZ recombination rate (m) known to occur for each genotype (in recombinations per cell per generation). The calculated mean (λ) was then used as the parameter of a Poisson distribution, to work out the probability of 'N' independent clones arising in a single thymus lobe, using the formula $(\lambda^N e^{-\lambda})/(N!)$. The total fraction of lobes labelled (fL) was calculated as (100% - N=0). Calculations were carried out using Microsoft Excel.

Table 5.5 Expected thymic epithelial recombination frequencies from different *laacZ* x *laacZ* cross embryos

Embryo age	17.5	16.5	15.5	14.5	13.5	12.5
TEC # (Nt)	$1.41x10^5$	$1.01x10^5$	$5.14x10^4$	$3.18x10^4$	$1.37x10^4$	$8.23x10^3$
Genotype	***R26laacZ1.1*$^{+/+}$**					
Rec. Rate(m)	$1.63x10^{-5}$					
mNt (λ)	2.294	1.646	0.838	0.518	0.224	0.134
% of thymus lobes displaying N independent clones						
N=0	10.1%	19.3%	43.2%	59.6%	79.9%	87.4%
N=1	23.1%	31.7%	36.3%	30.9%	17.9%	11.7%
N=2	26.5%	26.1%	15.2%	8.0%	2.0%	0.8%
N=3	20.3%	14.3%	4.2%	1.4%	0.1%	0.0%
N=4	11.6%	5.9%	0.9%	0.2%	0.0%	0.0%
N=5	5.3%	1.9%	0.1%	0.0%	0.0%	0.0%
Total labeled (*fL*)	89.9%	80.7%	56.8%	40.4%	20.1%	12.6%
Genotype	***R26laacZ0.3*$^{+/+}$**					
Rec. Rate(m)	$3.32x10^{-6}$					
mNt (λ)	0.467	0.335	0.171	0.106	0.046	0.027
% of thymus lobes displaying N independent clones						
N=0	62.7%	71.5%	84.3%	90.0%	95.5%	97.3%
N=1	29.3%	24.0%	14.4%	9.5%	4.4%	2.7%
N=2	6.8%	4.0%	1.2%	0.5%	0.1%	0.0%
N=3	1.1%	0.4%	0.1%	0.0%	0.0%	0.0%
N=4	0.1%	0.0%	0.0%	0.0%	0.0%	0.0%
N=5	0.0%	0.0%	0.0%	0.0%	0.0%	0.0%
Total labeled (*fL*)	37.3%	28.5%	15.7%	10.0%	4.5%	2.7%
Genotype	***R26laacZ1.1/R26laacZ0.3***					
Rec. Rate(m)	$9.81x10^{-6}$					
mNt (λ)	1.380	0.990	0.505	0.312	0.135	0.081
% of thymus lobes displaying N independent clones						
N=0	25.1%	37.1%	60.4%	73.2%	87.4%	92.2%
N=1	34.7%	36.8%	30.5%	22.8%	11.8%	7.4%
N=2	24.0%	18.2%	7.7%	3.6%	0.8%	0.3%
N=3	11.0%	6.0%	1.3%	0.4%	0.0%	0.0%
N=4	3.8%	1.5%	0.2%	0.0%	0.0%	0.0%
N=5	1.1%	0.3%	0.0%	0.0%	0.0%	0.0%
Total labeled (*fL*)	74.9%	62.9%	39.6%	26.8%	12.6%	7.8%

For explanation, see Table 5.4. Recombination frequencies (m) for *laacZ* x *laacZ* crosses were obtained by adding the recombination frequencies of each parental genotype. Data on the two combinations of genotype/developmental stage investigated in this thesis are outlined in red.

5.2.2. Detection of thymic epithelial clones

5.2.2.1. β-galactosidase expression in the embryonic thymus under control of the ROSA26 promoter

To demonstrate that cells in the E16.5 thymus were able to produce β-gal, by expression of *lacZ* under the control of the ROSA26 promoter, *R26lacZ*$^{+/-}$ mice that ubiquitously expressed β-gal were crossed with CBA/BL6 wild-type animals, resulting in both *R26lacZ*$^{+/-}$ and *R26lacZ*$^{-/-}$ embryos. Thymus lobes were removed from embryos by microdissection, rinsed in cold PBS and fixed in 'old embryo fix' (OEF, see materials and methods) overnight at 4^{o}C. Lobes were subsequently washed with X-gal wash and stained at 37^{o}C for 24 hours with X-gal (see materials and methods). After fixing in X-gal-fix (XGF, see materials and methods) overnight at 4^{o}C, lobes were examined. Staining revealed blue cells throughout thymus lobes from *R26lacZ*$^{+/-}$ embryos, whereas wild-type littermates were negative for X-gal staining (Figure 5.4).

5.2.2.2. Production of R26laacZ0.3$^{+/+}$ *E16.5 thymus lobes*

Initial *R26laacZ0.3*$^{+/+}$ embryos were generated by homozygous *R26laacZ0.3*$^{+/+}$ crosses. This resulted in litters of a uniform *R26laacZ0.3*$^{+/+}$ genotype. In total 15 litters were dissected, with 192 thymus lobes being removed from embryos at E16.5. Lobes were treated in the same manner as positive/negative controls (see section 5.2.2.1). After staining/fixation, lobes were put into 30%, 50% and 80% glycerol (in PBS) overnight at 4^{o}C, sequentially. This was done in order to clear the tissue, so that any β-gal^{+} cells present might show up more clearly. Lobes were then stored in 80% glycerol at 4^{o}C to await analysis.

5.2.2.3. Detection and analysis of E16.5 β-gal^{+} clones

X-gal stained E16.5 *R26laacz0.3*$^{+/+}$ thymus lobes in 80% glycerol were examined under a light microscope, in order to look for blue β-gal^{+} cells resulting from any *laacZ-lacZ* recombination events that may have occurred. Any observed clones were photographed. The number of clones observed was well below the expected level. From predictions in Table 5.5, it was calculated that around 64 TEC clones would be

generated from a sample of 192 thymus lobes with this particular age/genotype combination (Table 5.6). However, only 14 clones were observed, of any cell type. This seems even lower when the expected number of clones of any cell type is taken into account, with the total number of clones expected from this sample being around 624 (Table 5.7). This was calculated by the same means used in section 5.2, with a mean number of 3.25 clones of any type expected to occur in each E16.5 lobe (Table 5.7).

Clones detected here were all on or near the surface of the thymus. Most β-gal$^+$ cells occurred singly or in pairs. Representative photographs of all E16.5 clone types are shown in Figure 5.5. The location of clones in Figure 5.5 suggests either a capsular mesenchymal or subcapsular epithelial identity. Panel C in particular appears to be of extrathymic mesenchymal origin. The topology of these clones indicates a dispersive mode of growth and significant cell mixing, since individual cells are frequently separated by a long distance (particularly F and G). In Figure 5.5B, several clusters of 2 cells can be seen. This could indicate either recent cell division, or a switch from a dispersive to a coherent mode of growth (Figure 1.7).

5.2.2.4. Production of R26laacZ1.1$^{+/+}$ *E15.5 thymus lobes*

Due to the lower than expected labelling frequencies observed using the homozygous *R26laacZ0.3* embryos, it was decided to use the larger 1.1kb *laacZ* duplication. *R26laacZ1.1*$^{+/+}$ embryos were expected to give an increased recombination frequency, resulting in an increase in the observed number of labelled clones. E15.5 *R26laacZ1.1*$^{+/+}$ embryos were used in this analysis, because their smaller size would make it easier to see labelled cells in the interior of the thymus. Also, the ratio of epithelial cells to non-epithelial cells is higher (16.2% ±4.1% of total thymus at E15.5 as opposed to 8.8% ±2.4% at E16.5, Figure 3.3.), boosting the epithelial proportion amongst total clones. At E15.5, a mean number of 0.84 epithelial clones per lobe were calculated – 2.5 times as many as would be expected to occur in *R26laacZ0.3*$^{+/+}$ thymus lobes (Table 5.5, Figure 5.5). A total of 254 lobes were removed from *R26laacZ1.1*$^{+/+}$ E15.5 embryos. These were stained and cleared in the manner described for E16.5 thymus above.

Table 5.6 Expected/observed TEC clone numbers

Embryo genotype	*R26laacZ0.3*$^{+/+}$	*R26laacZ1.1*$^{+/+}$
Embryo age	16.5	15.5
Mean expected TEC clones per lobe (λ)	0.34	0.84
% of lobes expected with N>0 TEC clones (*fL*)	28.5%	56.8%
No. lobes examined (*S*)	192	254
No. lobes expected to contain TEC clones (*nL*)	54.7	144.2
Total no. TEC clones expected (*nC*)	64.4	212.9
No. clones observed (any lineage)	14	19

The number of lobes expected to contain labelled TECs (nL), out of a total of 'S' lobes, was calculated by multiplying S by the percentage of lobes expected to have labelled TECs (fL). fL was calculated as described in Table 5.4.

The total number of TEC clones expected (nC) was calculated as S x λ. (λ was calculated as described in Table 5.4). Values for fL and λ taken from Table 5.5

.

Table 5.7 Expected number and frequency of total thymus clones

Embryo genotype	*R26laacZ0.3*$^{+/+}$	*R26laacZ1.1*$^{+/+}$
Embryo age	16.5	15.5
Recomb. Rate (m)	3.32×10^{-6}	1.63×10^{-5}
Total cells (Nt)	9.79×10^{5}	2.36×10^{5}
Mean expected total clones per lobe (λ)	3.25	3.85
% of lobes expected with N>0 clones (*fL*)	96.1%	97.9%
No. lobes expected to contain clones (*nL*)	184.5	248.7
Total no. clones expected (any lineage) (*nC*)	624.0	977.9

Here, the number of clones of any lineage expected to occur in the sample described in Table 5.6 was calculated. λ was calculated as mNt, as described in Table 5.4. The total number of cells in the thymus (Nt) was calculated in Chapter Three. Values for nL and nC were calculated as described for Table 5.6, above.

5.2.2.5. Detection and analysis of E15.5 β-gal$^+$ clones

E15.5 thymus lobes were analysed by the same method as E16.5 lobes, described in section 5.2.2.3. From 254 E15.5 lobes, 19 clones were observed. Once again, this is well below the expected number – from this sample a total of 144 TEC clones was calculated to have been present (Table 5.6). This is particularly surprising when it is considered that almost 98% of these lobes were expected to harbour clones encompassing any type of cell. A mean of 3.85 clones of any kind was calculated to occur per lobe, giving an expected total of 978 independent labelling events for this sample of 254 lobes. In E16.5 and E15.5 lobes, the observed number of clones was 2% and 3% respectively of the expected total number.

Of the 19 E15.5 clones observed, the majority were very similar to those in Figure 5.5. These consisted of a very small number of cells, most frequently 1 or 2, located on the outside of the thymus. Two larger clones were seen, however. Clone 1.1/14 was composed of around 40 cells, and was located as a region of extrathymic tissue on the outside of the lobe (Figure 5.6). Clone 1.1/16 was composed of several hundred cells, and was immediately visible to the naked eye. When examined under the microscope, blue patches both on the surface and within the interior of the lobe were obvious (Figure 5.7A). This clone was cryo-sectioned, whereupon it was seen that labelled cells covered a large proportion of the lobe's surface, particularly toward one pole. Labelled cells also extended deep within the lobe, forming elongated clusters that often extended from the perimeter of the thymus (Figure 5.7B-D). The staining pattern correlates extremely closely with that seen when using the ER-TR7 monoclonal antibody to identify thymic mesenchyme (Figure 5.7E). Unfortunately, direct staining of tissue from this clone with the ER-TR7 antibody was not possible, since the antibody appears sensitive to the X-gal staining process.

It was decided to section a number of *R26laacZ1.1*$^{+/+}$ lobes, in case there were β-gal$^+$ cells within the thymus that could not be visualized when examining an intact lobe – a distinct possibility since the vast majority of labelled cells observed were on the periphery of the organ. A total of 64 E15.5, X-gal stained thymus lobes were fully sectioned, with the sections captured on glass slides. Sections were all carefully

examined under a light microscope. From a sample of 64 E15.5 lobes, a total of approximately 246 clones of any cell type would be expected, due to a calculated mean of 3.85 *laacZ* recombination events occurring per lobe. Upon examining the sections, 17 lobes were found to have labelled cells, representative examples of which are shown in Figure 5.8 and Figure 5.9. Most of these had only one or two β-gal^{+} cells, located in the thymic capsule (Figure 5.8). One lobe contained a large clone consisting of 23 cells, found on multiple adjacent sections (Figure 5.9). This clone was also located on the periphery of the thymus, appearing to be either extra-thymic connective tissue, or part of the capsule that had lifted away during the staining process. Lobes were also hemisected in order to increase the chances of locating clones within the interior of the thymus, but this did not lead to extra clones being discovered. None of the sectioned lobes revealed any clones within the thymic parenchyma that could be considered as epithelial, and therefore of further interest in this project.

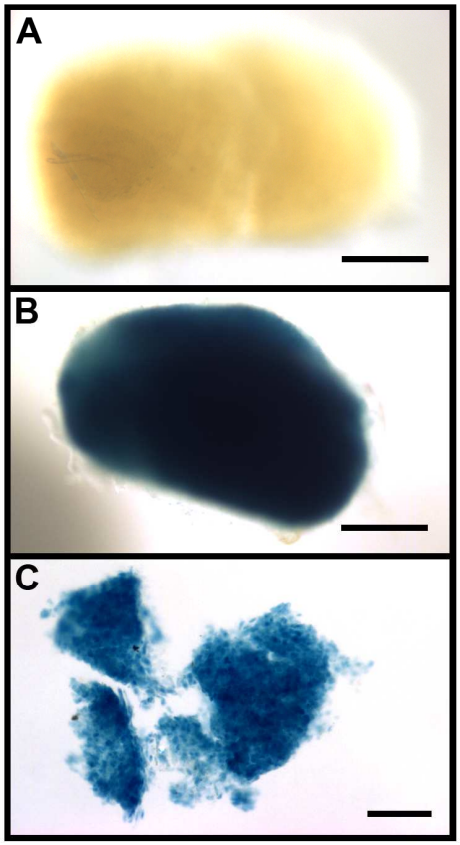

Figure 5.4 *R26lacZ*$^{+/-}$ thymus lobe showing X-gal staining

Panel **A** shows negative control *R26lacZ*$^{-/-}$ E16.5 thymus after staining with X-gal. Panel **B** shows positive control E16.5 thymus from *R26lacZ*$^{+/-}$ littermate. In panel **C**, a positively stained lobe was teased apart to show stain penetration into interior of thymus. Lobes were stained for 24 hours at 37^{o}C. Scale bars: A, B – 400 µm; C – 100 µm.

Figure 5.5 Examples of β-gal^{+} cells from *R26laacZ0.3*$^{+/+}$ E16.5 thymus

See following page

Shown here are representative examples of β-gal^{+} clones seen in R26laacZ0.3$^{+/+}$ E16.5 thymus lobes. Black arrowheads indicate labelled cells. Where clones are large and spread over a wide area, the outer extents of clone boundaries are marked by a black dotted line (**B** and **C**). The numbers of labelled cells shown in each example are as follows: **A**-1, **B**-29, **C**-11, **D**-4, **E**-3, **F**-6, and **G**-8. In **Fa** and **Fb**, multiple images represent changes in depth of focus required to visualise labelled cells in different areas of the same thymus lobe. **Ga**, **Gb** and **Gc** also represent one lobe. Scale bars are 200µm.

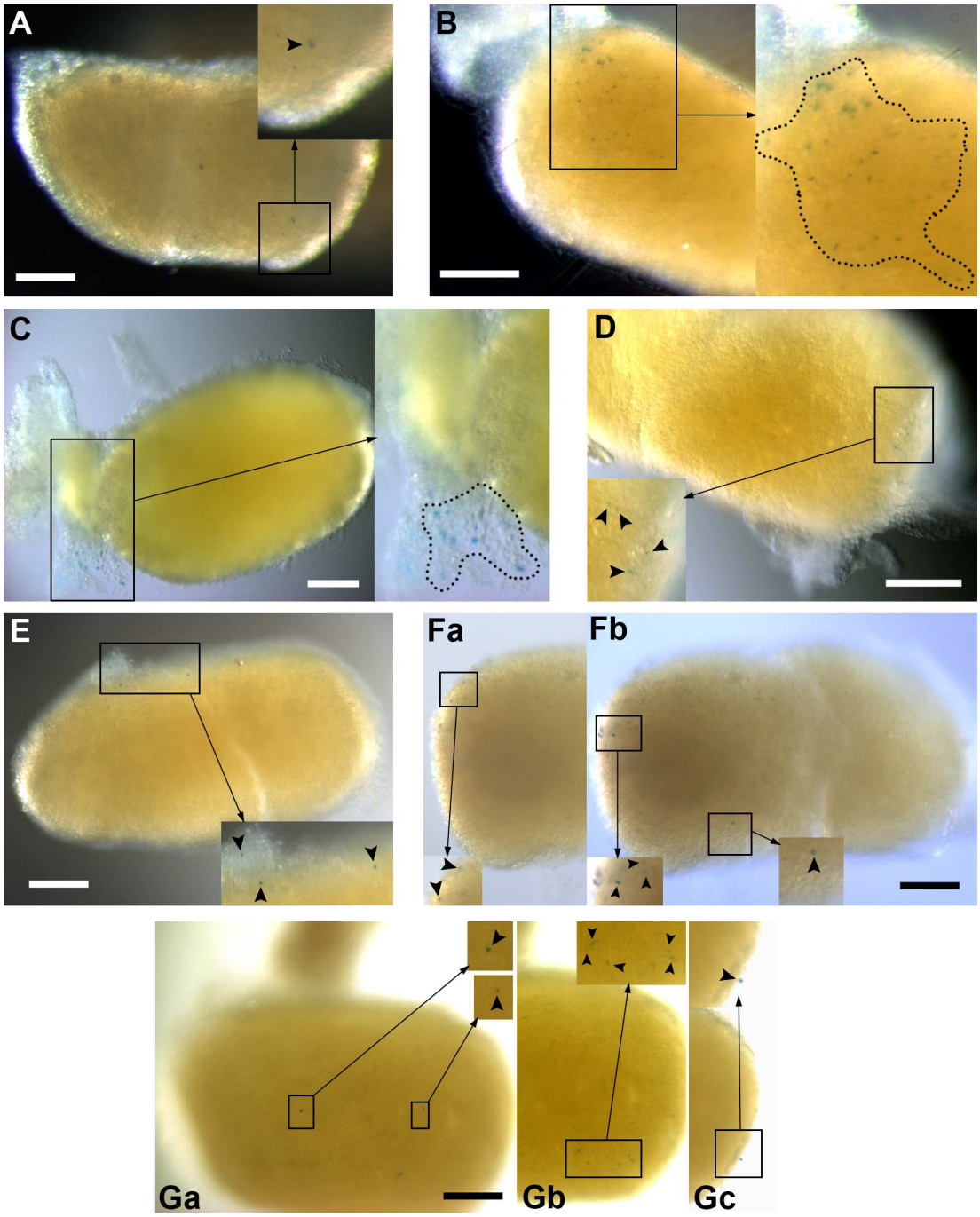

Figure 5.5 Examples of β-gal+ cells from *R26laacZ0.3*+/+ E16.5 thymus

For legend, see previous page.

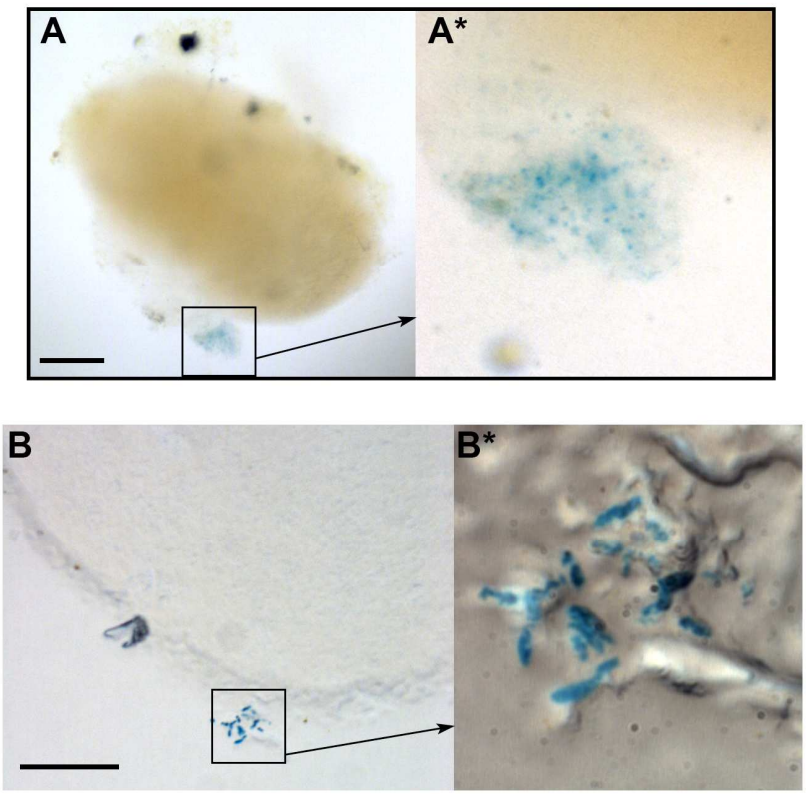

Figure 5.6 Clone 1.1/14 – a large clone in capsular/extrathymic tissue

A) Whole-mount X-gal stain of E15.5 R26laacZ1.1$^{+/+}$ thymus lobe, showing clone 1.1/14.

B) Cryo-section through clone 1.1/14, showing blue X-gal-stained nuclei. Scale bars – in A is 200µm, in B is 100µm.

Figure 5.7 Clone 1.1/16 – a large clone of apparent mesenchymal origin

See following page.

(**A**) Whole-mount X-gal stain of E15.5 R26laacZ1.1$^{+/+}$ thymus lobe showing clone 1.1/16. Hundreds of labelled cells were observed, and were concentrated toward one pole of the lobe. In a horizontal progression towards the opposite pole the number of labelled cells decreased, and the final 30-40% was completely unlabelled. White dashed line indicates approximate orientation of tissue sections. (**B**) Greyscale image of frozen section through clone 1.1/16. (**C, D**) Magnified view of panel **B**, showing detail of labelled cells. Red, dotted lines show clustered nature of labelled cells, both in the thymus interior (**C**) and in the outer capsule (**D**). Green colour shows DAPI stain, giving position of cell nuclei. (**E**) ER-TR7 stain of E15.5 thymus for comparison, demonstrating similarity between distribution of ER-TR7^{+} mesenchyme and β-gal^{+} cells in clone 1.1/16. Scale bars - A is 200µm; B and E are 100µm.

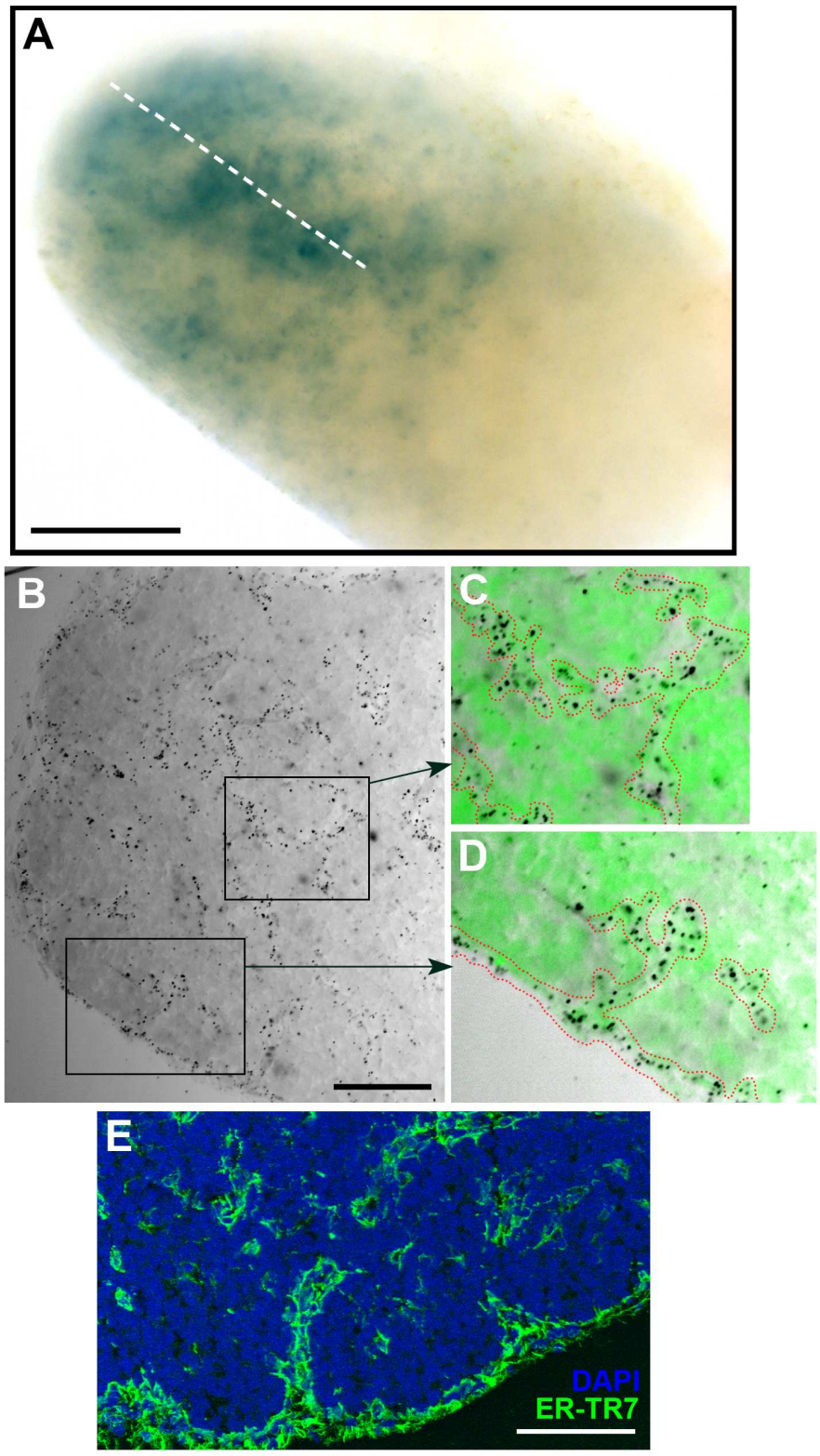

Figure 5.7 Clone 1.1/16 – a large clone of apparent mesenchymal origin

For legend, see previous page.

Figure 5.8 Sections through *R26laacZ1.1*$^{+/+}$ lobes showing examples of β-gal^{+} labelled cells

See following page.

(**A-H**) 8 representative examples of clones observed after sectioning a sample of 64 E15.5 thymus lobes. Nearly all clones observed in this analysis were located on the outside of the thymus. Some were obviously in the capsule (**A, C, G**), while others may have originated from extrathymic tissue (**D, E, H**). Two cells were observed that may be subcapsular (**B, F**). Red arrowheads point to blue cells. Scale bars are 100μm.

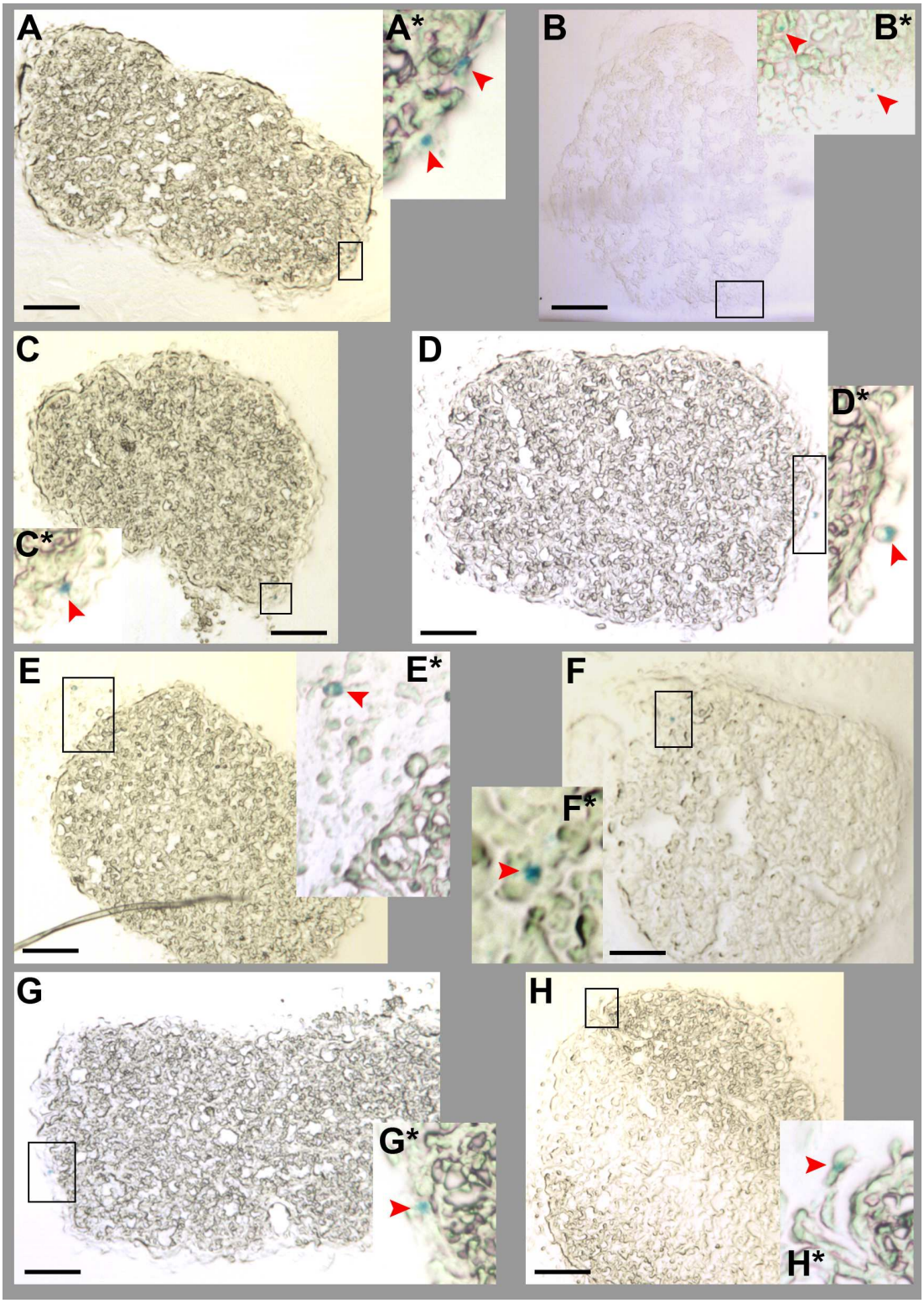

Figure 5.8 Sections through *R26laacZ1.1*+/+ lobes showing examples of β-gal+ labelled cells

For legend, see previous page.

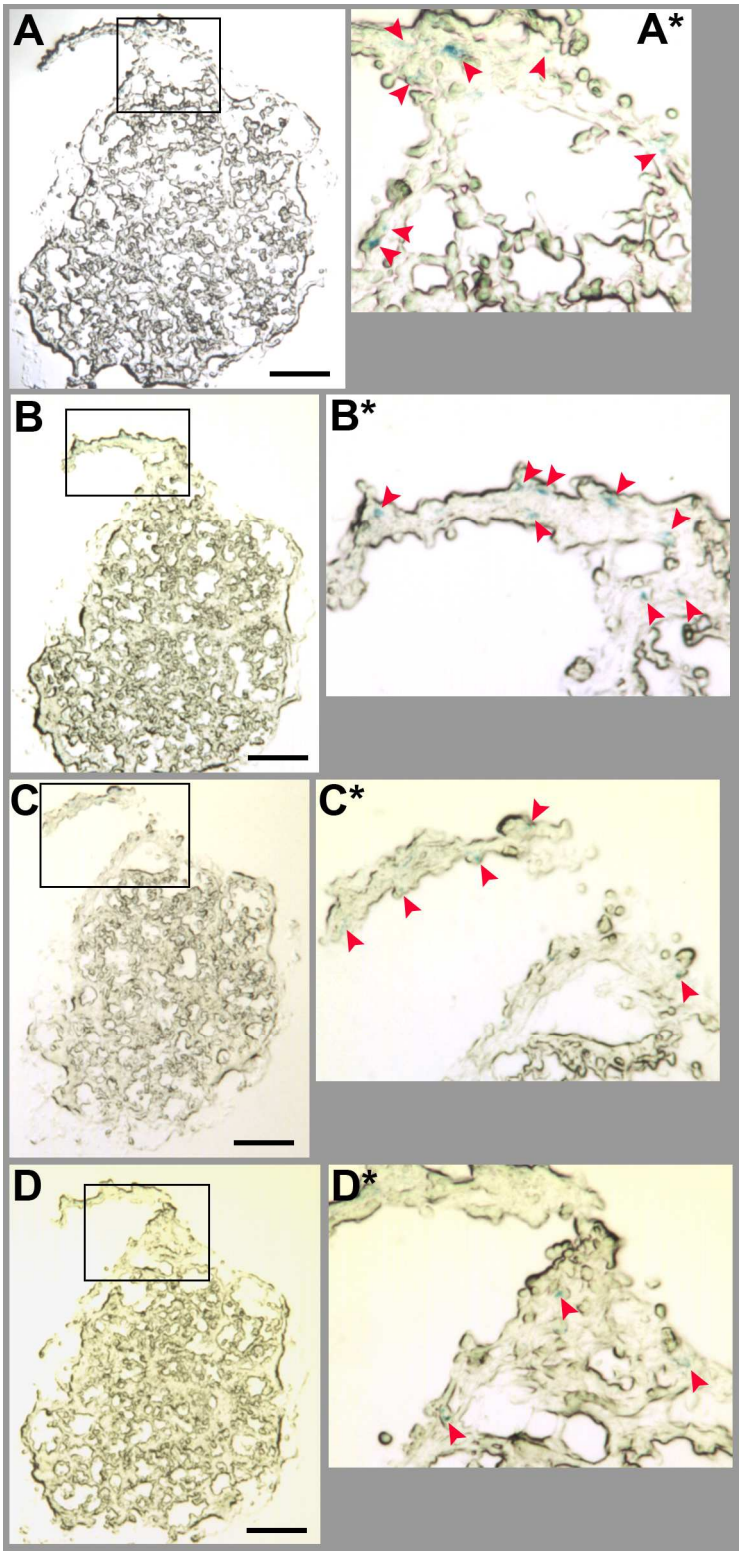

Figure 5.9 Sections through a 23-cell clone

(**A-D**) Adjacent sections through a single E15.5 thymus lobe, showing a clone comprised of 23 cells. Red arrowheads point to blue cells. Scale bars are 100µm.

5.2.2.6. Weak staining in R26lacZ$^{+/-}$ *control thymus sections*

Since the vast majority of labelled lobes exhibited β-gal^{+} cells only on or near the surface of the thymus, it was considered whether or not reagents used in the X-gal staining process were able to penetrate into the interior of the thymus successfully. To investigate this, *R26lacZ*$^{+/-}$ positive control lobes were stained with X-gal as in section 5.2.2.1. These were then frozen in OCT and sectioned using a cryostat (see materials and methods). It was seen that although whole X-gal-stained lobes were dark blue in appearance, the β-gal^{+} cells were much paler when observed in section, and individual nuclei were not well defined (Figure 5.10). However, it was concluded that this was not due to poor tissue penetration of the staining process, since cells on the periphery of the thymus stained with the same intensity as those in the centre of the organ (Figure 5.10). In a large number of cells, a single tiny area of intense staining was visible in the form of a small dot. These dots appeared to be either perinuclear or just outside the cell nucleus adjacent to the outer membrane (Figure 5.10C,D). Some cells did display the expected X-gal staining morphology, with the whole nucleus appearing as dark blue. These occurred predominantly in clusters, mostly at the edge of the thymus but also in the interior of the lobe (Figure 5.10A). Often, the areas of strongest staining appeared in extrathymic tissue that had remained attached to the thymus following dissection (Figure 5.10B).

Figure 5.10 Cross-section of β-gal^{+} control thymus reveals weak staining

See following Page

A) Cross section through an E16.5 R26lacZ$^{+/-}$ thymus lobe, showing poor resolution of nuclear X-gal staining. Cells that show an obvious, darkly stained nucleus are infrequent, occurring individually (black arrowheads), or in clusters (marked by dotted black lines). Staining appears in most cells as a single, intense dot (red arrowheads).

B) Prominent, darkly stained nuclei are most frequently observed around the edge of the thymus (black arrowheads), or in extrathymic tissue still attached to lobes after dissection (within black dotted line).

C) The size of the dots of X-gal staining (left panel) is demonstrated in comparison to the nucleus by a DAPI stain (pale blue in left panel, dark blue in right panel). Only small numbers of nuclei appear to be completely X-gal stained as expected (white arrowheads).

D) Magnified view, showing the position of the 'dot' staining to be on the edge of the nucleus (black arrowheads). Left panel shows brightfield only, right panel shows brightfield plus DAPI overlay.

Scale bars in A and B are 200µm, scale bars in C and D are 50µm.

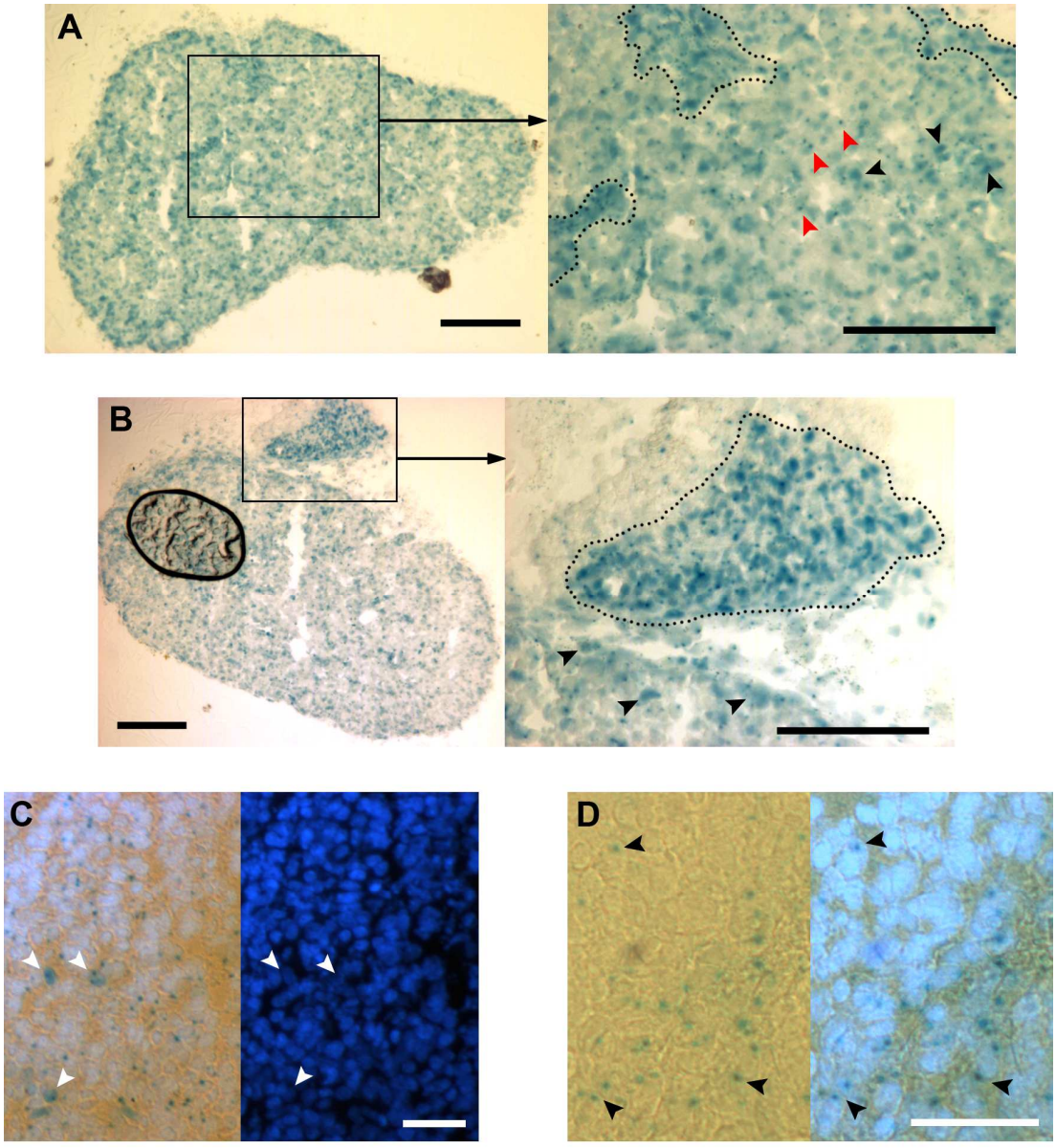

Figure 5.10 Cross-section of β-gal+ control thymus reveals weak staining

For legend, see previous page

5.2.3. Optimisation of X-gal staining

5.2.3.1. Pre-stain tissue fixation

It was decided to optimise the X-gal staining process, in order to achieve the maximum possible staining intensity and give a better chance of locating the presumptively substantial number of β-gal^{+} clones that were not detected. Optimisation of X-gal staining was investigated using *R26lacZ*$^{+/-}$ mice constitutively expressing β-galactosidase.

The first variable investigated was the method of tissue fixation. Fixatives are used in order to preserve morphology within the tissue, and to prevent its degradation by microbes. However, since X-gal staining relies on the enzymatic activity of β-galactosidase produced within the cell, it was important not to over-fix the tissue. OEF (which utilises glutaraldehyde and formaldehyde as fixatives, see materials and methods) and two sources of formaldehyde - one made as a 4% solution of paraformaldehyde (PFA) in PBS, the other as a 10% dilution of formalin - were used for varying durations, as summarised in Table 5.8. Both sources of formaldehyde resulted in a similar working concentration.

Table 5.8 Effects of fixative variation on X-gal staining

Fixative	Duration	Result
OEF (0.2% glutaraldehyde, 1% formaldehyde)	overnight	original condition
	3 hours	no improvement
	1 hour	no improvement
	10 min	no improvement
4% formaldehyde (4% PFA)	overnight	worse
	3 hours	no improvement
	1 hour	no improvement
	10 min	slight improvement
3.7% formaldehyde (10 % formalin)	overnight	worse
	3 hours	no improvement
	1 hour	no improvement
	10 min	no improvement

A brief 10-minute fixation with 4% PFA appeared to result in a slightly stronger stain than the original OEF overnight fixation (not pictured). The prominent 'dot'

morphology described in section 5.2.2.3 was still present. Fixation in 10% formalin for an identical time did not result in a similar improvement, possibly due to the presence of methanol. Methanol is added to formalin in small amounts by the manufacturer as a stabilising agent, but may cause conformational changes to proteins and hence affect the enzymatic activity of β-galactosidase. This is not an issue with freshly dissolved PFA.

Although both glutaraldehyde and formaldehyde operate in a similar manner by cross-linking protein molecules, glutaraldehyde has a higher molecular weight. This can limit its ability to diffuse into tissues, and likewise may affect the penetration of X-gal substrate into cells. Glutaraldehyde fixation can also cause significant auto-fluorescence in tissue. This would likely pose problems in this analysis, where cell types would be identified by confocal microscopy in conjunction with fluorescently tagged antibodies.

In conclusion, it was decided to use 4% PFA for 10 minutes in all future tissue fixation prior to X-gal staining.

5.2.3.2. Duration and temperature of X-gal staining

Next, the conditions of the X-gal staining step were investigated. One of the most obvious parameters that could be adjusted was the length of time for which the tissue was in contact with the X-gal staining reagent. Since enzymatic reactions such as processing of X-gal substrate by β-galactosidase can also be sensitive to temperature, it was decided to investigate the effect of staining duration at two temperatures. All tissues have endogenous β-galactosidase activity due to lysosomes, which can result in non-specific background staining - the stain was performed out 25^{o}C to reduce this phenomenon. Staining was also carried out at 37^{o}C, as performed previously in this chapter. Results are summarised in Table 5.9.

It was seen that a 48-hour stain gave marginally better results than a 24-hour stain. This difference is imperceptible when looking at photographs, and hence not shown here. Increasing the stain time to 72 hours did not give any further improvement. There did not appear to be any difference between staining the tissue at 37^{o}C or

25°C. It was decided that future X-gal staining would take place for 48 hours, at 25°C (for reasons of practical convenience).

Table 5.9 Effects of time and temperature on X-gal staining

Temperature	Duration	Result
37 °C	24h	original condition
	48h	Slight improvement
	72h	Slight improvement
25 °C	24h	no improvement
	48h	Slight improvement
	72h	Slight improvement

5.2.4. X-gal staining of whole-mount vs. sectioned tissue

Previous results in section 5.2.2.3 showed uniform staining between cells both deep in the centre of the thymus and on its periphery, indicating there were no problems involving penetration of staining reagents into the interior of the organ. To confirm that diffusion of reagents through the outer capsule of the organ was not an issue, X-gal staining of tissue sections was investigated.

Freshly dissected E16.5 *R26lacZ*$^{+/-}$ thymus lobes were embedded in either OCT compound or 15% sucrose/7% gelatine and snap-frozen, before being sectioned onto glass microscope slides (see Chapter Two: Materials and Methods).

Frozen sections from each embedding medium were firstly subject to variations in fixative (OEF or 4% PFA) and in fixation time, as summarised in Table 5.10. These samples all underwent an X-gal stain of 24 hours at 25°C. Little or no improvement was observed between any of these conditions and the X-gal staining pattern seen on sections of whole-mount-stained thymus.

Variations in X-gal staining temperature and duration on slides were also investigated. Sections from both OCT-frozen and sucrose/gelatine-frozen tissue were briefly fixed in 4% PFA, before undergoing the X-gal staining process. Conditions were varied in the same manner as in whole-mount thymus staining, seen in Table 5.9. Once again, no differences were observed compared to the whole-

mount stained thymus. Thus, it can be concluded that the poor X-gal staining seen here in the embryonic thymus is definitely not due to difficulties encountered by the fixation/staining reagents in penetrating through the thymic capsule into the interior of the organ.

Table 5.10 Effects of embedding medium, type of fixative and duration of fixation upon X-gal staining of frozen thymus sections

Embedded	Fixative	Duration	Result (compared to wholemount stain)
OCT	OEF	2 min	No change
		10 min	No change
		30 min	No change
	4% PFA	2 min	No change
		10 min	No change
		30 min	No change
Gelatin/ sucrose	OEF	2 min	No change
		10 min	No change
		30 min	No change
	4% PFA	2 min	No change
		10 min	No change
		30 min	No change

5.2.4.1. Attempted sensitivity increase by alkaline treatment

It has been noted that in some cases X-gal staining can be enhanced by following the staining step with alkaline treatment (Tanahashi and Tabira, 2000). In the staining reaction, the X-gal substrate (5-bromo-4-chloro-3-indolyl-β-D-galactopyranoside) is hydrolysed by β-galactosidase to produce galactose and 5-bromo-4-chloro-3-hydroxyindole (Figure 5.11). The latter product self-couples following oxidation, to give the insoluble blue precipitate required to visualise the result of the reaction (Pearson et al., 1963). Alkaline treatment immediately following incubation with X-gal increases oxidation of any residual 5-bromo-4-chloro-3-hydroxyindole from the hydrolysis step, increasing levels of the blue precipitate and therefore giving increased sensitivity to the assay.

Addition of 1M sodium carbonate (Na_2CO_3) for 20 minutes was tried after X-gal staining of whole lobes, and also on frozen sections following X-gal staining upon slides (for details, see materials and methods). Upon subsequent examination of alkaline-treated tissue, however, it was clear that no improvement in staining sensitivity had occurred (not shown).

5.2.4.2. Detection of β-gal⁺ cells by confocal microscopy

Anti-β-galactosidase antibody was investigated as an alternative means of detecting β-gal$^+$ cells. Three antibodies from different manufacturers were tried on frozen E15.5 *R26lacZ*$^{+/-}$ positive control thymus sections, with both fresh and formaldehyde-fixed tissue. The most successful of these antibodies showed a similar staining pattern to the X-gal stain. Once again, small positively stained dots were visible, occurring just outside the nucleus (Figure 5.12). This result provides additional support for the conclusion that the X-gal staining results obtained above are a true reflection of the pattern of β-gal expression, and not a result of a sub-standard staining protocol/technique.

5.2.5. Staining of E10.5 R26laacZ1.1$^{+/+}$ *embryos*

E10.5 *R26laacZ1.1*$^{+/+}$ embryos were examined for the presence of clones, to confirm that there were no inherent problems with my staining technique or with the intrinsic ability of the mice to produce detectable clones *per se*. 199 E10.5 embryos were collected (fixed in 4% PFA at 4°C for 10 mins, X-gal stained at RT for 48h) and examined. Most embryos contained multiple clones, as expected due to the high *laacZ* recombination rate seen in these homozygous *R26laacZ1.1* embryos (1.63×10^{-5} recombinations per cell per generation). Clones of all sizes from <10 cells to several hundred cells were easily detected, both on the surface and within embryos, in all three germ layers. It was therefore concluded that there are no inherent problems with the methods of histology and detection I have used in this chapter.

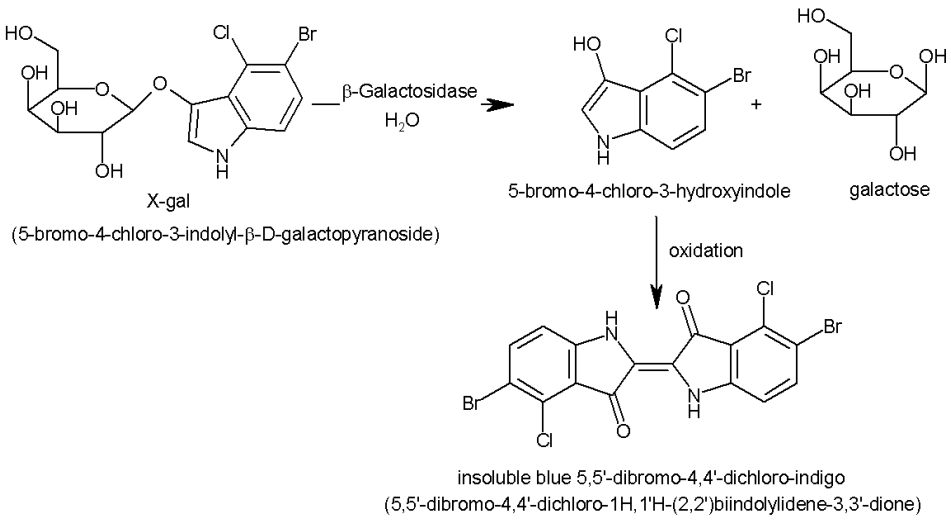

Figure 5.11 Reaction of X-gal to produce an insoluble blue precipitate

The above reaction shows the two-step process involved in the X-gal staining reaction. The first step involves hydrolysis of X-gal by β-galactosidase, the product of which dimerises following a second oxidation step. This produces the insoluble blue precipitate that enables detection of β-gal$^+$ cells.

(Picture from http://upload.wikimedia.org/wikipedia/en/5/5b/X-gal_reaction.png)

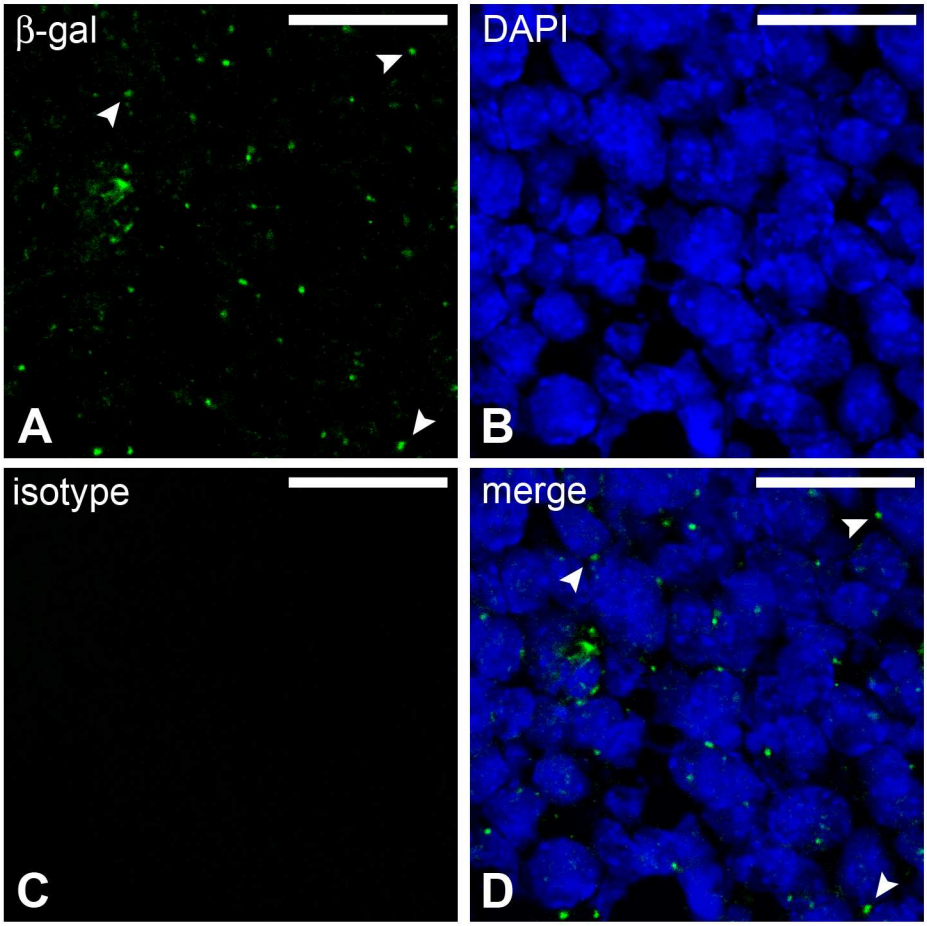

Figure 5.12 Anti-β-galactosidase antibody shows a similar pattern to X-gal staining

(**A**) Immunostaining of R26lacZ$^{+/-}$ positive control E15.5 thymus shows similar results to X-gal staining. When compared to DAPI staining, it can once again be seen that a single, small localisation of β-gal is present on the outer edge of the nucleus (**B** and **D**). (**C**) Rabbit IgG isotype control was negative, when used with the same secondary antibody as in **A**. Wild-type E15.5 thymus also showed negative when treated with anti-β-gal. Scale bars are 20μm.

5.3. Discussion

From these experiments, it was concluded that the *laacZ* system, under the control of the ROSA26 promoter, is unsuitable for undertaking clonal analysis of the thymic epithelium at E15.5 or E16.5.

The observed numbers of thymus clones were far below what was expected (around 2% of the calculated number). The vast majority of clones discovered were tiny (1 or 2 cells), and nearly always within the thymic capsule or extrathymic. Although a prevalence of small clones would be expected, their spatial distribution was not. By definition, the ubiquitous expression of *R26laacZ* should produce labelled cells in all lineages, occurring throughout the organ. There is, however, anecdotal evidence that ROSA26 is not well expressed in $CD45^+$ cells - the most numerous thymic component at E15.5 and E16.5, and therefore the population within which the majority of clones were expected to occur. There may be a possibility that thymic epithelial cells may also express ROSA26 poorly. This would leave thymic mesenchyme as the major cell type able to produce detectable clones (as documented in Chapter Three), and may account for the observation of a disproportionate number of labelled cells belonging to this population. The greatest concentration of thymic mesenchyme occurs around the outside of the organ, in the capsule. Together, these factors may explain why most labelled cells were observed in this part of the thymus.

A weak staining pattern was observed in thymus lobes constitutively expressing β-gal, with staining apparent only as a single, intense, dot in most cells. This may indicate low levels of β-galactosidase protein expression, since staining with an anti-β-gal antibody showed a similar morphology. The dots of staining were localized on the edge of cell nuclei. If β-gal was expressed in a similar fashion in *laacZ-lacZ* cells, it may account for the difficulty in locating clones, since small groups of cells exhibiting this staining pattern would be extremely difficult to detect. A similar 'prominent blue spot' pattern has been described in pancreatic β-cells from *R26lacZ*$^{+/+}$ embryos (Percival and Slack, 1999). In addition, studies of primordial germ cells in *R26lacZ* embryos also report a 'cyan perinuclear dot of X-gal precipitate' (Adams and McLaren, 2002, Bielinska et al., 2007).

One possible explanation behind the problems in detecting βgal$^+$ cells is epigenetic silencing, due to cytosine methylation at CpG dinucleotides. CpG dinucleotides are not uniformly distributed, averaging only 1% of the vertebrate genome (Takai and Jones, 2002). However, CpG 'islands' of 300 – 3,000 base pairs, containing a higher frequency of CpG dinucleotides, are found in or near approximately 40% of mammalian gene promoters; frequently in those of widely expressed genes, and rarely in those exhibiting strict expression patterns (Fatemi et al., 2005, Saxonov et al., 2006, Gardiner-Garden and Frommer, 1987). CpG dinucleotides are prone to methylation by methyltransferases, leading to recruitment of chromatin proteins and silencing – 70% to 80% of mammalian CpG cytosines are methylated (Jabbari and Bernardi, 2004). However, CpG islands are somehow protected from hypermethylation under normal circumstances.

Bacterial DNA tends to have a higher proportion of CpG dinucleotides than is found in most vertebrates. These sequences can cause problems when introduced to the mammalian genome – CpG rich reporter transgenes can act as foci for *de novo* methylation, which can spread in *cis* by means that are poorly understood. This can result in the aberrant methylation and consequent inactivation of some promoters that are located in CpG islands. An experiment in transgenic mice where the CpG content of an introduced *lacZ* reporter was reduced demonstrated this (Chevalier-Mariette et al., 2003). The *lacZ* reporter was placed under the control of a transgenic human promoter of the α-subunit of the elongation factor 1 of translation (EF1α), a widely expressed gene included in a CpG island with a high (6.2%) CpG content. Three variants of the *lacZ* reporter with varying CpG content were used. The original *lacZ* had a CpG content of 9.24%. Two mutant alleles, *lagZ* and *lagoZ*, were engineered and had CpG contents of 1.6% and 0.06% respectively. These used alternate codons to encode the same amino acids as the original *lacZ* sequence. Histological studies using X-gal showed very poor β-galactosidase expression in *lacZ* mice. In *lagZ* mice expression was poor in most tissues, although levels were varied. In *lagoZ* mice, with the lowest CpG content, stronger expression of β-galactosidase was observed. Methylation studies revealed that, in the mice with the weakest transgene expression (*EF1αlacZ*), the CpG island where the EF1α promoter

was located had been hypermethylated, and consequently expression was silenced. Conversely, the promoter in the *EF1αlagoZ* mice escaped methylation, allowing transgene expression in most tissues examined (Chevalier-Mariette et al., 2003).

Furthermore, a recent study examining expression of *lacZ* under the control of the ubiquitous β-actin promoter also reported widespread silencing of the transgene (Strathdee et al., 2008). In ES cells and early embryonic (E9.5) tissue, *lacZ* expression was widespread, although a broad variation in expression levels was observed. As mice aged, *lacZ* expression became restricted to certain tissues, and within those was seen to be patchy. The β-actin promoter, located in a CpG island, was seen to be hypermethylated, particularly in differentiated cells (Strathdee et al., 2008).

To examine whether a similar mechanism of epigenetic silencing may be possible in the *R26lacZ* transgene used in my clonal analysis experiments in this chapter, I looked at the CpG content of the ROSA26 promoter (Figure 5.13). From a total of 534 base pairs in this sequence, there are 62 CpG dinucleotides. At 11.6%, this confirms that the ROSA26 promoter is contained within a CpG island. It is therefore entirely possible that, when placed adjacent to the CpG-rich *lacZ* reporter gene, *de novo* methylation spreads in *cis* from the reporter to the CpG-rich ROSA26 promoter sequence and results in silencing of the transgene in certain tissues.

Since I have shown, using E10.5 embryos, that the transgenic mice used in this chapter can produce β-gal$^+$ clones, and that my histological and detection techniques are able to display labelled cells at that age, it is likely that there are age-specific or tissue-specific problems with *R26lacZ* expression in these mouse lines.

It is possible to test the hypothesis of genetic silencing in specific thymus components. One could sort and collect the different thymic components by flow cytometry. RNA isolation and RT-PCR would then provide an answer as to whether RNA transcripts for β-galactosidase were being produced in any particular cell subsets.

```
  1 ctcgagttag gcccaacgcg gcgccacggc gtttcctggc cgggaatggc ccgtacccgt
 61 gaggtggggg tgggggcag aaaaggcgga gcgagccgga ggcgggagg gggagggcca
121 ggggcggagg gggccggcac tactgtgttg gcggactggc gggactaggg ctgcgtgagt
181 ctctgagcgc aggcgggcgg cggccgcccc tccccgggcg gcggcagcgg cggcagcggc
241 ggcagctcac tcagccgcgct gcccgagcgg aaacgccact gaccgcacgg ggattcccag
301 tgccgggcgcc aggggcacgc gggacacgcc ccctccgccc gcgccattgg cctctccgcc
361 caccgcccca cacttattgg ccggtgcgcc gccaatcagc ggaggctgcc ggggccgcct
421 aaagaagagg ctgtgctttg gggctccggc tcctcagaga gcctcggcta ggtaggggat
481 cgggactctg gcgggagggc ggcttggtgc gtttgcgggg atgggcggcc gcgg
```

Figure 5.13 CpG dinucleotides within ROSA26 promoter sequence

Mus Musculus ROSA26 region 534 bp promoter sequence DNA (GenBank: U83173). Position of CpG dinucleotides is highlighted in blue. From a possible 533 dinucleotide pairings, 62 (11.6%) are CpG.

Chapter 6. Concluding remarks

The work detailed in this thesis aimed to assess the lineage potential of fetal thymic epithelial progenitor cells, with regards to their ability to give rise to cortex and/or medulla, as thymus ontogeny proceeds.

I used a *ROSA26laacZ* non-invasive clonal labelling system to generate a library of clones for retrospective analysis. Since the *laacZ-lacZ* recombination rate had already been ascertained in ES cells (for two variants of the transgene, *R26laacZ0.3* and *R26laacZ1.1*), the theoretical average number of independent thymic epithelial cell clones in a thymus lobe of a given age could be calculated if the number of TECs present at that age were known.

Therefore, I began in Chapter Three by analysing the number of TECs present within a single developing thymus lobe from early until late organogenesis (E12.5 – E17.5). Due to the lack of detailed quantitative data on all thymic fetal cell populations, I also quantified haematopoietic, mesenchymal and endothelial populations at these time points. Consequently a defined data set now exists of thymic cell population sizes changes through thymus ontogeny, which will be of value to future studies of thymic developmental composition and kinetics.

In Chapter Four, I examined the Plet1^{+} content of the TEC population. Here, I discovered that there is no significant change in the absolute number of Plet1^{+} TECs between E12.5 and E17.5. Furthermore, I used DNA quantification to demonstrate that the proportion (and thus the absolute number) of Plet1^{+} TECs undergoing proliferation at any one time decreases as thymus ontogeny proceeds.

My experimental results from Chapter Four are consistent with a developmental model in which Plet1^{-} transit amplifying (TA) cells are produced from the Plet1^{+} population. A continual increase in the total TEC population size, coupled with a continual decrease in the rate of Plet1^{+} proliferation, suggests that fully differentiated TECs are produced from a dynamic population of Plet1^{-} TA TECs with high proliferative capabilities.

Recently, some doubt has been cast over the nature and identity of TEPCs. A recent investigation compared the ability of Plet1^{+} and Plet1^{-} TECs to generate a functional

thymic microenvironment. The authors stated there were no differences in proliferative potential, organisational abilities, and T-cell maturation, between Plet1^{+} and Plet1^{-} TECs from E14, E16 or E18 mouse embryos (Rossi et al., 2007a). Expression of genes associated with epithelial progenitor status in other tissues, such as p63 and BCRP-1, was also seen to occur at comparable levels in both TEC subsets.

Discrepancies between these results and those of earlier work in E15.5 TECs by Gill *et al*, where Plet1^{-} TECs did not form a functional thymic microenvironment, may be due to a larger number of TECs (2,500 vs. 100,000) being reaggregated in this instance (Rossi et al., 2007a, Gill et al., 2002). In addition, the earlier study allowed grafted tissue to develop for 8 weeks as opposed to a 4-week time window in the Rossi *et al* paper. It may be that the maintenance and survival of 100,000 cells for 4 weeks is more feasible than that of only 2,500 cells for twice that period.

However, it can also be seen from the work done in Chapter Four of this thesis that the Plet1^{-} population contains a large number of proliferating cells. It is likely that these are a transit amplifying population that can go on to produce differentiated, functional thymic epithelium.

In an attempt to track the proliferative behaviour of individual cells over time, I attempted an ultimately unsuccessful *in vitro* double-labelling of TECs with halogenated thymidine analogues. However, some preliminary work using BrdU labelling showed 90% of cells proliferating in the 26 hours prior to E14.5, confirming Plet1+ TECs to be highly active during early thymus organogenesis.

As a follow-up experiment, a set of 26-hour BrdU pulses beginning at different time points during organogenesis (similar to those in Figure 4.10), would be interesting. Starting with E12.5 and progressing in 12-hour intervals until E17.5, these additional experiments would indicate which of the two proliferation models shown in Figure 2.9 was more likely. BrdU has been used previously to examine TEC proliferation from E15 to E18, but on the epithelial population as a whole and not the Plet1^{+} population specifically (Anderson et al., 1998).

Future work could also follow up the BrdU labelling with a chase period, where it could be seen whether the BrdU was retained by Plet1^{+} cells. Retention of BrdU in some cells but not in others would indicate non-uniform division, where as the loss of BrdU in all Plet1^{+} cells would indicate the uniform division model where all cells continue to proliferate, but at a reduced rate.

In Chapter Five, I used the data on TEC number from Chapter Three to calculate the mean number of independent epithelial clones potentially occurring in a single thymus lobe. This information was calculated for each 24-hour time point from E12.5 until E17.5, resulting in data for each heterozygous and homozygous combination of wild-type, *R26laacZ0.3* and *R26laacZ1.1* genotypes. These findings resulted in selection and analysis of E16.5 *R26laacZ0.3*$^{+/+}$ embryos.

Upon subsequent collection, processing and analysis of thymus lobes, I observed a far lower than expected number of clones - none of which could be classified as epithelial. Consequently, I analysed thymus lobes from E15.5 *R26laacZ1.1*$^{+/+}$ embryos, in an attempt to increase the level of clone generation and observation. However, similar results were observed, with no epithelial clones seen. I extensively analysed and optimised the histological techniques involved in embryo fixation, X-gal staining and clone visualisation, and concluded that the problem lay in expression of the *ROSA26lacZ* transgene. My analysis of the *ROSA26* promoter revealed a high CpG dinucleotide content which, in combination with the high CpG content of the *lacZ* reporter sequence, has in theory a high likelihood of undergoing methylation-induced silencing.

In retrospect, if I repeated this work, I would address the problems of this transgene as a reporter of genetic recombination by re-engineering the *laacZ* sequence. Point mutations altering CpG dinucleotides could be introduced, enabling alternate codons for the appropriate amino acids to be used.

In an ideal situation, I would use a mouse where the *laacZ* gene was expressed in a thymic epithelial-specific manner. This could be achieved by creating a *Foxn1laacZ* mouse, as *Foxn1Cre* paired with a *R26laacZ* reporter would probably inherit the same silenced expression pattern as I found during my work.

List of Figures

List of Tables

References

AALTONEN, J., HORELLI-KUITUNEN, N., FAN, J. B., BJORSES, P., PERHEENTUPA, J., MYERS, R., PALOTIE, A. & PELTONEN, L. (1997) High-resolution physical and transcriptional mapping of the autoimmune polyendocrinopathy-candidiasis-ectodermal dystrophy locus on chromosome 21q22.3 by FISH. *Genome Res,* 7, 820-9.

ADAMS, I. R. & MCLAREN, A. (2002) Sexually dimorphic development of mouse primordial germ cells: switching from oogenesis to spermatogenesis. *Development,* 129, 1155-64.

ALEXIADES, M. R. & CEPKO, C. (1996) Quantitative analysis of proliferation and cell cycle length during development of the rat retina. *Dev Dyn,* 205, 293-307.

ANDERSON, G., JENKINSON, E. J., MOORE, N. C. & OWEN, J. J. (1993) MHC class II-positive epithelium and mesenchyme cells are both required for T-cell development in the thymus. *Nature,* 362, 70-3.

ANDERSON, G., OWEN, J. J., MOORE, N. C. & JENKINSON, E. J. (1994) Thymic epithelial cells provide unique signals for positive selection of CD4+CD8+ thymocytes in vitro. *J Exp Med,* 179, 2027-31.

ANDERSON, K. L., MOORE, N. C., MCLOUGHLIN, D. E., JENKINSON, E. J. & OWEN, J. J. (1998) Studies on thymic epithelial cells in vitro. *Dev Comp Immunol,* 22, 367-77.

ANDERSON, M., ANDERSON, S. K. & FARR, A. G. (2000) Thymic vasculature: organizer of the medullary epithelial compartment? *Int Immunol,* 12, 1105-10.

ANDERSON, M. S., VENANZI, E. S., KLEIN, L., CHEN, Z., BERZINS, S. P., TURLEY, S. J., VON BOEHMER, H., BRONSON, R., DIERICH, A., BENOIST, C. & MATHIS, D. (2002) Projection of an immunological self shadow within the thymus by the aire protein. *Science,* 298, 1395-401.

ANDREE, H. A., REUTELINGSPERGER, C. P., HAUPTMANN, R., HEMKER, H. C., HERMENS, W. T. & WILLEMS, G. M. (1990) Binding of vascular anticoagulant alpha (VAC alpha) to planar phospholipid bilayers. *J Biol Chem,* 265, 4923-8.

ANNUNZIATO, F., ROMAGNANI, P., COSMI, L., BELTRAME, C., STEINER, B. H., LAZZERI, E., RAPORT, C. J., GALLI, G., MANETTI, R., MAVILIA, C., VANINI, V., CHANTRY, D., MAGGI, E. & ROMAGNANI, S. (2000) Macrophage-derived chemokine and EBI1-ligand chemokine attract human thymocytes in different stage of development and are produced by distinct subsets of medullary epithelial cells: possible implications for negative selection. *J Immunol,* 165, 238-46.

ATEN, J. A., BAKKER, P. J., STAP, J., BOSCHMAN, G. A. & VEENHOF, C. H. (1992) DNA double labelling with IdUrd and CldUrd for spatial and temporal analysis of cell proliferation and DNA replication. *Histochem J,* 24, 251-9.

AUERBACH, R. (1960) Morphogenetic interactions in the development of the mouse thymus gland. *Dev Biol,* 2, 271-84.

BAKKER, P. J., STAP, J., TUKKER, C. J., VAN OVEN, C. H., VEENHOF, C. H. & ATEN, J. (1991) An indirect immunofluorescence double staining procedure for the simultaneous flow cytometric measurement of iodo- and chlorodeoxyuridine incorporated into DNA. *Cytometry,* 12, 366-72.

BALCIUNAITE, G., CEREDIG, R. & ROLINK, A. G. (2005) The earliest subpopulation of mouse thymocytes contains potent T, significant macrophage, and natural killer cell but no B-lymphocyte potential. *Blood,* 105, 1930-6.

BARKER, N., VAN ES, J. H., KUIPERS, J., KUJALA, P., VAN DEN BORN, M., COZIJNSEN, M., HAEGEBARTH, A., KORVING, J., BEGTHEL, H., PETERS, P. J. & CLEVERS, H. (2007) Identification of stem cells in small intestine and colon by marker gene Lgr5. *Nature,* 449, 1003-7.

BARRANDON, Y. & GREEN, H. (1987) Three clonal types of keratinocyte with different capacities for multiplication. *Proc Natl Acad Sci U S A,* 84, 2302-6.

BENNETT, A. R., FARLEY, A., BLAIR, N. F., GORDON, J., SHARP, L. & BLACKBURN, C. C. (2002) Identification and characterization of thymic epithelial progenitor cells. *Immunity,* 16, 803-14.

BETSHOLTZ, C. (2003) Biology of platelet-derived growth factors in development. *Birth Defects Res C Embryo Today,* 69, 272-85.

BHUSHAN, A., ITOH, N., KATO, S., THIERY, J. P., CZERNICHOW, P., BELLUSCI, S. & SCHARFMANN, R. (2001) Fgf10 is essential for maintaining the proliferative capacity of epithelial progenitor cells during early pancreatic organogenesis. *Development,* 128, 5109-17.

BIELINSKA, M., SEEHRA, A., TOPPARI, J., HEIKINHEIMO, M. & WILSON, D. B. (2007) GATA-4 is required for sex steroidogenic cell development in the fetal mouse. *Dev Dyn,* 236, 203-13.

BLACKBURN, C. C., AUGUSTINE, C. L., LI, R., HARVEY, R. P., MALIN, M. A., BOYD, R. L., MILLER, J. F. & MORAHAN, G. (1996) The nu gene acts cell-autonomously and is required for differentiation of thymic epithelial progenitors. *Proc Natl Acad Sci U S A,* 93, 5742-6.

BLACKBURN, C. C. & MANLEY, N. R. (2004) Developing a new paradigm for thymus organogenesis. *Nat Rev Immunol,* 4, 278-89.

BLANPAIN, C., LOWRY, W. E., GEOGHEGAN, A., POLAK, L. & FUCHS, E. (2004) Self-renewal, multipotency, and the existence of two cell populations within an epithelial stem cell niche. *Cell,* 118, 635-48.

BLAU, J. N. (1973) Hassall's corpuscles--a site of thymocyte death. *Br J Exp Pathol,* 54, 634-7.

BLEUL, C. C., CORBEAUX, T., REUTER, A., FISCH, P., MONTING, J. S. & BOEHM, T. (2006) Formation of a functional thymus initiated by a postnatal epithelial progenitor cell. *Nature,* 441, 992-6.

BOCK, T., PAKKENBERG, B. & BUSCHARD, K. (2003) Increased islet volume but unchanged islet number in ob/ob mice. *Diabetes,* 52, 1716-22.

BOCKMAN, D. E. & KIRBY, M. L. (1984) Dependence of thymus development on derivatives of the neural crest. *Science,* 223, 498-500.

BOEHM, T., SCHEU, S., PFEFFER, K. & BLEUL, C. C. (2003) Thymic medullary epithelial cell differentiation, thymocyte emigration, and the control of autoimmunity require lympho-epithelial cross talk via LTbetaR. *J Exp Med,* 198, 757-69.

BONNEROT, C. & NICOLAS, J. F. (1993) Clonal analysis in the intact mouse embryo by intragenic homologous recombination. *C R Acad Sci III,* 316, 1207-17.

BORKOWSKI, T. A., NELSON, A. J., FARR, A. G. & UDEY, M. C. (1996) Expression of gp40, the murine homologue of human epithelial cell adhesion molecule (Ep-CAM), by murine dendritic cells. *Eur J Immunol,* 26, 110-4.

BOYD, R. L., TUCEK, C. L., GODFREY, D. I., IZON, D. J., WILSON, T. J., DAVIDSON, N. J., BEAN, A. G., LADYMAN, H. M., RITTER, M. A. & HUGO, P. (1993) The thymic microenvironment. *Immunol Today,* 14, 445-59.

BOYD, R. L., WILSON, T. J., BEAN, A. G., WARD, H. A. & GERSHWIN, M. E. (1992) Phenotypic characterization of chicken thymic stromal elements. *Dev Immunol,* 2, 51-66.

BREKELMANS, P. & VAN EWIJK, W. (1990) Phenotypic characterization of murine thymic microenvironments. *Semin Immunol,* 2, 13-24.

BROOKS, S. E., GU, X., KAUFMANN, P. M., MARCUS, D. M. & CALDWELL, R. B. (1998) Modulation of VEGF production by pH and glucose in retinal Muller cells. *Curr Eye Res,* 17, 875-82.

BRUGNERA, E., BHANDOOLA, A., CIBOTTI, R., YU, Q., GUINTER, T. I., YAMASHITA, Y., SHARROW, S. O. & SINGER, A. (2000) Coreceptor reversal in the thymus: signaled CD4+8+ thymocytes initially terminate CD8 transcription even when differentiating into CD8+ T cells. *Immunity,* 13, 59-71.

BUTLER, A. E., JANSON, J., SOELLER, W. C. & BUTLER, P. C. (2003) Increased beta-cell apoptosis prevents adaptive increase in beta-cell mass in mouse model of type 2 diabetes: evidence for role of islet amyloid formation rather than direct action of amyloid. *Diabetes,* 52, 2304-14.

CAI, W. B., ROBERTS, S. A. & POTTEN, C. S. (1997) The number of clonogenic cells in crypts in three regions of murine large intestine. *Int J Radiat Biol,* 71, 573-9.

CANDI, E., RUFINI, A., TERRINONI, A., GIAMBOI-MIRAGLIA, A., LENA, A. M., MANTOVANI, R., KNIGHT, R. & MELINO, G. (2007) DeltaNp63 regulates thymic development through enhanced expression of FgfR2 and Jag2. *Proc Natl Acad Sci U S A,* 104, 11999-2004.

CEPKO, C. L., FIELDS-BERRY, S., RYDER, E., AUSTIN, C. & GOLDEN, J. (1998) Lineage analysis using retroviral vectors. *Curr Top Dev Biol,* 36, 51-74.

CHAPMAN, D. L., GARVEY, N., HANCOCK, S., ALEXIOU, M., AGULNIK, S. I., GIBSON-BROWN, J. J., CEBRA-THOMAS, J., BOLLAG, R. J., SILVER, L. M.

& PAPAIOANNOU, V. E. (1996) Expression of the T-box family genes, Tbx1-Tbx5, during early mouse development. *Dev Dyn,* 206, 379-90.

CHEN, L., XIAO, S. & MANLEY, N. R. (2009) Foxn1 is required to maintain the postnatal thymic microenvironment in a dosage-sensitive manner. *Blood,* 113, 567-74.

CHEVALIER-MARIETTE, C., HENRY, I., MONTFORT, L., CAPGRAS, S., FORLANI, S., MUSCHLER, J. & NICOLAS, J. F. (2003) CpG content affects gene silencing in mice: evidence from novel transgenes. *Genome Biol,* 4, R53.

CIRNE-LIMA, E. O., VAN EWIJK, W. & SAVINO, W. (1993) Cortical and medullary phenotypes within a mouse thymic epithelial cell line. *In Vitro Cell Dev Biol Anim,* 29A, 443-5.

CLAYTON, E., DOUPE, D. P., KLEIN, A. M., WINTON, D. J., SIMONS, B. D. & JONES, P. H. (2007) A single type of progenitor cell maintains normal epidermis. *Nature,* 446, 185-9.

CORDIER, A. C. & HAUMONT, S. M. (1980) Development of thymus, parathyroids, and ultimo-branchial bodies in NMRI and nude mice. *Am J Anat,* 157, 227-63.

CORDIER, A. C. & HEREMANS, J. F. (1975) Nude mouse embryo: ectodermal nature of the primordial thymic defect. *Scand J Immunol,* 4, 193-6.

COTSARELIS, G., SUN, T. T. & LAVKER, R. M. (1990) Label-retaining cells reside in the bulge area of pilosebaceous unit: implications for follicular stem cells, hair cycle, and skin carcinogenesis. *Cell,* 61, 1329-37.

DANIELIAN, P. S., MUCCINO, D., ROWITCH, D. H., MICHAEL, S. K. & MCMAHON, A. P. (1998) Modification of gene activity in mouse embryos in utero by a tamoxifen-inducible form of Cre recombinase. *Curr Biol,* 8, 1323-6.

DEPRETER, M. G., BLAIR, N. F., GASKELL, T. L., NOWELL, C. S., DAVERN, K., PAGLIOCCA, A., STENHOUSE, F. H., FARLEY, A. M., FRASER, A., VRANA, J., ROBERTSON, K., MORAHAN, G., TOMLINSON, S. R. & BLACKBURN, C. C. (2008) Identification of Plet-1 as a specific marker of early thymic epithelial progenitor cells. *Proc Natl Acad Sci U S A,* 105, 961-6.

DERBINSKI, J., SCHULTE, A., KYEWSKI, B. & KLEIN, L. (2001) Promiscuous gene expression in medullary thymic epithelial cells mirrors the peripheral self. *Nat Immunol,* 2, 1032-9.

DOOLEY, J., ERICKSON, M. & FARR, A. G. (2008) Alterations of the medullary epithelial compartment in the Aire-deficient thymus: implications for programs of thymic epithelial differentiation. *J Immunol,* 181, 5225-32.

DOR, Y., BROWN, J., MARTINEZ, O. I. & MELTON, D. A. (2004) Adult pancreatic beta-cells are formed by self-duplication rather than stem-cell differentiation. *Nature,* 429, 41-6.

DUDLEY, E. C., PETRIE, H. T., SHAH, L. M., OWEN, M. J. & HAYDAY, A. C. (1994) T cell receptor beta chain gene rearrangement and selection during thymocyte development in adult mice. *Immunity,* 1, 83-93.

EGAWA, T. & LITTMAN, D. R. (2008) ThPOK acts late in specification of the helper T cell lineage and suppresses Runx-mediated commitment to the cytotoxic T cell lineage. *Nat Immunol,* 9, 1131-9.

EIREW, P., STINGL, J., RAOUF, A., TURASHVILI, G., APARICIO, S., EMERMAN, J. T. & EAVES, C. J. (2008) A method for quantifying normal human mammary epithelial stem cells with in vivo regenerative ability. *Nat Med,* 14, 1384-9.

ELOY-TRINQUET, S. & NICOLAS, J. F. (2002) Cell coherence during production of the presomitic mesoderm and somitogenesis in the mouse embryo. *Development,* 129, 3609-19.

FADOK, V. A., VOELKER, D. R., CAMPBELL, P. A., COHEN, J. J., BRATTON, D. L. & HENSON, P. M. (1992) Exposure of phosphatidylserine on the surface of apoptotic lymphocytes triggers specific recognition and removal by macrophages. *J Immunol,* 148, 2207-16.

FARR, A. G., DOOLEY, J. L. & ERICKSON, M. (2002) Organization of thymic medullary epithelial heterogeneity: implications for mechanisms of epithelial differentiation. *Immunol Rev,* 189, 20-7.

FARR, A. G. & NAKANE, P. K. (1983) Cells bearing Ia antigens in the murine thymus. An ultrastructural study. *Am J Pathol,* 111, 88-97.

FATEMI, M., PAO, M. M., JEONG, S., GAL-YAM, E. N., EGGER, G., WEISENBERGER, D. J. & JONES, P. A. (2005) Footprinting of mammalian promoters: use of a CpG DNA methyltransferase revealing nucleosome positions at a single molecule level. *Nucleic Acids Res,* 33, e176.

FLETCHER, A. L., SEACH, N., REISEGER, J. J., LOWEN, T. E., HAMMETT, M. V., SCOTT, H. S. & BOYD, R. L. (2009) Reduced thymic Aire expression and abnormal NF-kappa B2 signaling in a model of systemic autoimmunity. *J Immunol,* 182, 2690-9.

FOSTER, K., SHERIDAN, J., VEIGA-FERNANDES, H., RODERICK, K., PACHNIS, V., ADAMS, R., BLACKBURN, C., KIOUSSIS, D. & COLES, M. (2008) Contribution of neural crest-derived cells in the embryonic and adult thymus. *J Immunol,* 180, 3183-9.

FRIEDRICH, G. & SORIANO, P. (1991) Promoter traps in embryonic stem cells: a genetic screen to identify and mutate developmental genes in mice. *Genes Dev,* 5, 1513-23.

GARDINER-GARDEN, M. & FROMMER, M. (1987) CpG islands in vertebrate genomes. *J Mol Biol,* 196, 261-82.

GILL, J., MALIN, M., HOLLANDER, G. A. & BOYD, R. (2002) Generation of a complete thymic microenvironment by MTS24(+) thymic epithelial cells. *Nat Immunol,* 3, 635-42.

GODFREY, D. I., IZON, D. J., TUCEK, C. L., WILSON, T. J. & BOYD, R. L. (1990) The phenotypic heterogeneity of mouse thymic stromal cells. *Immunology,* 70, 66-74.

GODFREY, D. I., KENNEDY, J., SUDA, T. & ZLOTNIK, A. (1993) A developmental pathway involving four phenotypically and functionally distinct subsets of CD3-CD4-CD8- triple-negative adult mouse thymocytes defined by CD44 and CD25 expression. *J Immunol,* 150, 4244-52.

GODFREY, D. I. & ZLOTNIK, A. (1993) Control points in early T-cell development. *Immunol Today,* 14, 547-53.

GORDON, J., BENNETT, A. R., BLACKBURN, C. C. & MANLEY, N. R. (2001) Gcm2 and Foxn1 mark early parathyroid- and thymus-specific domains in the developing third pharyngeal pouch. *Mech Dev,* 103, 141-3.

GORDON, J., WILSON, V. A., BLAIR, N. F., SHERIDAN, J., FARLEY, A., WILSON, L., MANLEY, N. R. & BLACKBURN, C. C. (2004) Functional evidence for a single endodermal origin for the thymic epithelium. *Nat Immunol,* 5, 546-53.

GORDON, J., XIAO, S., HUGHES, B., 3RD, SU, D. M., NAVARRE, S. P., CONDIE, B. G. & MANLEY, N. R. (2007) Specific expression of lacZ and cre recombinase in fetal thymic epithelial cells by multiplex gene targeting at the Foxn1 locus. *BMC Dev Biol,* 7, 69.

GRAY, D., ABRAMSON, J., BENOIST, C. & MATHIS, D. (2007a) Proliferative arrest and rapid turnover of thymic epithelial cells expressing Aire. *J Exp Med,* 204, 2521-8.

GRAY, D. H., CHIDGEY, A. P. & BOYD, R. L. (2002) Analysis of thymic stromal cell populations using flow cytometry. *J Immunol Methods,* 260, 15-28.

GRAY, D. H., SEACH, N., UENO, T., MILTON, M. K., LISTON, A., LEW, A. M., GOODNOW, C. C. & BOYD, R. L. (2006) Developmental kinetics, turnover, and stimulatory capacity of thymic epithelial cells. *Blood,* 108, 3777-85.

GRAY, D. H., TULL, D., UENO, T., SEACH, N., CLASSON, B. J., CHIDGEY, A., MCCONVILLE, M. J. & BOYD, R. L. (2007b) A unique thymic fibroblast population revealed by the monoclonal antibody MTS-15. *J Immunol,* 178, 4956-65.

GROETTRUP, M. & VON BOEHMER, H. (1993) A role for a pre-T-cell receptor in T-cell development. *Immunol Today,* 14, 610-4.

GUNTHER, T., CHEN, Z. F., KIM, J., PRIEMEL, M., RUEGER, J. M., AMLING, M., MOSELEY, J. M., MARTIN, T. J., ANDERSON, D. J. & KARSENTY, G. (2000) Genetic ablation of parathyroid glands reveals another source of parathyroid hormone. *Nature,* 406, 199-203.

HAEGEBARTH, A. & CLEVERS, H. (2009) Wnt signaling, lgr5, and stem cells in the intestine and skin. *Am J Pathol,* 174, 715-21.

HAMAZAKI, Y., FUJITA, H., KOBAYASHI, T., CHOI, Y., SCOTT, H. S., MATSUMOTO, M. & MINATO, N. (2007) Medullary thymic epithelial cells expressing Aire represent a unique lineage derived from cells expressing claudin. *Nat Immunol,* 8, 304-11.

HE, W., ZHANG, Y., DENG, Y. & KABELITZ, D. (1995) Induction of TCR-gamma delta expression on triple-negative (CD3-4-8-) human thymocytes. Comparative analysis of the effects of IL-4 and IL-7. *J Immunol,* 154, 3726-31.

HETZER-EGGER, C., SCHORPP, M., HAAS-ASSENBAUM, A., BALLING, R., PETERS, H. & BOEHM, T. (2002) Thymopoiesis requires Pax9 function in thymic epithelial cells. *Eur J Immunol,* 32, 1175-81.

HOFMEISTER, R., KHALED, A. R., BENBERNOU, N., RAJNAVOLGYI, E., MUEGGE, K. & DURUM, S. K. (1999) Interleukin-7: physiological roles and mechanisms of action. *Cytokine Growth Factor Rev,* 10, 41-60.

HOLLANDER, G. A., WANG, B., NICHOGIANNOPOULOU, A., PLATENBURG, P. P., VAN EWIJK, W., BURAKOFF, S. J., GUTIERREZ-RAMOS, J. C. & TERHORST, C. (1995) Developmental control point in induction of thymic cortex regulated by a subpopulation of prothymocytes. *Nature,* 373, 350-3.

HOLMQUIST, G. P. (1987) Role of replication time in the control of tissue-specific gene expression. *Am J Hum Genet,* 40, 151-73.

HORSLEY, V., O'CARROLL, D., TOOZE, R., OHINATA, Y., SAITOU, M., OBUKHANYCH, T., NUSSENZWEIG, M., TARAKHOVSKY, A. & FUCHS, E. (2006) Blimp1 defines a progenitor population that governs cellular input to the sebaceous gland. *Cell,* 126, 597-609.

HUBERT, F. X., KINKEL, S. A., WEBSTER, K. E., CANNON, P., CREWTHER, P. E., PROEITTO, A. I., WU, L., HEATH, W. R. & SCOTT, H. S. (2008) A specific anti-Aire antibody reveals aire expression is restricted to medullary thymic epithelial cells and not expressed in periphery. *J Immunol,* 180, 3824-32.

IRLA, M., HUGUES, S., GILL, J., NITTA, T., HIKOSAKA, Y., WILLIAMS, I. R., HUBERT, F. X., SCOTT, H. S., TAKAHAMA, Y., HOLLANDER, G. A. & REITH, W. (2008) Autoantigen-specific interactions with CD4+ thymocytes control mature medullary thymic epithelial cell cellularity. *Immunity,* 29, 451-63.

ITO, M., LIU, Y., YANG, Z., NGUYEN, J., LIANG, F., MORRIS, R. J. & COTSARELIS, G. (2005) Stem cells in the hair follicle bulge contribute to wound repair but not to homeostasis of the epidermis. *Nat Med,* 11, 1351-4.

ITOI, M. & AMAGAI, T. (1998) Inductive role of fibroblastic cell lines in development of the mouse thymus anlage in organ culture. *Cell Immunol,* 183, 32-41.

ITOI, M., KAWAMOTO, H., KATSURA, Y. & AMAGAI, T. (2001) Two distinct steps of immigration of hematopoietic progenitors into the early thymus anlage. *Int Immunol,* 13, 1203-11.

ITOI, M., TSUKAMOTO, N., YOSHIDA, H. & AMAGAI, T. (2007) Mesenchymal cells are required for functional development of thymic epithelial cells. *Int Immunol,* 19, 953-64.

JABBARI, K. & BERNARDI, G. (2004) Cytosine methylation and CpG, TpG (CpA) and TpA frequencies. *Gene,* 333, 143-9.

JAKS, V., BARKER, N., KASPER, M., VAN ES, J. H., SNIPPERT, H. J., CLEVERS, H. & TOFTGARD, R. (2008) Lgr5 marks cycling, yet long-lived, hair follicle stem cells. *Nat Genet,* 40, 1291-9.

JENKINSON, E. J., VAN EWIJK, W. & OWEN, J. J. (1981) Major histocompatibility complex antigen expression on the epithelium of the developing thymus in normal and nude mice. *J Exp Med,* 153, 280-92.

JENKINSON, W. E., BACON, A., WHITE, A. J., ANDERSON, G. & JENKINSON, E. J. (2008) An epithelial progenitor pool regulates thymus growth. *J Immunol,* 181, 6101-8.

JENKINSON, W. E., JENKINSON, E. J. & ANDERSON, G. (2003) Differential requirement for mesenchyme in the proliferation and maturation of thymic epithelial progenitors. *J Exp Med,* 198, 325-32.

JENKINSON, W. E., ROSSI, S. W., JENKINSON, E. J. & ANDERSON, G. (2005) Development of functional thymic epithelial cells occurs independently of lymphostromal interactions. *Mech Dev,* 122, 1294-9.

JENKINSON, W. E., ROSSI, S. W., PARNELL, S. M., JENKINSON, E. J. & ANDERSON, G. (2007) PDGFRalpha-expressing mesenchyme regulates thymus growth and the availability of intrathymic niches. *Blood,* 109, 954-60.

JENSEN, U. B., YAN, X., TRIEL, C., WOO, S. H., CHRISTENSEN, R. & OWENS, D. M. (2008) A distinct population of clonogenic and multipotent murine follicular keratinocytes residing in the upper isthmus. *J Cell Sci,* 121, 609-17.

JEROME, L. A. & PAPAIOANNOU, V. E. (2001) DiGeorge syndrome phenotype in mice mutant for the T-box gene, Tbx1. *Nat Genet,* 27, 286-91.

JIANG, X., ROWITCH, D. H., SORIANO, P., MCMAHON, A. P. & SUCOV, H. M. (2000) Fate of the mammalian cardiac neural crest. *Development,* 127, 1607-16.

KAMINSKI, W. E., LINDAHL, P., LIN, N. L., BROUDY, V. C., CROSBY, J. R., HELLSTROM, M., SWOLIN, B., BOWEN-POPE, D. F., MARTIN, P. J., ROSS, R., BETSHOLTZ, C. & RAINES, E. W. (2001) Basis of hematopoietic defects in platelet-derived growth factor (PDGF)-B and PDGF beta-receptor null mice. *Blood,* 97, 1990-8.

KAMPINGA, J., BERGES, S., BOYD, R. L., BREKELMANS, P., COLIC, M., VAN EWIJK, W., KENDALL, M. D., LADYMAN, H., NIEUWENHUIS, P., RITTER, M. A. & ET AL. (1989) Thymic epithelial antibodies: immunohistological analysis and introduction of nomenclature. *Thymus,* 13, 165-73.

KANARIOU, M., HUBY, R., LADYMAN, H., COLIC, M., SIVOLAPENKO, G., LAMPERT, I. & RITTER, M. (1989) Immunosuppression with cyclosporin A alters the thymic microenvironment. *Clin Exp Immunol,* 78, 263-70.

KATO, S. (1997) Thymic microvascular system. *Microsc Res Tech,* 38, 287-99.

KATO, S. & SCHOEFL, G. I. (1989) Microvasculature of normal and involuted mouse thymus. Light- and electron-microscopic study. *Acta Anat (Basel),* 135, 1-11.

KENDALL, M. D. (1989) The morphology of perivascular spaces in the thymus. *Thymus,* 13, 157-64.

KENDALL, M. D. (1991) Functional anatomy of the thymic microenvironment. *J Anat,* 177, 1-29.

KENDALL, M. D. & AL-SHAWAF, A. A. (1991) Innervation of the rat thymus gland. *Brain Behav Immun,* 5, 9-28.

KLUG, D. B., CARTER, C., CROUCH, E., ROOP, D., CONTI, C. J. & RICHIE, E. R. (1998) Interdependence of cortical thymic epithelial cell differentiation and T-lineage commitment. *Proc Natl Acad Sci U S A,* 95, 11822-7.

KLUG, D. B., CARTER, C., GIMENEZ-CONTI, I. B. & RICHIE, E. R. (2002) Cutting edge: thymocyte-independent and thymocyte-dependent phases of epithelial patterning in the fetal thymus. *J Immunol,* 169, 2842-5.

KOBAYASHI, K., ROCHAT, A. & BARRANDON, Y. (1993) Segregation of keratinocyte colony-forming cells in the bulge of the rat vibrissa. *Proc Natl Acad Sci U S A,* 90, 7391-5.

KOHU, K., SATO, T., OHNO, S., HAYASHI, K., UCHINO, R., ABE, N., NAKAZATO, M., YOSHIDA, N., KIKUCHI, T., IWAKURA, Y., INOUE, Y., WATANABE, T., HABU, S. & SATAKE, M. (2005) Overexpression of the Runx3 transcription factor increases the proportion of mature thymocytes of the CD8 single-positive lineage. *J Immunol,* 174, 2627-36.

KRUMLAUF, R. (1994) Hox genes in vertebrate development. *Cell,* 78, 191-201.

KURODA, N., MITANI, T., TAKEDA, N., ISHIMARU, N., ARAKAKI, R., HAYASHI, Y., BANDO, Y., IZUMI, K., TAKAHASHI, T., NOMURA, T., SAKAGUCHI, S., UENO, T., TAKAHAMA, Y., UCHIDA, D., SUN, S., KAJIURA, F., MOURI, Y., HAN, H., MATSUSHIMA, A., YAMADA, G. & MATSUMOTO, M. (2005) Development of autoimmunity against transcriptionally unrepressed target antigen in the thymus of Aire-deficient mice. *J Immunol,* 174, 1862-70.

KUSHNER, J. A., YE, J., SCHUBERT, M., BURKS, D. J., DOW, M. A., FLINT, C. L., DUTTA, S., WRIGHT, C. V., MONTMINY, M. R. & WHITE, M. F. (2002) Pdx1 restores beta cell function in Irs2 knockout mice. *J Clin Invest,* 109, 1193-201.

KYEWSKI, B., DERBINSKI, J., GOTTER, J. & KLEIN, L. (2002) Promiscuous gene expression and central T-cell tolerance: more than meets the eye. *Trends Immunol,* 23, 364-71.

LACLEF, C., SOUIL, E., DEMIGNON, J. & MAIRE, P. (2003) Thymus, kidney and craniofacial abnormalities in Six 1 deficient mice. *Mech Dev,* 120, 669-79.

LAUFER, T. M., DEKONING, J., MARKOWITZ, J. S., LO, D. & GLIMCHER, L. H. (1996) Unopposed positive selection and autoreactivity in mice expressing class II MHC only on thymic cortex. *Nature,* 383, 81-5.

LE DOUARIN, N. & JOTEREAU, F. (1973) [Embryologic origin of thymus lymphocytes in bird embryos]. *C R Acad Sci Hebd Seances Acad Sci D,* 276, 629-32.

LE DOUARIN, N. M. (1974) Cell recognition based on natural morphological nuclear markers. *Med Biol,* 52, 281-319.

LE DOUARIN, N. M. & JOTEREAU, F. V. (1975) Tracing of cells of the avian thymus through embryonic life in interspecific chimeras. *J Exp Med,* 142, 17-40.

LE LIEVRE, C. S. & LE DOUARIN, N. M. (1975) Mesenchymal derivatives of the neural crest: analysis of chimaeric quail and chick embryos. *J Embryol Exp Morphol,* 34, 125-54.

LE, P. T., LAZORICK, S., WHICHARD, L. P., HAYNES, B. F. & SINGER, K. H. (1991) Regulation of cytokine production in the human thymus: epidermal growth factor and transforming growth factor alpha regulate mRNA levels of interleukin 1 alpha (IL-1 alpha), IL-1 beta, and IL-6 in human thymic epithelial cells at a post-transcriptional level. *J Exp Med,* 174, 1147-57.

LECHLER, T. & FUCHS, E. (2005) Asymmetric cell divisions promote stratification and differentiation of mammalian skin. *Nature,* 437, 275-80.

LEUNG, D. W., CACHIANES, G., KUANG, W. J., GOEDDEL, D. V. & FERRARA, N. (1989) Vascular endothelial growth factor is a secreted angiogenic mitogen. *Science,* 246, 1306-9.

LI, A., LIU, X., DUAN, B. & MA, J. (2005) Thymic nurse cells support CD4-CD8+ thymocytes to differentiate into CD4+CD8+ cells. *Cell Mol Immunol,* 2, 301-5.

LI, Y., PEZZANO, M., PHILP, D., REID, V. & GUYDEN, J. (1992) Thymic nurse cells exclusively bind and internalize CD4+CD8+ thymocytes. *Cell Immunol,* 140, 495-506.

LIND, E. F., PROCKOP, S. E., PORRITT, H. E. & PETRIE, H. T. (2001) Mapping precursor movement through the postnatal thymus reveals specific microenvironments supporting defined stages of early lymphoid development. *J Exp Med,* 194, 127-34.

LINDAHL, P., JOHANSSON, B. R., LEVEEN, P. & BETSHOLTZ, C. (1997) Pericyte loss and microaneurysm formation in PDGF-B-deficient mice. *Science,* 277, 242-5.

LINDBLOM, P., GERHARDT, H., LIEBNER, S., ABRAMSSON, A., ENGE, M., HELLSTROM, M., BACKSTROM, G., FREDRIKSSON, S., LANDEGREN, U., NYSTROM, H. C., BERGSTROM, G., DEJANA, E., OSTMAN, A., LINDAHL, P. & BETSHOLTZ, C. (2003) Endothelial PDGF-B retention is required for proper investment of pericytes in the microvessel wall. *Genes Dev,* 17, 1835-40.

LISTON, A., LESAGE, S., WILSON, J., PELTONEN, L. & GOODNOW, C. C. (2003) Aire regulates negative selection of organ-specific T cells. *Nat Immunol,* 4, 350-4.

LIU, X. & BOSSELUT, R. (2004) Duration of TCR signaling controls CD4-CD8 lineage differentiation in vivo. *Nat Immunol,* 5, 280-8.

LOEFFLER, M., BRATKE, T., PAULUS, U., LI, Y. Q. & POTTEN, C. S. (1997) Clonality and life cycles of intestinal crypts explained by a state dependent stochastic model of epithelial stem cell organization. *J Theor Biol,* 186, 41-54.

LURIA, S. E. & DELBRUCK, M. (1943) Mutations of Bacteria from Virus Sensitivity to Virus Resistance. *Genetics,* 28, 491-511.

MANLEY, N. R. (2000) Thymus organogenesis and molecular mechanisms of thymic epithelial cell differentiation. *Semin Immunol,* 12, 421-8.

MANLEY, N. R. & BLACKBURN, C. C. (2003) A developmental look at thymus organogenesis: where do the non-hematopoietic cells in the thymus come from? *Curr Opin Immunol,* 15, 225-32.

MANLEY, N. R. & CAPECCHI, M. R. (1995) The role of Hoxa-3 in mouse thymus and thyroid development. *Development,* 121, 1989-2003.

MANLEY, N. R. & CAPECCHI, M. R. (1998) Hox group 3 paralogs regulate the development and migration of the thymus, thyroid, and parathyroid glands. *Dev Biol,* 195, 1-15.

MARSHMAN, E., BOOTH, C. & POTTEN, C. S. (2002) The intestinal epithelial stem cell. *Bioessays,* 24, 91-8.

MARTINEZ, M., SAMMS, M., HENDRIX, T. M., ADEOSUN, O., PEZZANO, M. & GUYDEN, J. C. (2007) Thymic nurse cell multicellular complexes in HY-TCR transgenic mice demonstrate their association with MHC restriction. *Exp Biol Med (Maywood),* 232, 780-8.

MATHIS, L., BONNEROT, C., PUELLES, L. & NICOLAS, J. F. (1997) Retrospective clonal analysis of the cerebellum using genetic laacZ/lacZ mouse mosaics. *Development,* 124, 4089-104.

MEILHAC, S. M., KELLY, R. G., ROCANCOURT, D., ELOY-TRINQUET, S., NICOLAS, J. F. & BUCKINGHAM, M. E. (2003) A retrospective clonal analysis of the myocardium reveals two phases of clonal growth in the developing mouse heart. *Development,* 130, 3877-89.

MERKENSCHLAGER, M., GRAF, D., LOVATT, M., BOMMHARDT, U., ZAMOYSKA, R. & FISHER, A. G. (1997) How many thymocytes audition for selection? *J Exp Med,* 186, 1149-58.

MIGNINI, F., STRECCIONI, V. & AMENTA, F. (2003) Autonomic innervation of immune organs and neuroimmune modulation. *Auton Autacoid Pharmacol,* 23, 1-25.

MORI, K., ITOI, M., TSUKAMOTO, N., KUBO, H. & AMAGAI, T. (2007) The perivascular space as a path of hematopoietic progenitor cells and mature T cells between the blood circulation and the thymic parenchyma. *Int Immunol,* 19, 745-53.

MORRIS, L., GORDON, J. & BLACKBURN, C. C. (2006) Identification of a tandem duplicated array in the Rhox alpha locus on mouse chromosome X. *Mamm Genome,* 17, 178-87.

MUEGGE, K., VILA, M. P. & DURUM, S. K. (1993) Interleukin-7: a cofactor for V(D)J rearrangement of the T cell receptor beta gene. *Science,* 261, 93-5.

MULLER, S. M., STOLT, C. C., TERSZOWSKI, G., BLUM, C., AMAGAI, T., KESSARIS, N., IANNARELLI, P., RICHARDSON, W. D., WEGNER, M. & RODEWALD, H. R. (2008) Neural crest origin of perivascular mesenchyme in the adult thymus. *J Immunol,* 180, 5344-51.

MULLER, S. M., TERSZOWSKI, G., BLUM, C., HALLER, C., ANQUEZ, V., KUSCHERT, S., CARMELIET, P., AUGUSTIN, H. G. & RODEWALD, H. R. (2005) Gene targeting of VEGF-A in thymus epithelium disrupts thymus blood vessel architecture. *Proc Natl Acad Sci U S A,* 102, 10587-92.

MUROI, S., NAOE, Y., MIYAMOTO, C., AKIYAMA, K., IKAWA, T., MASUDA, K., KAWAMOTO, H. & TANIUCHI, I. (2008) Cascading suppression of transcriptional silencers by ThPOK seals helper T cell fate. *Nat Immunol,* 9, 1113-21.

NEHLS, M., KYEWSKI, B., MESSERLE, M., WALDSCHUTZ, R., SCHUDDEKOPF, K., SMITH, A. J. & BOEHM, T. (1996) Two genetically separable steps in the differentiation of thymic epithelium. *Science,* 272, 886-9.

NELSON, A. J., DUNN, R. J., PEACH, R., ARUFFO, A. & FARR, A. G. (1996) The murine homolog of human Ep-CAM, a homotypic adhesion molecule, is expressed by thymocytes and thymic epithelial cells. *Eur J Immunol,* 26, 401-8.

NEUBUSER, A., KOSEKI, H. & BALLING, R. (1995) Characterization and developmental expression of Pax9, a paired-box-containing gene related to Pax1. *Dev Biol,* 170, 701-16.

NICOLAS, J. F., MATHIS, L., BONNEROT, C. & SAURIN, W. (1996) Evidence in the mouse for self-renewing stem cells in the formation of a segmented longitudinal structure, the myotome. *Development,* 122, 2933-46.

NIJHOF, J. G., BRAUN, K. M., GIANGRECO, A., VAN PELT, C., KAWAMOTO, H., BOYD, R. L., WILLEMZE, R., MULLENDERS, L. H., WATT, F. M., DE GRUIJL, F. R. & VAN EWIJK, W. (2006) The cell-surface marker MTS24 identifies a novel population of follicular keratinocytes with characteristics of progenitor cells. *Development,* 133, 3027-37.

NISHIO, H., MATSUI, K., TSUJI, H., TAMURA, A. & SUZUKI, K. (2001) Immunolocalization of the mitogen-activated protein kinase signaling pathway in Hassall's corpuscles of the human thymus. *Acta Histochem,* 103, 89-98.

NOWAK, J. A., POLAK, L., PASOLLI, H. A. & FUCHS, E. (2008) Hair follicle stem cells are specified and function in early skin morphogenesis. *Cell Stem Cell,* 3, 33-43.

OFFIELD, M. F., JETTON, T. L., LABOSKY, P. A., RAY, M., STEIN, R. W., MAGNUSON, M. A., HOGAN, B. L. & WRIGHT, C. V. (1996) PDX-1 is required for pancreatic outgrowth and differentiation of the rostral duodenum. *Development,* 122, 983-95.

OP DEN KAMP, J. A. (1979) Lipid asymmetry in membranes. *Annu Rev Biochem,* 48, 47-71.

ORR-URTREGER, A. & LONAI, P. (1992) Platelet-derived growth factor-A and its receptor are expressed in separate, but adjacent cell layers of the mouse embryo. *Development,* 115, 1045-58.

OSHIMA, H., ROCHAT, A., KEDZIA, C., KOBAYASHI, K. & BARRANDON, Y. (2001) Morphogenesis and renewal of hair follicles from adult multipotent stem cells. *Cell,* 104, 233-45.

OZERDEM, U. & STALLCUP, W. B. (2003) Early contribution of pericytes to angiogenic sprouting and tube formation. *Angiogenesis,* 6, 241-9.

PAI, S. Y., TRUITT, M. L., TING, C. N., LEIDEN, J. M., GLIMCHER, L. H. & HO, I. C. (2003) Critical roles for transcription factor GATA-3 in thymocyte development. *Immunity,* 19, 863-75.

PALMER, D. B., VINEY, J. L., RITTER, M. A., HAYDAY, A. C. & OWEN, M. J. (1993) Expression of the alpha beta T-cell receptor is necessary for the generation of the thymic medulla. *Dev Immunol,* 3, 175-9.

PEARSON, B., WOLF, P. L. & VAZQUEZ, J. (1963) A Comparative Study of a Series of New Indolyl Compounds to Localize Beta-Galactosidase in Tissues. *Lab Invest,* 12, 1249-59.

PENIT, C., LUCAS, B. & VASSEUR, F. (1995) Cell expansion and growth arrest phases during the transition from precursor (CD4-8-) to immature (CD4+8+) thymocytes in normal and genetically modified mice. *J Immunol,* 154, 5103-13.

PENIT, C., LUCAS, B., VASSEUR, F., RIEKER, T. & BOYD, R. L. (1996) Thymic medulla epithelial cells acquire specific markers by post-mitotic maturation. *Dev Immunol,* 5, 25-36.

PERCIVAL, A. C. & SLACK, J. M. (1999) Analysis of pancreatic development using a cell lineage label. *Exp Cell Res,* 247, 123-32.

PETIT, A. C., LEGUE, E. & NICOLAS, J. F. (2005) Methods in clonal analysis and applications. *Reprod Nutr Dev,* 45, 321-39.

PETRIE, H. T., HUGO, P., SCOLLAY, R. & SHORTMAN, K. (1990) Lineage relationships and developmental kinetics of immature thymocytes: CD3, CD4, and CD8 acquisition in vivo and in vitro. *J Exp Med,* 172, 1583-8.

PETRIE, H. T., LIVAK, F., SCHATZ, D. G., STRASSER, A., CRISPE, I. N. & SHORTMAN, K. (1993) Multiple rearrangements in T cell receptor alpha chain genes maximize the production of useful thymocytes. *J Exp Med,* 178, 615-22.

PORRITT, H. E., RUMFELT, L. L., TABRIZIFARD, S., SCHMITT, T. M., ZUNIGA-PFLUCKER, J. C. & PETRIE, H. T. (2004) Heterogeneity among DN1 prothymocytes reveals multiple progenitors with different capacities to generate T cell and non-T cell lineages. *Immunity,* 20, 735-45.

POTTEN, C. S. (1977) Extreme sensitivity of some intestinal crypt cells to X and gamma irradiation. *Nature,* 269, 518-21.

POTTEN, C. S. (1998) Stem cells in gastrointestinal epithelium: numbers, characteristics and death. *Philos Trans R Soc Lond B Biol Sci,* 353, 821-30.

REVEST, J. M., SUNIARA, R. K., KERR, K., OWEN, J. J. & DICKSON, C. (2001) Development of the thymus requires signaling through the fibroblast growth factor receptor R2-IIIb. *J Immunol,* 167, 1954-61.

ROBERTS, S. A. & POTTEN, C. S. (1994) Clonogen content of intestinal crypts: its deduction using a microcolony assay on whole mount preparations and its dependence on radiation dose. *Int J Radiat Biol,* 65, 477-81.

ROCHAT, A., KOBAYASHI, K. & BARRANDON, Y. (1994) Location of stem cells of human hair follicles by clonal analysis. *Cell,* 76, 1063-73.

RODEWALD, H. R., PAUL, S., HALLER, C., BLUETHMANN, H. & BLUM, C. (2001) Thymus medulla consisting of epithelial islets each derived from a single progenitor. *Nature,* 414, 763-8.

ROMAGNANI, P., ANNUNZIATO, F., MANETTI, R., MAVILIA, C., LASAGNI, L., MANUELLI, C., VANNELLI, G. B., VANINI, V., MAGGI, E., PUPILLI, C. & ROMAGNANI, S. (1998) High CD30 ligand expression by epithelial cells and Hassal's corpuscles in the medulla of human thymus. *Blood,* 91, 3323-32.

ROPKE, C., VAN SOEST, P., PLATENBURG, P. P. & VAN EWIJK, W. (1995) A common stem cell for murine cortical and medullary thymic epithelial cells? *Dev Immunol,* 4, 149-56.

ROSSI, S. W., CHIDGEY, A. P., PARNELL, S. M., JENKINSON, W. E., SCOTT, H. S., BOYD, R. L., JENKINSON, E. J. & ANDERSON, G. (2007a) Redefining epithelial progenitor potential in the developing thymus. *Eur J Immunol,* 37, 2411-8.

ROSSI, S. W., JENKINSON, W. E., ANDERSON, G. & JENKINSON, E. J. (2006) Clonal analysis reveals a common progenitor for thymic cortical and medullary epithelium. *Nature,* 441, 988-91.

ROSSI, S. W., KIM, M. Y., LEIBBRANDT, A., PARNELL, S. M., JENKINSON, W. E., GLANVILLE, S. H., MCCONNELL, F. M., SCOTT, H. S., PENNINGER, J. M., JENKINSON, E. J., LANE, P. J. & ANDERSON, G. (2007b) RANK signals from CD4(+)3(-) inducer cells regulate development of Aire-expressing epithelial cells in the thymic medulla. *J Exp Med,* 204, 1267-72.

SALMOND, R. J., FILBY, A., QURESHI, I., CASERTA, S. & ZAMOYSKA, R. (2009) T-cell receptor proximal signaling via the Src-family kinases, Lck and Fyn, influences T-cell activation, differentiation, and tolerance. *Immunol Rev,* 228, 9-22.

SANES, J. R. (1994) Lineage tracing. The laatest in lineaage. *Curr Biol,* 4, 1162-4.

SANES, J. R., RUBENSTEIN, J. L. & NICOLAS, J. F. (1986) Use of a recombinant retrovirus to study post-implantation cell lineage in mouse embryos. *Embo J,* 5, 3133-42.

SAUER, B. (1998) Inducible gene targeting in mice using the Cre/lox system. *Methods,* 14, 381-92.

SAVINO, W. & DARDENNE, M. (1988a) Developmental studies on expression of monoclonal antibody-defined cytokeratins by thymic epithelial cells from normal and autoimmune mice. *J Histochem Cytochem,* 36, 1123-9.

SAVINO, W. & DARDENNE, M. (1988b) Immunohistochemical studies on a human thymic epithelial cell subset defined by the anti-cytokeratin 18 monoclonal antibody. *Cell Tissue Res,* 254, 225-31.

SAXONOV, S., BERG, P. & BRUTLAG, D. L. (2006) A genome-wide analysis of CpG dinucleotides in the human genome distinguishes two distinct classes of promoters. *Proc Natl Acad Sci U S A,* 103, 1412-7.

SCHEIFF, J. M., CORDIER, A. C. & HAUMONT, S. (1978) The thymus of Nu/+ mice. *Anat Embryol (Berl),* 153, 115-22.

SCHLUEP, M., WILLCOX, N., RITTER, M. A., NEWSOM-DAVIS, J., LARCHE, M. & BROWN, A. N. (1988) Myasthenia gravis thymus: clinical, histological and culture correlations. *J Autoimmun,* 1, 445-67.

SCOLLAY, R., WILSON, A. & SHORTMAN, K. (1984) Thymus cell migration: analysis of thymus emigrants with markers that distinguish medullary thymocytes from peripheral T cells. *J Immunol,* 132, 1089-94.

SEACH, N., UENO, T., FLETCHER, A. L., LOWEN, T., MATTESICH, M., ENGWERDA, C. R., SCOTT, H. S., WARE, C. F., CHIDGEY, A. P., GRAY, D. H. & BOYD, R. L. (2008) The lymphotoxin pathway regulates Aire-independent expression of ectopic genes and chemokines in thymic stromal cells. *J Immunol,* 180, 5384-92.

SEMPOWSKI, G. D., GOODING, M. E., LIAO, H. X., LE, P. T. & HAYNES, B. F. (2002) T cell receptor excision circle assessment of thymopoiesis in aging mice. *Mol Immunol,* 38, 841-8.

SENELAR, R., ESCOLA, M. J., ESCOLA, R., SERROU, B. & SERRE, A. (1976) Relationship between Hassall's corpuscles and thymocytes fate in guinea-pig foetus. *Biomedicine,* 24, 112-22.

SENOO, M., PINTO, F., CRUM, C. P. & MCKEON, F. (2007) p63 Is essential for the proliferative potential of stem cells in stratified epithelia. *Cell,* 129, 523-36.

SHACKLETON, M., VAILLANT, F., SIMPSON, K. J., STINGL, J., SMYTH, G. K., ASSELIN-LABAT, M. L., WU, L., LINDEMAN, G. J. & VISVADER, J. E. (2006) Generation of a functional mammary gland from a single stem cell. *Nature,* 439, 84-8.

SHAKIB, S., DESANTI, G. E., JENKINSON, W. E., PARNELL, S. M., JENKINSON, E. J. & ANDERSON, G. (2009) Checkpoints in the development of thymic cortical epithelial cells. *J Immunol,* 182, 130-7.

SHINOHARA, T. & HONJO, T. (1996) Epidermal growth factor can replace thymic mesenchyme in induction of embryonic thymus morphogenesis in vitro. *Eur J Immunol,* 26, 747-52.

SHINOHARA, T. & HONJO, T. (1997) Studies in vitro on the mechanism of the epithelial/mesenchymal interaction in the early fetal thymus. *Eur J Immunol,* 27, 522-9.

SHORES, E. W., VAN EWIJK, W. & SINGER, A. (1991) Disorganization and restoration of thymic medullary epithelial cells in T cell receptor-negative scid mice: evidence that receptor-bearing lymphocytes influence maturation of the thymic microenvironment. *Eur J Immunol,* 21, 1657-61.

SINGER, A. (2002) New perspectives on a developmental dilemma: the kinetic signaling model and the importance of signal duration for the CD4/CD8 lineage decision. *Curr Opin Immunol,* 14, 207-15.

SORIANO, P. (1999) Generalized lacZ expression with the ROSA26 Cre reporter strain. *Nat Genet,* 21, 70-1.

STINGL, J., EAVES, C. J., ZANDIEH, I. & EMERMAN, J. T. (2001) Characterization of bipotent mammary epithelial progenitor cells in normal adult human breast tissue. *Breast Cancer Res Treat,* 67, 93-109.

STINGL, J., EIREW, P., RICKETSON, I., SHACKLETON, M., VAILLANT, F., CHOI, D., LI, H. I. & EAVES, C. J. (2006) Purification and unique properties of mammary epithelial stem cells. *Nature,* 439, 993-7.

STRATHDEE, D., WHITELAW, C. B. & CLARK, A. J. (2008) Distal transgene insertion affects CpG island maintenance during differentiation. *J Biol Chem,* 283, 11509-15.

SU, D., ELLIS, S., NAPIER, A., LEE, K. & MANLEY, N. R. (2001) Hoxa3 and pax1 regulate epithelial cell death and proliferation during thymus and parathyroid organogenesis. *Dev Biol,* 236, 316-29.

SUNIARA, R. K., JENKINSON, E. J. & OWEN, J. J. (2000) An essential role for thymic mesenchyme in early T cell development. *J Exp Med,* 191, 1051-6.

SURH, C. D., GAO, E. K., KOSAKA, H., LO, D., AHN, C., MURPHY, D. B., KARLSSON, L., PETERSON, P. & SPRENT, J. (1992) Two subsets of epithelial cells in the thymic medulla. *J Exp Med,* 176, 495-505.

SUTHERLAND, J. S., GOLDBERG, G. L., HAMMETT, M. V., ULDRICH, A. P., BERZINS, S. P., HENG, T. S., BLAZAR, B. R., MILLAR, J. L., MALIN, M. A., CHIDGEY, A. P. & BOYD, R. L. (2005) Activation of thymic regeneration in mice and humans following androgen blockade. *J Immunol,* 175, 2741-53.

TAKAHAMA, Y. (2006) Journey through the thymus: stromal guides for T-cell development and selection. *Nat Rev Immunol,* 6, 127-35.

TAKAI, D. & JONES, P. A. (2002) Comprehensive analysis of CpG islands in human chromosomes 21 and 22. *Proc Natl Acad Sci U S A,* 99, 3740-5.

TAKAKURA, N., YOSHIDA, H., OGURA, Y., KATAOKA, H., NISHIKAWA, S. & NISHIKAWA, S. (1997) PDGFR alpha expression during mouse embryogenesis: immunolocalization analyzed by whole-mount immunohistostaining using the monoclonal anti-mouse PDGFR alpha antibody APA5. *J Histochem Cytochem,* 45, 883-93.

TANAHASHI, H. & TABIRA, T. (2000) Alkaline treatment after X-Gal staining reaction for Escherichia coli beta-galactosidase enhances sensitivity. *Anal Biochem,* 279, 122-3.

TAUB, D. D. & LONGO, D. L. (2005) Insights into thymic aging and regeneration. *Immunol Rev,* 205, 72-93.

TAYLOR, G., LEHRER, M. S., JENSEN, P. J., SUN, T. T. & LAVKER, R. M. (2000) Involvement of follicular stem cells in forming not only the follicle but also the epidermis. *Cell,* 102, 451-61.

TETA, M., RANKIN, M. M., LONG, S. Y., STEIN, G. M. & KUSHNER, J. A. (2007) Growth and regeneration of adult beta cells does not involve specialized progenitors. *Dev Cell,* 12, 817-26.

TZOUANACOU, E., WEGENER, A., WYMEERSCH, F. J., WILSON, V. & NICOLAS, J. F. (2009) Redefining the progression of lineage segregations during mammalian embryogenesis by clonal analysis. *Dev Cell*, 17, 365-76.

VALERO, R., BARON, M. L., GUERIN, S., BELIARD, S., LELOUARD, H., KAHN-PERLES, B., VIALETTES, B., NGUYEN, C., IMBERT, J. & NAQUET, P. (2002) A defective NF-kappa B/RelB pathway in autoimmune-prone New Zealand black mice is associated with inefficient expansion of thymocyte and dendritic cells. *J Immunol,* 169, 185-92.

VAN BUUL-OFFERS, S. C., DE HAAN, K., REIJNEN-GRESNIGT, M. G., MEINSMA, D., JANSEN, M., OEI, S. L., BONTE, E. J., SUSSENBACH, J. S. & VAN DEN BRANDE, J. L. (1995) Overexpression of human insulin-like growth factor-II in transgenic mice causes increased growth of the thymus. *J Endocrinol,* 144, 491-502.

VAN DE WIJNGAERT, F. P., KENDALL, M. D., SCHUURMAN, H. J., RADEMAKERS, L. H. & KATER, L. (1984) Heterogeneity of epithelial cells in the human thymus. An ultrastructural study. *Cell Tissue Res,* 237, 227-37.

VAN EWIJK, W., HOLLANDER, G., TERHORST, C. & WANG, B. (2000) Stepwise development of thymic microenvironments in vivo is regulated by thymocyte subsets. *Development,* 127, 1583-91.

VAN EWIJK, W., ROUSE, R. V. & WEISSMAN, I. L. (1980) Distribution of H-2 microenvironments in the mouse thymus. Immunoelectron microscopic identification of I-A and H-2K bearing cells. *J Histochem Cytochem,* 28, 1089-99.

VAN EWIJK, W., SHORES, E. W. & SINGER, A. (1994) Crosstalk in the mouse thymus. *Immunol Today,* 15, 214-7.

VAN VLIET, E., MELIS, M. & VAN EWIJK, W. (1984) Monoclonal antibodies to stromal cell types of the mouse thymus. *Eur J Immunol,* 14, 524-9.

VERMES, I., HAANEN, C., STEFFENS-NAKKEN, H. & REUTELINGSPERGER, C. (1995) A novel assay for apoptosis. Flow cytometric detection of phosphatidylserine expression on early apoptotic cells using fluorescein labelled Annexin V. *J Immunol Methods,* 184, 39-51.

VITELLI, F., MORISHIMA, M., TADDEI, I., LINDSAY, E. A. & BALDINI, A. (2002) Tbx1 mutation causes multiple cardiovascular defects and disrupts neural crest and cranial nerve migratory pathways. *Hum Mol Genet,* 11, 915-22.

VON GAUDECKER, B., KENDALL, M. D. & RITTER, M. A. (1997) Immuno-electron microscopy of the thymic epithelial microenvironment. *Microsc Res Tech,* 38, 237-49.

WALLIN, J., EIBEL, H., NEUBUSER, A., WILTING, J., KOSEKI, H. & BALLING, R. (1996) Pax1 is expressed during development of the thymus epithelium and is required for normal T-cell maturation. *Development,* 122, 23-30.

WANG, B., BIRON, C., SHE, J., HIGGINS, K., SUNSHINE, M. J., LACY, E., LONBERG, N. & TERHORST, C. (1994) A block in both early T lymphocyte and

natural killer cell development in transgenic mice with high-copy numbers of the human CD3E gene. *Proc Natl Acad Sci U S A,* 91, 9402-6.

WANG, L., WILDT, K. F., ZHU, J., ZHANG, X., FEIGENBAUM, L., TESSAROLLO, L., PAUL, W. E., FOWLKES, B. J. & BOSSELUT, R. (2008) Distinct functions for the transcription factors GATA-3 and ThPOK during intrathymic differentiation of CD4(+) T cells. *Nat Immunol,* 9, 1122-30.

WATANABE, N., WANG, Y. H., LEE, H. K., ITO, T., WANG, Y. H., CAO, W. & LIU, Y. J. (2005) Hassall's corpuscles instruct dendritic cells to induce CD4+CD25+ regulatory T cells in human thymus. *Nature,* 436, 1181-5.

WEKERLE, H. & KETELSEN, U. P. (1980) Thymic nurse cells--Ia-bearing epithelium involved in T-lymphocyte differentiation? *Nature,* 283, 402-4.

WEKERLE, H., KETELSEN, U. P. & ERNST, M. (1980) Thymic nurse cells. Lymphoepithelial cell complexes in murine thymuses: morphological and serological characterization. *J Exp Med,* 151, 925-44.

WILSON, A., HELD, W. & MACDONALD, H. R. (1994a) Two waves of recombinase gene expression in developing thymocytes. *J Exp Med,* 179, 1355-60.

WILSON, C., COTSARELIS, G., WEI, Z. G., FRYER, E., MARGOLIS-FRYER, J., OSTEAD, M., TOKAREK, R., SUN, T. T. & LAVKER, R. M. (1994b) Cells within the bulge region of mouse hair follicle transiently proliferate during early anagen: heterogeneity and functional differences of various hair cycles. *Differentiation,* 55, 127-36.

XU, H., CERRATO, F. & BALDINI, A. (2005) Timed mutation and cell-fate mapping reveal reiterated roles of Tbx1 during embryogenesis, and a crucial function during segmentation of the pharyngeal system via regulation of endoderm expansion. *Development,* 132, 4387-95.

XU, P. X., ZHENG, W., LACLEF, C., MAIRE, P., MAAS, R. L., PETERS, H. & XU, X. (2002) Eya1 is required for the morphogenesis of mammalian thymus, parathyroid and thyroid. *Development,* 129, 3033-44.

XU, X., D'HOKER, J., STANGE, G., BONNE, S., DE LEU, N., XIAO, X., VAN DE CASTEELE, M., MELLITZER, G., LING, Z., PIPELEERS, D., BOUWENS, L., SCHARFMANN, R., GRADWOHL, G. & HEIMBERG, H. (2008) Beta cells can be generated from endogenous progenitors in injured adult mouse pancreas. *Cell,* 132, 197-207.

YAMAZAKI, H., SAKATA, E., YAMANE, T., YANAGISAWA, A., ABE, K., YAMAMURA, K., HAYASHI, S. & KUNISADA, T. (2005) Presence and distribution of neural crest-derived cells in the murine developing thymus and their potential for differentiation. *Int Immunol,* 17, 549-58.

YANG, S. J., AHN, S., PARK, C. S., HOLMES, K. L., WESTRUP, J., CHANG, C. H. & KIM, M. G. (2006) The quantitative assessment of MHC II on thymic epithelium: implications in cortical thymocyte development. *Int Immunol,* 18, 729-39.

ZAITSEVA, M., KAWAMURA, T., LOOMIS, R., GOLDSTEIN, H., BLAUVELT, A. & GOLDING, H. (2002) Stromal-derived factor 1 expression in the human thymus. *J Immunol,* 168, 2609-17.

ZAMBROWICZ, B. P., IMAMOTO, A., FIERING, S., HERZENBERG, L. A., KERR, W. G. & SORIANO, P. (1997) Disruption of overlapping transcripts in the ROSA beta geo 26 gene trap strain leads to widespread expression of beta-galactosidase in mouse embryos and hematopoietic cells. *Proc Natl Acad Sci U S A,* 94, 3789-94.

ZHOU, Q., LAW, A. C., RAJAGOPAL, J., ANDERSON, W. J., GRAY, P. A. & MELTON, D. A. (2007) A multipotent progenitor domain guides pancreatic organogenesis. *Dev Cell,* 13, 103-14.

ZOU, D., SILVIUS, D., DAVENPORT, J., GRIFONE, R., MAIRE, P. & XU, P. X. (2006) Patterning of the third pharyngeal pouch into thymus/parathyroid by Six and Eya1. *Dev Biol,* 293, 499-512.